Department of Communications and Networking

Enabling Time-Synchronized and Interference-Aware Initialization of Wireless Sensor Networks

Aamir Mahmood

A!

DOCTORAL DISSERTATIONS

Aalto University publication series
DOCTORAL DISSERTATIONS 8/2014

Enabling Time-Synchronized and Interference-Aware Initialization of Wireless Sensor Networks

Aamir Mahmood

A doctoral dissertation completed for the degree of Doctor of Science (Technology) to be defended, with the permission of the Aalto University School of Electrical Engineering, at a public examination held at the lecture hall TU2 of the school on 31 January 2014 at 12 noon.

Aalto University
School of Electrical Engineering
Department of Communications and Networking

Supervising professor
Professor Riku Jäntti

Preliminary examiners
Professor Karl Henrik Johansson, KTH, Sweden
Professor Ismo Hakala, University of Jyväskylä, Finland

Opponent
Professor Mikael Johansson, KTH, Sweden

Aalto University publication series
DOCTORAL DISSERTATIONS 8/2014

ISBN 978-952-60-5536-7
ISBN 978-952-60-5537-4 (pdf)
ISSN-L 1799-4934
ISSN 1799-4934 (printed)
ISSN 1799-4942 (pdf)
http://urn.fi/URN:ISBN:978-952-60-5537-4

Unigrafia Oy
Helsinki 2014

Finland

441 697
Printed matter

Aalto University

Abstract

Aalto University, P.O. Box 11000, FI-00076 Aalto www.aalto.fi

Author
Aamir Mahmood

Name of the doctoral dissertation
Enabling Time-Synchronized and Interference-Aware Initialization of Wireless Sensor Networks

Publisher School of Electrical Engineering

Unit Department of Communications and Networking

Series Aalto University publication series DOCTORAL DISSERTATIONS 8/2014

Field of research Communications Engineering

Manuscript submitted 22 August 2013 **Date of the defence** 31 January 2014

Permission to publish granted (date) 4 December 2013 **Language** English

☐ **Monograph** ☒ **Article dissertation (summary + original articles)**

Abstract

Wireless sensor networks (WSNs) provide ad hoc wireless infrastructure to spatially distributed sensors to interact with physical or environmental phenomena. WSNs can offer a multitude of applications given that the sensors are able to collaborate and self-organize. These requirements are essential to accurately capture and reliably fuse the observations towards the application logic. This thesis studies time synchronization and interference management schemes to enable collaboration and self-organization in low-power WSNs.

Network-wide time synchronization is required both for the concurrent actuation of sensors and reliable data aggregation. Time synchronization is achieved by a clock synchronization algorithm which estimates the clock offset and clock skew at a sensor with respect to a reference time. The reference time is diffused in the network by a messaging protocol. This thesis studies clock offset and skew estimation methods for broadcast-based exchange of the reference time. The offset estimation is based on a study to eliminate the delay factors in the communication path. For skew estimation based on linear-regression, the correlation between time synchronization period and regression size is studied. In addition, a maximum-likelihood skew estimator, which minimizes the estimation error variance, is validated.

From an application's perspective, the time synchronization service should provide the desired synchronization accuracy in a transparent and energy-efficient manner. This thesis demonstrates this ability by extending the proposed time synchronization methods for a) tight synchronization among vibration samples in a structural health monitoring application, b) communication scheduling in time and frequency.

WSNs deployed in shared unlicensed bands need to analyze and mitigate interference. The low-power transmissions of sensor nodes are otherwise prone to corruption from high-power transmissions of coexisting wireless networks. Therein, this thesis proposes coexistence models for energy-detection based link-quality estimation. The coexistence models are utilized to formulate low-complexity coexistence enhancement algorithms named channel ranking. A ranking algorithm creates an ordered list of the candidate channels using a channel quality metric (CQM). The algorithms differ with respect to their design of CQM, the main design factor being the availability of network connectivity information which is usually unknown upon network initialization.

Keywords time synchronization, coexistence modeling, channel ranking

ISBN (printed) 978-952-60-5536-7 **ISBN (pdf)** 978-952-60-5537-4

ISSN-L 1799-4934 **ISSN (printed)** 1799-4934 **ISSN (pdf)** 1799-4942

Location of publisher Helsinki **Location of printing** Helsinki **Year** 2014

Pages 228 **urn** http://urn.fi/URN:ISBN:978-952-60-5537-4

Preface

Praise be to Allah. The research work presented in this thesis is carried out during 2008 – 2013 at the Department of Communications and Networking, Aalto University. The main theme of the work falls in the scope of MIDE funded ISMO project. I would like to acknowledge the financial grant from Nokia Foundation.

Although hard to acknowledge all, many people contributed directly and indirectly in the completion of the thesis. First of all, my sincere gratitude to my supervisor, Prof. Riku Jäntti, for his guidance and mentoring in these years. I would like to thank him for providing detailed instructions which greatly improved the quality of the work. Besides work, special thanks for the inspiration to long-distance running.

During this period, I got the opportunity to work with my colleagues Mr. Konstantinos Koufos, Maurizio Bocca, Huseyin Yiğitler, M. M. Aftab Hossain, Hamidreza Shariatmadari and Emre Ilke Cosar. I am thankful to all for their contributions and lively discussions. I would also like to thank the pre-examiners of the thesis, Prof. Karl Henrik Johansson and Prof. Ismo Hakala for their time and valuable feedback.

For experimental studies, I am thankful to Mr. Viktor Nässi for his technical support on setting up test-beds. Help from Sari Kiveliö and Sanna Patana on administrative matters is also greatly acknowledged.

At the end, *Jeetay Raho*, stay blessed remarks to my family and friends for their love, prayers and support. Ammarah! Thank you for giving meaning to my life.

Espoo, January 7, 2014,

Aamir Mahmood

Contents

List of Publications

This thesis consists of an overview and of the following publications which are referred to in the text by their Roman numerals.

I A. Mahmood, R. Jäntti. Time synchronization accuracy for real-time wireless sensor networks. In *IEEE Malaysia International Conference on Communications, MICC*, pp. 652 – 657, December 2009.

II H. Yiğitler, A. Mahmood, R. Virrankoski, R. Jäntti. Recursive clock skew estimation for wireless sensor networks using reference broadcasts. *IET Wireless Sensor Systems*, pp. 338 – 350, December 2012.

III M. Bocca, A. Mahmood, L. M. Eriksson, J. Kullaa, R. Jäntti. A synchronized wireless sensor network for experimental modal analysis in structural health monitoring. *Computer-Aided Civil and Infrastructure Engineering*, Volume 26, issue 7, pp. 483 – 499, October 2011.

IV E. I. Cosar, A. Mahmood, M. Bjorkbom. A-Stack: a real-time protocol stack for IEEE 802.15.4 radios. In *IEEE Conference on Local Computer Networks, LCN*, pp. 1020 – 1023, October 2011.

V M. M. A. Hossain, A. Mahmood, R. Jäntti. Channel ranking algorithms for cognitive coexistence of IEEE 802.15.4. In *IEEE International Symposium on Personal, Indoor and Mobile Radio Communications, PIMRC*, pp. 112 – 116, September 2009.

VI A. Mahmood, R. Jäntti. A decision theoretic approach for channel ranking in crowded unlicensed bands. *Wireless Networks*, Volume 17, issue 4, pp. 907 – 919, May 2011.

VII A. Mahmood, K. Koufos, R. Jäntti. Channel ranking algorithm and ranking error bounds: a two channel case. In *IEEE International Symposium on Personal, Indoor and Mobile Radio Communications, PIMRC*, pp. 1071 – 1076, September 2011.

VIII A. Mahmood, H. Yiğitler, R. Jäntti. Stochastic packet collision modeling in coexisting wireless networks for link quality evaluation. In *IEEE International Conference on Communications, ICC*, pp. 508 – 513, June 2013.

IX H. Shariatmadari, A. Mahmood, R. Jäntti. Channel ranking based on packet delivery ratio estimation in wireless sensor networks. In *IEEE Wireless Communications and Networking Conference, WCNC*, pp. 59 – 64, April 2013.

Author's Contribution

Publication I: "Time synchronization accuracy for real-time wireless sensor networks"

The author designed and implemented the synchronization framework for enhancing the accuracy of time synchronization. R. Jäntti supervised the work.

Publication II: "Recursive clock skew estimation for wireless sensor networks using reference broadcasts"

The author contributed to the validation of the clock skew estimator proposed by H. Yiğitler. The author also provided the clock skew data of the nodes. He participated in writing Sections 1,2 and 8 and editing the rest of the paper. This work is supervised by R. Virrankoski and R. Jäntti.

Publication III: "A synchronized wireless sensor network for experimental modal analysis in structural health monitoring"

The author designed and implemented the time synchronization protocol and interfaces for synchronized execution of the sampling task in the network. The author wrote Sections 2.6 and 2.7 and commented on the rest of the paper.

Publication IV: "A-Stack: a real-time protocol stack for IEEE 802.15.4 radios"

The author developed the interfaces for the generation of timer events from a synchronized clock required by TDMA scheduler initialization, time-slot generation and task synchronization. The author participated in the validation of the design with E. I. Cosar.

Publication V: "Channel ranking algorithms for cognitive coexistence of IEEE 802.15.4"

The author contributed to the design of experimental setup for coexistence analysis and channel ranking algorithm together with M. M. A. Hossain. The paper was written jointly by the first two authors. R. Jäntti motivated this study.

Publication VI: "A decision theoretic approach for channel ranking in crowded unlicensed bands"

The author proposed the channel ranking algorithm and validated it using the channel energy measurements from a real environment. This work is supervised by R. Jäntti.

Publication VII: "Channel ranking algorithm and ranking error bounds: a two channel case"

The author proposed the channel ranking algorithm and performed simulations. K. Koufos instructed in designing the numerical solution to evaluate ranking error probability. The author wrote the paper in the supervision of R. Jäntti.

Publication VIII: "Stochastic packet collision modeling in coexisting wireless networks for link quality evaluation"

The author motivated this study based on the limitations of the existing deterministic packet collision models. R. Jäntti proposed the stochastic packet collision model. The author derived the collision-time distributions using this model with the help of H. Yiğitler. The author also studied

the distributions approximating the realistic traffic scenarios. The author wrote the paper.

Publication IX: "Channel ranking based on packet delivery ratio estimation in wireless sensor networks"

The author proposed the PDR model and instructed H. Shariatmadari for the experimental validation of the model. The author revised the paper written by H. Shariatmadari under the supervision of R. Jäntti.

List of Abbreviations

ACH	Adaptive Channel Hopping
AHP	Analytic Hierarchy Process
AWGN	Additive White Gaussian Noise
BCA	Broadcast Collision Avoidance
BER	Bit Error Rate
CDF	Cumulative Distribution Function
CQM	Channel Quality Metric
CSMA/CA	Carrier Sense Multiple Access - Collision Avoidance
CTD	Collision Time Distribution
DSA	Dynamic Spectrum Access
DSSS	Direct Sequence Spread Spectrum
ERA	Eigensystem Realization Algorithm
FCF	Frame Control Field
FTSP	Flooding Time Synchronization Protocol
GPS	Global Positioning System
IoT	Internet of Things
ISR	Interrupt Service Routine
LOS	Line Of Sight
LQI	Link Quality Indicator
LR-WPAN	Low Rate Wireless Personal Area Networks

LS	Least Squares
LTS	Lightweight Tree-based Synchronization
MCU	MicroController Unit
ML	Maximum Likelihood
NLOS	Non Line Of Sight
NTP	Network Time Protocol
OFDM	Orthogonal Frequency Division Multiplexing
OQPSK	Offset Quadrature Phase Shift Keying
PAN	Personal Area Network
PDF	Probability Density Function
PDR	Packet Delivery Ratio
PER	Packet Error Rate
PPM	Parts Per Million
PTP	Precision Time Protocol
RBS	Reference Broadcast Synchronization
REP	Ranking Error Probability
RSSI	Received Signal Strength Indicator
RT-WSN	Real-Time Wireless Sensor Network
SHM	Structural Health Monitoring
SINR	Signal to Noise plus Interference Ratio
SISO	Single Input Single Output
SNR	Signal to Noise Ratio
SoC	System-on-Chip
SSI-COV	Covariance-based Stochastic Subspace Identification
TDMA	Time Division Multiple Access
TDP	Time Diffusion Protocol

TMS	Tiny/Mini-Sync
TPSN	Timing-sync Protocol for Sensor Networks
TS	Time Synchronization
TSMP	Time Synchronized Mesh Protocol
TxCCRy	Timer *x* Compare Control Register *y*
WLAN	Wireless Local Area Network
WSN	Wireless Sensor Network

List of Symbols

Greek Symbols

α	Shape parameter of a distribution
$\alpha_o(\cdot)$	*on* state variable
β	Scale parameter of a distribution
$\beta_o(\cdot)$	*off* state variable
γ	Decision threshold
$\gamma(\cdot,\cdot)$	Lower incomplete gamma function
$\Gamma(\cdot)$	Gamma function
$\Gamma(\cdot,\cdot)$	Upper incomplete gamma function
δ	Clock skew
Δt	Time error
Δ_τ	Time duration of the critical path
ε	Clock accuracy
ζ	Pulse shaping factor
η	Busy time
$\bar{\eta}$	Mean busy time
η^R	Residual busy time
θ	Clock offset
λ	Packet rate
λ'	Eigenvalue
μ	Mean
ξ	Idle time
$\bar{\xi}$	Mean idle time
ξ^R	Residual idle time
π	Mixture probability
ρ	Activity factor
$\hat{\rho}$	Estimated activity factor

$\hat{\rho}_k$	Estimated activity factor on channel k
$\rho_k^{'}$	Normalized activity factor on channel k
$\rho_{\max}$	Maximum activity factor
σ	Standard deviation
τ_{dec}	Decoding time
τ_{enc}	Encoding time
$\tau_{\text{int}-\text{handling}}$	Interrupt handling time
τ_{prop}	Propagation time
$\tau_{\text{ts}-\text{tx}}$	Timestamp insert time at transmitter
$\tau_{\text{ts}-\text{rx}}$	Timestamp read time at receiver
υ	Regression size
φ	Phase shift in a mode shape
$\chi(\cdot)$	State of a stochastic process
$\omega_0(\cdot,\cdot)$	Collision-time distribution in *off* observed state
$\omega_1(\cdot,\cdot)$	Collision-time distribution in *on* observed state

Latin Symbols

a	Clock skew ratio
$\hat{a}$	Clock skew ratio estimate
a_S	Synchronization accuracy
$\mathbf{A}$	Pairwise comparison matrix
C	Number of available channels
C_h	Hardware clock counter
C^i	Time report of a clock i
C_j^i	Time report of a clock i at jth synchronization instant
C_l	Logical clock counter
$\mathcal{CN}$	Complex Gaussian distribution
dI	Step size for discretized interference power
E_b	Signal energy per bit
f	Natural frequency
f_c	Clock frequency
$f(\cdot)$	Interference function
F_k	Fitness of channel k
$F(\cdot,\cdot)$	Collision time distribution function
$g(\cdot)$	PDF of idle time
$G(\cdot)$	CDF of idle time
$G_n(\cdot)$	n-fold convolution of $G(\cdot)$

$G_n^R(\cdot)$	$G_{n-1}(\cdot)$ convolved with CDF of residual idle time
H_0	Hypothesis 0
H_1	Hypothesis 1
$H(\cdot)$	CDF of busy time
$H_n(\cdot)$	n-fold convolution of $H(\cdot)$
$H_n^R(\cdot)$	$H_{n-1}(\cdot)$ convolved with CDF of residual busy time
I	Interference power
$\bar{I}$	Average interference power
$\hat{I}$	Estimated average interference power
$\hat{I}_k$	Estimated average interference power on channel k
I_k'	Normalized interference power on channel k
$I_{\min}$	Minimum interference power
$I_{\max}$	Maximum interference power
k	Channel index
k_c	Value of a counter at arbitrary time
k_{cj}^i	Value of a counter i at jth synchronization instant
ℓ	Number of interfered bits in a LR-WPAN packet
L	Decision statistic
M	Number of macro-samples
M_r	Number of independent Erlang distributions
N	Number of collected energy samples
$\hat{N}$	Number of decision variables exceeding a decision threshold
N_b	Number of bits in a LR-WPAN packet
N_I	Number of discretized interference levels
N_o	Noise spectral density
N_{T_s}	Number of decision variables in a sampling duration
$p(\cdot\|\cdot)$	Conditional probability
P_e	Bit error rate
P_{e_0}	Bit error rate without interference
P_{e_1}	Bit error rate under interference
P_N	Noise power
Pr_{fa}	False alarm probability
$\mathrm{Pr}_{\varepsilon}$	Ranking error probability
$\mathrm{Pr}_{\varepsilon j}$	Ranking error probability in jth error-case
Pr_{cj}	Probability of occurrence of jth error-case
q_0	Bit success rate without interference
q_1	Bit success rate under interference
$Q(\cdot)$	Q function

r	Number of independent exponential distributions
R	Rank of a channel
R_b	Data rate
R_I	Rank of a channel based on interference signal strength
R_ρ	Rank of a channel based on interference activity factor
s_1, s_2, s_3	Locations of a sensor receiver
S	Signal power of a LR-WPAN link
S_k	Signal power of a LR-WPAN link on channel k
t	Real time
t_0	Time instant of an observation
t_r	Tick resolution of a clock
t_{local}	Local time of a clock
t_S	Synchronization probe interval
T	Packet duration of WLAN
T_b	Bit duration of LR-WPAN
T_0	Period of a clock counter
T_0^i	Period of a clock counter at node i
T_g	Guard time in time slots
T_I	Sampling or packet interval
T_{IA}	Mean packet inter-arrival time
T_s	Sampling duration
T_S	Synchronization interval
T_w	Packet duration of LR-WPAN
$U(\cdot, \cdot)$	Uniform distribution
$\mathbf{w}$	Eigenvector of pairwise comparison matrix
w_I	Weight factor for interference power
w_ρ	Weight factor for interference activity
W	Bandwidth
$W[n]$	nth noise sample
$x^{i,j}$	jth micro-sample in ith macro-sample
X^i	ith macro-sample
$X[n]$	nth channel energy sample
$Y[n]$	nth signal sample
z	Scaling factor
z_I	Scale for interference signal strength
z_ρ	Scale for interference activity factor

1. Introduction

1.1 Background

Environments we *live in* and *depend on* are full of phenomena of meaningful value. Our observations and responses to a phenomenon can change the perspective of our interaction with the physical world. The technological advancements in the field of wireless communication and embedded systems and their combination in the form of wireless sensor networks (WSNs) have revolutionized that perspective that was earlier marred by the lack of a cost-effective and easy-to-deploy requisite infrastructure.

WSNs provide ad hoc wireless infrastructure to spatially distributed sensors for the collection of sensory information. Each sensor is a self-powered unit which integrates sensing, computing and low-range communication capabilities [1]. These sensors, large in number, collaborate and self-organize to fuse the collected information towards a centralized application logic of the network.

Initially, wireless sensor networks were used in military applications; however, a wide range of application areas emerged in the last decade [2]. Industrial monitoring and control, environmental monitoring, structural health monitoring (SHM), agriculture, passive localization, home automation and area monitoring is still a conservative list of application areas as many more are envisioned.

In the future, it is assumed that WSNs will merge into the Internet of Things (IoT), a ubiquitous connectivity paradigm. The end sensors using WSN standards and principles will form a capillary network whereas the IoT will unravel the heterogeneity of isolated WSN islands using standardized protocols like the Internet. The recent standardization efforts are reflected by IoT solutions such as Smarter Planet [3] and

6LoWPAN [4].

The applications and usage scenarios of sensor networks are numerous. However, their realization offers unique challenges to the design of communication and networking techniques. The challenges arise from the very characteristics of a WSN; that is, energy and hardware constrained sensors deployed with high density to provide high fidelity measurements. As a result, the networking techniques must be power efficient, low in complexity and scalable enough to ensure reliable data collection from a sensor field with minimum network maintenance. The diversity in sensor network applications adds another dimension to the design challenges since each application has its own requirements.

The varying requirements among applications have resulted in a number of standards covering the radio and wireless mesh networking aspects of the communication protocol stack. The dominant radio standard for low-power WSN applications is IEEE 802.15.4 [5], known as low-rate wireless personal area network (LR-WPAN). However, no single networking standard dominates; for instance, Zigbee [6] provides several application profiles mainly for smart building automation whereas the standards targeted at wireless automation industry are WirelessHART [7] and ISA100.11a [8]. All these standards are built on IEEE 802.15.4 specifications mostly operating on a 2.4 GHz license-free band.

1.2 Motivation and Objectives

Despite the standardization efforts, adoption of wireless sensor networks in monitoring and automation applications is cautious [9]. The main concerns of technology adopters are; would it provide the results comparable to the existing (wired) infrastructure, can it be relied upon for time-critical operations. A plausible factor being the applications requiring deterministic network behavior in data collection and aggregation. The data collection, which extracts the raw sensor readings of a monitored event, often requires concurrent observations from multiple sensors. The data aggregation, on the other hand, requires reliable network connectivity to transfer the observations to a central point in the network. The network connectivity affects the communication reliability which in turn brings about increase in latency and energy consumption. Therefore, a WSN-based alternative to an existing infrastructure is viable only if the data collection and aggregation can yield a comparable performance. However,

enabling the desired network behavior within the WSN characteristics is challenging, owing to the lack of core network management functions.

The focus of this thesis is the provision of such management functions. These functions relate to the concurrent actuation of the sensors and communication scheduling, and network adaptation under wireless communication unreliability. All stand essential to set up WSN applications and their reliable operation.

In respect to concurrent actuation and observations of a physical phenomenon, time synchronization (TS) plays a crucial role. This role is essential for applications such as SHM, data fusion and localization. Energy efficient medium access scheduling also requires a common reading of time among the sensors. The provision of a common network-wide time scale in distributed systems requires the diffusion of a reference time in the network and a clock synchronization algorithm. The synchronization accuracy is a function of a local clock stability, frequency of the reference time distribution and robustness of the synchronization algorithm. WSN applications usually require synchronization accuracy in sub-microseconds. However, the low cost design of sensors results in higher clock instability, meanwhile the time distribution frequency is bounded by the energy constraints.

In this thesis, our first objective is to,"*design an energy-efficient TS framework which can fulfill the synchronization demands of a sensor network as well as its applications*". For this purpose, the design of a messaging protocol and clock skew estimation algorithm within the WSN constraints is considered. This design is validated by incorporating it to an SHM application for vibrational modal analysis and a time-synchronized communication protocol stack.

The communication reliability depends on the ability of a system to initialize and self-organize in adverse wireless propagation conditions. In sensor networks, establishing and maintaining network connectivity is affected by node failures, fading and radio interference. In this thesis, we focus on heterogeneous inter-network interference.

Interference in unlicensed bands is the main concern to communication reliability in low-power sensor networks. The unlicensed bands host wireless standards with heterogeneous channel partitioning, transmit power and medium access rules. As the application domain of these standards expands, the spectral coexistence in geographical co-location scenarios is imminent. Any high-power transmissions, for instance from WLAN

terminals in a 2.4 GHz ISM band, can easily degrade the communication quality of a low-budget sensor link. The packet loss affects the reliability and also the lifetime of a network owing to the energy drainage by packet retransmissions. Therefore, the integration of an interference avoidance strategy to the WSNs is of the utmost importance especially in industrial and home automation applications where wireless local area network (WLAN) systems are heavily deployed.

The second objective of the thesis is,"*coexistence performance modeling and enhancement in WSNs under heterogeneous inter-network interference*". Therein, coexistence modeling relates to link quality analysis in an interfered sensor network considering traffic and power characteristics of the interfering network. Whereas, coexistence enhancement builds on coexistence modeling study to design low-complexity channel ranking algorithms. The output of a channel ranking algorithm is an ordered list of channels with respect to a link-quality metric. The link-quality metric projects the interference disruption on a channel to a sensor link.

1.3 Contribution of the Thesis

This thesis is composed of a summary and nine publications. A brief overview of the contributions in each publication is given in this section.

1.3.1 Time Synchronization

In Publication I, we analyzed factors contributing to the clock offset under MAC layer time-stamping of reference broadcasts. By taking care of these factors in the clock offset budget, we achieved better time synchronization (TS) accuracy. In order to enhance the scalability of reference broadcast based TS protocols, a broadcast collision avoidance (BCA) scheme is proposed. In addition, we investigated the optimal data set size for the linear regression-based clock skew estimation.

In Publication II, we developed a recursive maximum-likelihood (ML) clock skew estimation algorithm for reference broadcast protocols. It is shown that the skew estimation using least square linear regression yields large estimation error variance owing to the correlation in the time records of the regression data set. The proposed recursive estimator utilizes a time-relation model that reflects the correlation in time records, thus achieving smallest estimation error variance as compared to the

existing ones as suggested by the experimental validation.

In Publication III, time synchronization is extended to distributed synchronized sampling in an SHM application. The SHM application, for the modal analysis of a monitored structure, requires accurate synchronicity among acceleration samples collected by the sensors. The proposed method ensured accurate synchronicity among samples (with TS error less than 10 μs) even at sampling frequency of up to 1 KHz. In terms of modal analysis performance, the measurements from such a synchronized wireless system deployed on a model bridge provided the precise identification of natural frequencies of vibration.

In Publication IV, a protocol stack named A-Stack is designed which provides a flexible development environment for prototyping reliable and real-time wireless sensor networks (RT-WSNs) applications. A-Stack incorporates time division multiple access (TDMA)-based medium access, multi-hop packet time-slot/channel scheduling, and network configuration and formation schemes.

A block diagram categorizing these contributions is shown in Fig. 1.1.

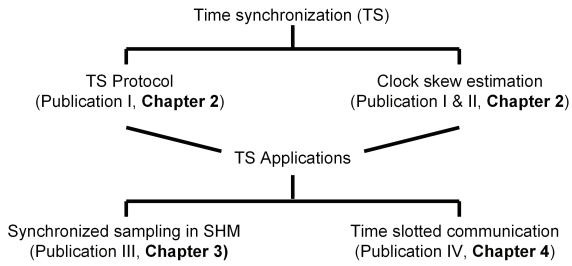

Figure 1.1. Contributions of the thesis on time synchronization

1.3.2 Interference-Aware Coexistence

In Publication V, the coexistence performance of a IEEE 802.15.4-based WSN link is evaluated under WLAN interference in a test-bed. The test-bed features the performance evaluation in different wireless channel models. The conditions for reliable link operation are identified in terms of interference parameters, strength level and activity factor. Based on these conditions, two channel ranking algorithms are proposed which learn the interference parameters using spectrum measurements and heuristically combine these parameters for channel ranking. The algorithms are verified in emulated and open-air channels.

In Publication VI, a channel ranking algorithm is developed based

on the identification and decision theoretic weighting of interference parameters using channel energy measurements. The ranking algorithm is suitable at WSN initialization with unknown signal levels of the adjacent links to a sensor node. We showed that weighting the interference parameters according to their individual influence on the fitness of a channel achieves significant improvement in channel ranking performance as compared to the heuristic approach of Publication V.

In Publication VII, a packet delivery ratio (PDR)-estimation-based channel ranking algorithm is developed where the PDR estimation is based on spectrum energy measurements. The PDR, including other parameters, depends on the WLAN traffic distribution which cannot be satisfactorily predicted with limited measurements. Because of this, the traffic distributions setting bounds on channel ranking performance are identified and these bounds are calculated for a given measurement time. The proposed algorithm establishes relative channel ranking based on the PDR estimation under the traffic distribution setting upper bound on ranking error.

The PDR of an interfered link depends on the collision-time distribution (CTD), which is a function of traffic distributions of the interfering and interfered networks. The existing packet collision models in the literature are deterministic which cannot be generalized to realistic traffic scenarios. In Publication VIII, a stochastic packet collision model is proposed for coexisting wireless networks by modeling the interference traffic as an alternating renewal process and analyzed it in particular for coexisting WSN and WLAN networks. The proposed collision-time model is utilized to derive theoretical CTDs for periodic, Poisson and gamma inter-arrival distributions. In addition, the model is verified by using a distribution fitted to the empirical channel-idle-time distribution shaped by a carrier sense multiple access with collision avoidance (CSMA/CA) rules in a multi-terminal WLAN network.

Contrary to Publication VII, which estimates PDR estimation with respect to the interference traffic distribution, in Publication IX, the proposed PDR estimation method identifies the interference characteristics by spectrum measurements with respect to the intended traffic distribution of the sensor link. The effectiveness of the proposed estimation scheme is verified using a sensor platform against the empirical PDR in emulated multi-path fading channels. Channel ranking in a real environment using this method of PDR estimation shows promising result

under interference from WLAN.

A block diagram categorizing these contributions is shown in Fig. 1.2.

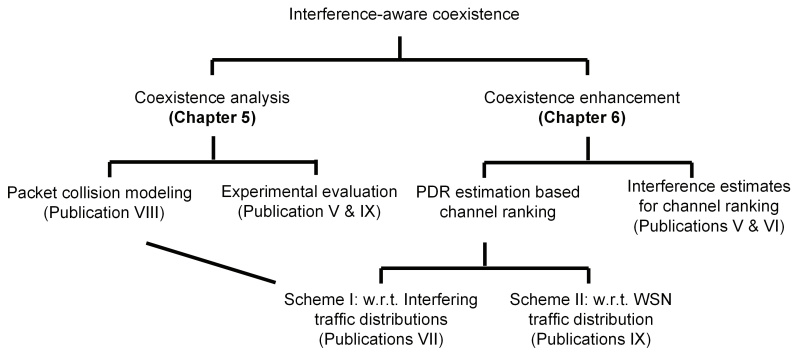

Figure 1.2. Contributions of the thesis on interference-aware coexistence of WSNs

1.4 Structure of the Thesis

The remainder of this thesis is organized in five chapters. Each chapter presents a short introduction to the subject and highlights the contributions in the subject area. An overview of the related work precedes our contributions and results.

Following this structure, Chapter 2 presents reference broadcast-based time synchronization techniques for clock offset adjustment and skew estimation. Time synchronization service is extended further by providing interfaces for task synchronization in WSN applications in Chapter 3 and Chapter 4. Chapter 3 exploits time synchronization service for modal analysis in structural health monitoring. Chapter 4 uses synchronized clocks for communication scheduling. Coexistence modeling of WSNs with WLAN is discussed in Chapter 5 with an objective of link-quality analysis and estimation. The coexistence modeling is extended to formulate coexistence enhancement algorithms in Chapter 6. Finally, conclusions and future research directions are outlined in Chapter 7.

2. Time Synchronization using Reference Broadcasts

Time synchronization (TS) is a fundamental service for initialization and maintenance of wireless sensor networks. From chronological ordering of information to the synchronous task execution, a common notion of time is a *must* requirement for WSN applications. The WSN applications require accurate network-wide time synchronization, often, in the order of a few microseconds. For example, sensor data fusion, structural health monitoring and distributed localization bring forth such synchronization accuracy demands. Moreover, a time-synchronized network can facilitate transmission scheduling such as TDMA and radio duty-cycling in an energy-efficient manner. Since the traditional synchronization schemes such as Network Time Protocol (NTP) [10] were designed for resourceful systems with relaxed accuracy requirements, the WSN community investigates the applicable class of solutions to meet the objectives.

Network-wide time synchronization, in general, is achieved by a combination of a messaging protocol and the clock synchronization algorithm [11]. A clock synchronization algorithm estimates the time offset and clock skew based on the local and received time information exchanged by a messaging protocol. A clock synchronization algorithm maintains long term synchronization by reducing the messaging. The messaging protocols can broadly be categorized as *handshake* [10, 12] and *broadcast* [13, 14] protocols. In a handshake protocol, a message sender synchronizes with the receiver, whereas, a set of receivers synchronize with the reference sender in a broadcast protocol. In this chapter, we studied the messaging protocol and clock skew estimation using reference broadcasts since the broadcast protocols are appreciated for their low-power demands. Our contribution can be summarized as:

- Analyzing the clock offset delay in the sender-receiver path to enhance synchronization accuracy.

- Optimizing the accuracy of clock skew estimation with least-squares linear regression by determining the effective regression data set size for different synchronization periods.
- Validating an efficient recursive maximum-likelihood clock skew estimator under correlated time measurements.

2.1 Oscillator, Clock and Synchronization

The source of time, in each individual sensor node, is a clock - essentially a timer - that counts the oscillations of a crystal oscillator at a particular frequency. Given that the oscillator runs at the expected frequency, the associated clock will always match with a reference clock. However, due to imperfections in low-quality oscillators, the clocks gradually diverge from the reference clock even if initially tuned perfectly [15]. An oscillator behavior is defined by:

- *Accuracy* – defines the agreement between the expected and actual frequency referred to as *frequency difference*. The accuracy of the commonly used oscillators in sensor nodes is 40 to 60 parts per million (PPM): meaning a clock can lose as much as 40 μs in a second.
- *Stability* – defines the tendency to stay at the same frequency over time. The short-term frequency deviations mainly caused by environmental factors are referred to as *clock skew*, whereas, long-term deviations due to aging are referred to as *clock drift* [13].

Considering these oscillator characteristics, the relationship of a clock A with respect to the ideal time (t) and a clock B can be modeled by Eq. (2.1) and Eq. (2.2) respectively without considering clock drift [15]. This relationship is also shown in Fig.2.1.

$$C^A(t) = \theta + \delta \cdot t \tag{2.1}$$

$$C^B = \theta + \delta \cdot C^A \tag{2.2}$$

where θ is the relative clock offset (phase difference) and δ is the relative clock skew (the change in phase difference with time) between the clocks.

The time offset adjustment provides instantaneous synchronization by masking the effect of other parameters, whereas the synchronous operation can be maintained only by identifying and correcting the clock skew

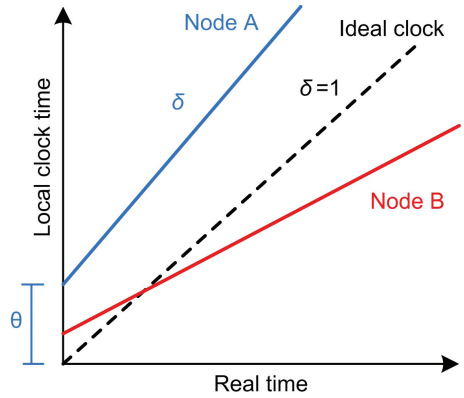

Figure 2.1. A simple clock model of sensor nodes [15]

[13]. Therefore the TS problem involves estimation and compensation of the clock skew after measuring the time difference at a fixed reference time instant.

Later in this chapter, we discuss messaging protocols for TS in Section 2.2 and clock skew estimation algorithms in Section 2.3 , along with our contributions based on Publication I and Publication II.

2.2 Time Synchronization Protocols

The rich knowledge on TS of distributed computer networks becomes ineffective when applied directly to energy and cost constrained WSNs [16]. NTP, ticking the Internet's clock in-phase for decades, provides the synchronization accuracy only in milliseconds and its passive listening is energy inefficient. Global position system (GPS) [17], on the other hand, can provide accuracy in nanoseconds but costs additional hardware and energy, and may also suffer indoor availability. Also, Precision Time Protocol (PTP) [18] provides accuracy in microseconds, however, the additional messaging consumes bandwidth and energy.

Owing to its unique design requirements, TS in WSNs has been extensively studied in the past decade. A complete overview of synchronization schemes in WSNs can be found in [11, 19]. Based on the exchange of time information in the network, the main theme of the existing protocols can broadly be categorized as:

Reference Broadcast Protocols: The variants of broadcast protocols, proposed in the literature, are Reference Broadcast Synchronization (RBS) [13], Flooding Time Synchronization Protocol (FTSP) [14] and Time

Diffusion Protocol (TDP) [20]. RBS is a *receiver-receiver* protocol since the nodes maintain a relative time by sharing the recorded reception time of a reference beacon. The reference beacon itself does not carry the time information of the beaconing node. However, the reference beacon in FTSP is timestamped at the origin as well at the reception, thus the nodes synchronize with the reference node instead of developing a receiver-receiver relationship. The timing in FTSP is diffused by the recipients of a reference beacon in hierarchical fashion. The TDP is a variant of RBS and FTSP in which one-hop nodes, already synchronized with the reference node, select a diffusion leader to broadcast the timing information to second tier nodes.

Handshake Protocols: The prime example of handshake protocols is Timing-sync Protocol for Sensor Networks (TPSN) [12] that uses two-way timing exchange. TPSN first creates a hierarchical network as in FTSP and then nodes at level n synchronize with the ones at level $(n-1)$. The other protocols exploiting this *sender-receiver* scheme are Tiny/Mini-Sync (TMS) [21] and Lightweight Tree-based Synchronization (LTS)[22].

A TS protocol, in general, can work at any layer of the communication stack. However, considering random and deterministic delays associated with each layer, acquiring accurate TS is challenging. The delays can be grouped into send, medium access, transmission, propagation and reception times [16]. The delays in the sender-receiver path reduce as the timestamping is moved down in the stack towards the physical layer. A common notion in recently proposed protocols is to timestamp the packets after the medium access has been granted. We analyzed the clock offset in the sender-receiver path under reference broadcasts and MAC layer timestamping in Publication I, which we discuss in detail in the following section.

2.2.1 μ-Sync Protocol

In Publication I, a reference broadcast-based TS protocol is studied with an objective of eliminating the delays and uncertainties in the sender-receiver path. A broadcast collision avoidance (BCA) model for enhancing the scalability of reference broadcast protocols is also outlined. In addition, we investigated the optimal data set size of the linear regression based clock skew estimation. The complete contribution is named as μ-Sync, since our proposal can provide synchronization accuracy of a few microseconds. In the following sections, we discuss the synchronization

protocol related details whereas the clock skew estimation is presented in Section 2.3.1.

The μ-Synch protocol is implemented on the Sensinode Nano.CC2430 [Appendix A.1.2] platform. The protocol works at the MAC layer of a communication stack, NanoStack [Appendix A.3]. It is integrated as an add-on feature to IEEE 802.15.4 MAC: transparent to the existing MAC message flow. A gateway node acting as a reference periodically generates a synchronization message called a *sync-beacon* at the MAC layer without a timestamp. The timestamp is added to the sync-beacon at the very last stage before transmission. The sync-beacon recipients record their local times on its reception and adjust their clocks based on a clock offset budget analysis as discussed later in Section. 2.2.1. The nodes located at the first hop diffuse the reference time using sync-beacons down in the network hierarchy.

The time report or timestamp of a clock consists of two parameters: a hardware-defined *hardware clock* and a software-defined *logical clock*. The hardware clock (C_h), a 16-bit counter, is derived from a hardware timer driven by a crystal oscillator. On Sensinode Nano.CC2430, the counter increments at each active clock edge with frequency (f_c) ranging from 0.25 MHz to 32 MHz. Therefore, the minimum tick resolution we can achieve is $t_r = 1/f_c = 4$ μs with a counter period T_0 = 262 ms. At each T_0, an interrupt is generated which is acknowledged with an update in the logical clock counter (C_l). Therefore, the time report of a node A is

$$C^A = C_l \cdot T_0 + k_c \cdot t_r \tag{2.3}$$

where k_c is the value of C_h at an arbitrary time. The timers in Nano.CC2430 are briefly explained in Appendix A.1.2.

Clock Offset Budget Analysis

The clock offset is the time difference between a reference clock and a child clock at a fixed time instant. By adjusting the clock offset, the child clock achieves instantaneous synchronization. For adjusting clock offset under reference broadcasts, the child node relies on the time report of the reference clock. The moment the child clock receives the time report, the reference clock advances by a certain amount depending on the time length of the critical path (Δ_τ) by which the reference clock has to be adjusted. The μ-Synch timestamps a sync-beacon before the microcontroller unit (MCU) signals to transmit it, therefore, the Δ_τ can

be written as

$$\Delta_\tau = \underbrace{\tau_{\text{ts-tx}} + \tau_{\text{enc}}}_{\text{Tx-side delays}} + \tau_{\text{prop}} + \underbrace{\tau_{\text{dec}} + \tau_{\text{int-handling}} + \tau_{\text{ts-rx}}}_{\text{Rx-side delays}} \tag{2.4}$$

The description of these time offset factors is as follows:

- Timestamp insert ($\tau_{\text{ts-tx}}$): the time needed to sample/insert timestamp in a message and enabling the radio to transmit the message.
- Message encoding (τ_{enc}): the deterministic time after the radio is enabled to encode a message and transforms it into radio waves.
- Propagation delay (τ_{prop}): the time taken by radio waves from a transmitter antenna to reach a receiver antenna. The propagation delay is less than a microsecond for distances smaller than 300 meters [14].
- Message decoding (τ_{dec}): the deterministic time at a receiver to transform and decode the radio waves into a binary message. The message reception is signaled by an interrupt.
- Interrupt handling ($\tau_{\text{int-handling}}$): the time between an interrupt is raised and MCU handles it.
- Timestamp read ($\tau_{\text{ts-rx}}$): the time to read the local time after the message reception interrupt is raised.

We measured Δ_τ between two nodes using an oscilloscope and compared it with the one obtained by computing each contributing factor in Δ_τ. In either case, Δ_τ is determined as the time difference between inserting a reference timestamp at transmitter at time instant t_1 and before reading the local time at the receiver at t_2. The average total Δ_τ is measured 1.1982 ms with negligible variations as compared to the tick resolution. The computed values of each factor in Δ_τ add up to a total of 1.1997 ms. The contributions of each element in the time offset is shown in Fig. 2.2. Therefore, by carefully performing the clock offset budget analysis in the sender-receiver path within the timestamping, the nodes achieve accurate instantaneous synchronization.

Clock Skew and Synchronization Period

The clocks need to be synchronized periodically due to the inaccuracy and instability inherited by crystal oscillators. The synchronization period (T_S), therefore, depends on the clock accuracy (ε) usually given in parts

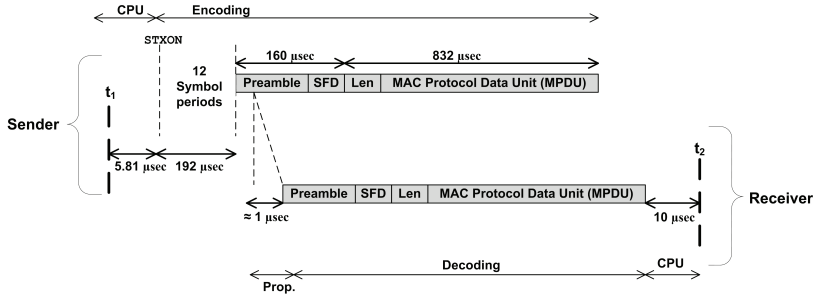

Figure 2.2. Disection of the critical path in reference broadcasts. The sync-beacon is 19 bytes including MAC header and frame control field (FCF))

per million (PPM) and the synchronization accuracy (a_S) required by an application. Using the worst-case clock skew experienced by a node (δ), we have $T_S = (a_S - \varepsilon)/\delta$.

We measured the clock skew of nodes with respect to a reference node with an oscilloscope. Figure 2.3(a) shows a trend in clock skew of five nodes. The worst-case δ we determined over tens of nodes is 2.4 μs/s. An enlarged view of a clock in Fig. 2.3(a) in Fig. 2.3(b) shows that the clock skew line, although linear, has fluctuations as high as $\pm$40 μs owing to the clocks' inaccuracy.

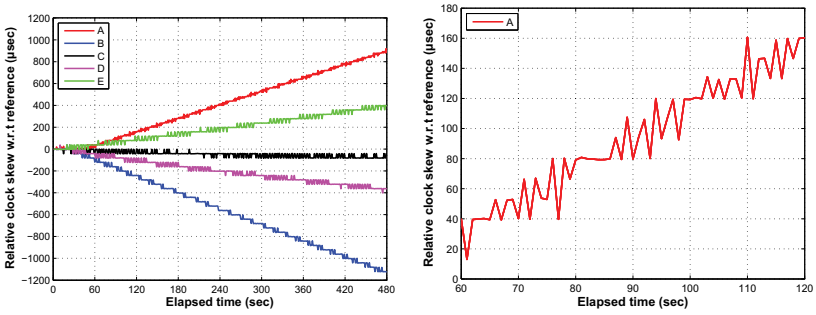

(a) Clock skew in Nano.2430 nodes

(b) Magnified view of clock A

Figure 2.3. Clock skew in Sensinode Nano.2430 nodes with respect to a reference node

Synchronization Accuracy Results

Using the clock offset budget analysis, we evaluated the synchronization accuracy of μ-Synch in single and multiple hop network configurations. In a single hop scenario, a reference node sends a sync-beacon periodically to synchronize the adjacent child nodes. The synchronization accuracy between a reference node and a child node is measured using an oscilloscope. Figure 2.4(a) shows the one hope synchronization error. The error remains close to zero, however, 3-5% reported error values, stemming

from the inaccuracy of the underlying oscillator, are at ± 40 μs. If these abnormal errors are ignored, the average synchronization error is 1.10 μs and the worst-case error is 3.67 μs. The multi-hop synchronization error, with/without ± 40 μs errors, is given in Fig. 2.4(b).

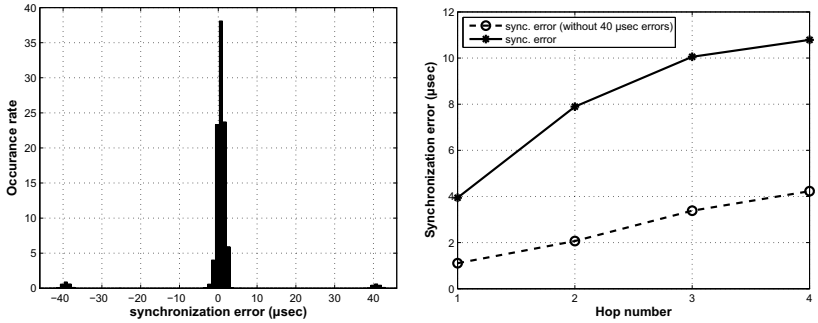

(a) One-hop synchronization error (b) Multi-hop synchronization error

Figure 2.4. Synchronization accuracy in μ-Synch

Network Scalability under Reference Broadcasts

The hierarchical network topology established by a reference broadcast protocol encounters scalability concerns in the diffusion of reference time in large networks. This is owing to the exponential increase in synch-beacons and their possible collisions that can easily degrade the quality of synchronization. We hypothesize a broadcast collision avoidance (BCA) mechanism to enhance the scalability under reference broadcasts. The BCA finds its motivation from the collisions mitigation method proposed in the IEEE 802.11s standard [23]. In this method, using the synchronized network, the nodes select a random sync-beacon transmission slot in a time-slotted window. The length of the time window depends on the required periodicity of the beacons. The nodes adjust their selections upon conflict with the nodes located up to two hops. The conflict is determined by embedding the transmission slot of the nodes in the sync-beacons.

2.3 Clock Skew Estimation Algorithms

Regardless of the underlying messaging scheme, the time difference between the clocks can be kept within required limits by frequently exchanging the time reports and by compensating for the time offset. The frequency of transmissions, however, is restrained by the energy constraints of the WSN applications. Pottie *et. al.* [24] demonstrated that

the energy required to transmit 1 Kb of data over 100 meters is equivalent to the energy required to execute 3 million instructions. This observation has led to the design of clock synchronization algorithms to decrease the number of required transmissions [13, 14, 25]. A clock synchronization algorithm uses past synchronization points to estimate the relative clock skew. In the following sections, we discuss two such clock skew estimation algorithms: least-squares (LS) linear regression and recursive maximum-likelihood (ML).

2.3.1 Least-Squares Linear Regression

In Publication I, we studied the LS linear-regression-based skew estimator. LS linear regression finds a best fit line through the time offset observations over time. The time offset and clock skew of a node's clock with respect to the reference node can be estimated from the intercept and slope of the line [13]. The main contribution, in this context, is the adaptation of the regression data set size as per the synchronization period and the linear time scale of the clock skew to keep the estimation error within limits. The existing literature [14], on the other hand, applies a fixed-size regression table irrespective of the linear time frame of the clocks. However, under different synchronization periods, the table can contain the past data points which deviate from the linearity resulting in large estimation errors.

At first, we analyzed the clock skew data, given in Fig. 2.3, for linearity using offline linear regression. The residual error of the regression line from the real data gives the clock estimation error. It is observed that the clock skew remains linear for a regression size holding data of only 16 minutes. In this case, the average residual error is 1.92 μs and the maximum error is 7.15 μs. As linear regression is performed over a longer period (2.5 hours) the average residual error increases to 5.51 μs. Besides, the linearity checks, the normal distribution of the residual error and a plot of residual error as a function of time, fails if the regression is applied to data longer than 16 minutes.

Therefore, there are two main limitations in linear-regression-based skew estimation in the real hardware over a long period: **a)** the deviations in the clock skew from linearity, **b)** limited memory to maintain the regression table and perform computations. Therefore, one has to find the optimal time range to perform regression.

The time offset, θ, and clock skew, δ, can be estimated from Eq. (2.5)

[26].

$$\hat{\theta} = \bar{y} - \hat{\delta}\bar{x} \tag{2.5}$$

where

$$\hat{\delta} = \sum_{i=1}^{\upsilon} (x_i - \bar{x})\,(y_i - \bar{y}) / \sum_{i=1}^{\upsilon} (x_i - \bar{x})^2$$

In Eq. (2.5), υ is the regression size, $x = C^B$ is the local time report of a node with mean $\bar{x}$, and $y = C^A$ is the reference time report with mean $\bar{y}$.

Computing $\hat{\delta}$ from Eq. (2.5) usually encounters finite word-length limitations in storing the square of a time report. However, this limitation can easily be avoided by updating $\hat{\delta}$ as Eq. (2.6).

$$\hat{\delta} = \frac{1}{\sum\limits_{i=1}^{\upsilon} \left(\frac{(x_i - \bar{x})}{\sum\limits_{i=1}^{\upsilon} (x_i - \bar{x})(y_i - \bar{y})} \times (x_i - \bar{x}) \right)} \tag{2.6}$$

Skew Estimation Methodology and Results

A node performs clock skew estimation using Eq. (2.6) by filling a regression table of size (υ) based on the time reports received every T_S s. A probe node inquires the two clocks using a probe packet every t_S s. The reference node timestamps the probe packet with its local time, whereas the child node timestamps the probe message with the estimated global time. The difference between the two time reports gives the estimation error.

Since the skew estimation error increases with data older than 13-16 minutes, the size of the regression table should be set accordingly. In Table 2.1, we compared the effect of two table sizes with respect to T_S on the synchronization error, which can be summarized as:

- *Table Size* υ_1: For sync-beacon period T_{S_1} and T_{S_2} since the estimation is performed over the past 4 and 16 minutes of data respectively, the table size υ_1 suits more to T_{S_2} than T_{S_1}.

- *Table Size* υ_2: For given T_{S_1} and T_{S_2}, the regression table holds data over the past 8 and 32 minutes. Therefore, table size υ_2 is appropriate for skew estimation given that the period is T_{S_1}. However, it exceeds the linear time scale of a clock for T_{S_2}, resulting in higher error.

In general, it can be concluded that the skew estimation error increases with the decrease in the sync-beacon period. Also, the time frame over which the clock skew estimation is performed depends on the linearity

Table 2.1. The effect of regression table size on synchronization error (μs). In each cell the first value is average and the second value is maximum synch. error

Period	Regression size	
	$v_1 = 8$	$v_2 = 16$
$T_{S_1} = 30,\ t_{S_1} = 17$	3.95 / 16	2.34 / 08
$T_{S_2} = 120, t_{S_2} = 57$	3.62 / 12	4.71 / 16

time frame of the clocks. Therefore, the time frame of skew estimation must be adjusted appropriately for a given synchronization period.

2.3.2 Recursive Maximum-Likelihood Estimation

As mentioned earlier, the clock skew estimation using LS linear regression is erroneous unless the linear regression is applied to a data set of appropriate size. In Publication II, we showed that since the received and local time reports are with reference to an absolute instant, the entries in the regression table are statistically correlated. Since, the LS linear regression is not an efficient estimator for a correlated set of measurements [27], its direct application results in estimation error variance higher than the lower bound. Therefore, tuning the regression size in Publication I in fact keeps the estimation error variance within the limits.

In Publication II, also, a time relation model, reflecting the correlation in time reports, is proposed and utilized to develop a recursive ML skew estimator. The experimental validation of the proposed estimator shows that the estimator achieves the smallest error variance as compared to the existing ones which can maintain an accuracy of less than 4 μs.

Experimental Evaluation

The performance of the developed estimator in Publication II is verified using the clock skew data set collected on a wireless sensor platform. The sensor platform and clock realization is the same as presented in Section 2.2.1. In a simple scenario of two nodes A and B, Node A sends a sync-beacon with its current local time (counter value, C^A) every T_S = 1 s. Node B compensates its time offset using the reference time transmitted by Node A for first five beacons. Later, the Node B stops synchronizing and runs undisciplined. Then on each sync-beacon reception at Node B, the clock difference between the nodes is retained for further evaluation.

The performance metric for a skew estimation algorithm is *time error*

which is the difference between the received reference time of Node A and the skew compensated time of Node B. As mentioned earlier in Section 2.2.1, the worst-case time error without skew compensation grows with 2.4 μs/s. For a sync-beacon index j and skew ratio estimate ($\hat{a}$) associated with jth beacon, we have

$$\text{Time error} = C_j^A - \hat{a}C_j^B$$

The time error performance of different clock skew estimation algorithms is compared in Fig. 2.5(a). This comparison is based on the recursive ML estimator and recursive LS estimator developed in Publication II, and LS linear regression with a table size of 8. The recursive ML estimator outperforms the other two estimators in time error and stability. The lowest performance of linear regression is mainly due to low response time and estimation error variance.

The experimental skew data has frequent abnormal jumps either due to the receiver timestamping procedure or the clocks' instability as discussed in Section 2.2.1. Therefore, a consistency check of the time data must be performed to avoid incorrect update of the clock skew estimate. A consistency check can be defined as

$$K_{\max} \geq \left| C_j^A - a\frac{T_0^A}{T_0^B}C_j^B \right| \tag{2.7}$$

where T_0^A and T_0^B denotes the nominal clock period of Node A and B respectively.

The received time report satisfying Eq. (2.7) is only considered for a time update. The $K_{\max}$ has to be adjusted according to the sync-beacon period and the communication delay between the timestamping procedure at both nodes. Figure 2.5(b) shows the effect of $K_{\max}$ on the time error under recursive ML estimator demanding a careful adjustment in $K_{\max}$ to minimize the synchronization error.

The quantitative statistical parameters of the time error distribution for different sync-beacon periods T_S are given in Table 2.2. The last column in the table gives the probability of time error larger than 3σ. Using these values, one can determine the appropriate synchronization period as per the required synchronization accuracy.

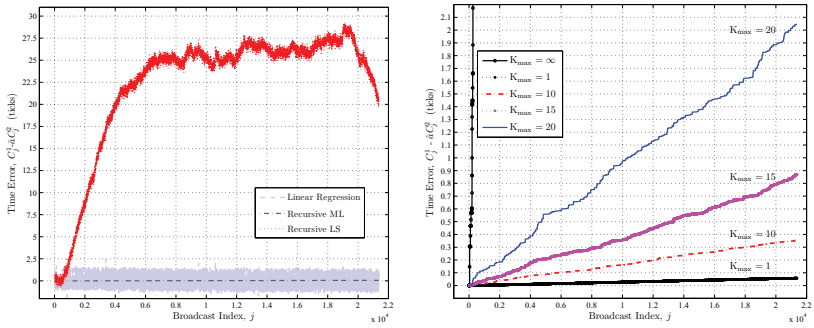

(a) Time error under different skew estimation algorithms

(b) Time error for the recursive clock skew estimator with different $K_{\max}$

Figure 2.5. Time error performance of the skew estimation algorithm(s)

Table 2.2. Timer error distribution parameters under the recursive ML estimator.

T_S	μ	σ	$\Pr\{\lvert k_{cj}^B - \hat{a}k_{cj}^A \rvert > 3\sigma\}$
60	0.176	0.961	1.12%
120	0.408	1.100	1.708%
300	1.640	3.954	1.960%

2.4 Summary

In this chapter, we focused on the time synchronization methods for maintaining discipline in the diverging clocks on low-cost wireless sensors. Time synchronization plays an intrinsic role in network organization and the realization of practical applications. The synchronization accuracy achieved by these proposed methods encouraged us to explore the challenges in their application-oriented usage. In Chapter 3, we discuss time synchronization requirements in structural health monitoring applications and develop a sampling application that can maintain tight synchronization among the accelerometer and therefore accurately identify the modal properties of a structure. In Chapter 4, a communication stack is developed providing time-synchronized, multi-channel and time-slotted communication suitable for real-time applications.

3. Time-Synchronized Wireless Structural Health Monitoring

3.1 Structural Health Monitoring

Structural health monitoring (SHM) is a process of adopting automated damage identification strategy for aerospace, civil and mechanical engineering infrastructures. It replaces the subjective and labor-intensive visual inspections to ensure structural integrity meets the life-safety standards during its life span. The main areas of SHM damage identification process [28] are:

- Observation of an infrastructure over time using periodically spaced sensory measurements
- Extraction of damage-sensitive features such as change in modal properties of the structure from these measurements
- Statistical analysis of these features to determine the current state of the infrastructure by damage detection, localization, quantification and prognostication [29]

The majority of proposed damage detection methods for civil structure such as dams, bridges, tunnels and buildings, concentrate on vibration-based damage detection. The vibration-based SHM allows damage identification from the changes in global vibration characteristics or damage-sensitive features using time series measurements. Some of the widely used features are the modal properties (e.g., natural frequency, damping ratio and mode-shape) of a structure [30]. These features are attractive for their physical meaning and can be identified using output-only methods without measuring the excitation owing to their independence from the input excitation system.

3.2 Wireless Structural Health Monitoring

SHM systems are traditionally wired, that is the measurements from the sensors, installed at different locations of a structure, are transferred to a central data repository through cables. In large structures since the large sampling points are required, the direct consequence of using cables is high system, installation and maintenance cost [31]. As a result, a lower number of sensors poorly scaled to the dimensions of a structure are installed which provide insight only to the low-order modal properties of the structure. Therefore, there is a need for higher monitoring fidelity by increasing the number of sensors [32]. The denser monitoring provides global damage detection as well as more detailed local investigation of the structure.

The denser monitoring, however, is only practical if the cost of the monitoring system is substantially reduced. Wireless sensor networks provide such a low-cost solution in large-scale physical systems. Yet, in order to provide a comparable functionality with wired SHM systems, a wireless SHM system has to overcome a number of challenges imposed by SHM applications; for instance high-frequency and high-fidelity synchronized sampling, and reliable collection of large amount of data.

3.3 Time-Synchronized Sampling for Modal Analysis

The sensitivity and accuracy of damage detection in structures depends on the accurate extraction of modal analysis parameters. The identification of modal parameters requires that the sampling process amongst the sensors must be synchronized during the sampling intervals so that the structural response time histories collected at different locations can be accurately aligned on a common time-scale. From the perspective of SHM applications, in [33][34][35], the effect of time synchronization (TS) error on output-only modal analysis is investigated. The commonly used output-only modal analysis techniques can be classified into two groups depending on their domain of operation (a) the frequency domain (non-parametric) approach and (b) the time domain (parametric) approach.

In [33][34], the effect of TS error on the reconstruction of mode shapes is investigated under a frequency domain modal analysis technique. This analysis concludes that the accuracy of mode-shape reconstruction under TS errors is a function of mode frequency. The higher modes, which are

better indicator of structural damage, are more sensitive to TS errors and a time error of even 30 μs can cause a significant reduction in the reconstruction of a higher mode shape. In [34], under the same frequency domain technique as in [33], it is shown that the presence of TS errors introduces errors in the amplitude and phase of each mode-shape component, however the main source of error in the identified mode shapes is the phase shift. The phase shift depends both on the TS errors and the mode frequency or natural frequency.

In [35][36][37], the correlation function of the structural responses is studied to analyze the effect of TS error on modal parameters. The correlation function of the structural responses can be used by time domain model identification schemes such as Eigensystem Realization Algorithm (ERA) [38] and Covariance-based Stochastic Subspace Identification (SSI-COV) [39][40] method to estimate the modal parameters. The analysis in [35][37] shows how the TS errors affect the modal parameters by entering into the correlation function. These studies conclude that the natural frequencies and damping ratios are unaffected by the TS errors. However, there are phase and amplitude errors in mode-shape reconstruction associated with TS error. Although the error in mode-shape amplitude is negligible, the phase error is meaningful as the mode-shape phases are important modal characteristics for damage indication.

The basic relationship between phase shift (φ_k) and natural frequency (f_k) of kth mode with a time error Δt is given as $\varphi_k = 2\pi f_k \Delta t$. Under this relationship, a TS error of 30 μs results in a 1.08-degree phase delay of a mode at 100 Hz, while the same TS error causes a 10-degree phase delay at 1 kHz. The phase delay tolerance depends on the application but as investigated in [41], even a 3.6-degree phase delay can cause a considerable reduction in the reliability of the mode-shape reconstruction.

3.4 Time Synchronization Techniques for SHM

In wired SHM systems, a traditional signal based synchronization technique, by sharing a sample clock signal among the sensors via coaxial cables, provides a high-precision synchronization. In [42], a signal-based synchronization technique is presented for SHM. However, it is not feasible to physically connect the entire network for distances over a few hundred meters, thus creating the demand for time-based synchronization techniques over wireless networks.

In time-based synchronization techniques, network entities have a common time reference which can be used for the generation of clocks and events. Time-based synchronization can be achieved with or without a direct connection between the measurement devices. IEEE 1588 [18], IRIG-B [43], NTP [10] are examples of time-based synchronization techniques in networked measurement systems. The time-based synchronization techniques for wireless sensor networks have already been discussed in Chapter 2. Here, we briefly look into the existing TS techniques in wireless networks for SHM.

In [44], a GPS receiver is attached to each data acquisition station which maintains a tight synchronization in the network with a synchronization mismatch of ± 25 ns. A GPS based solution, although, fulfills the stringent synchronization requirements of SHM applications, however, it does demand more power and the cost of additional hardware also becomes infeasible. In [45][33], a global beacon-based synchronization method is used where each wireless sensor resets its clock to zero at the reception of a synchronization beacon. However, in [45] an additional stable crystal oscillator is used to maintain synchronization during the sampling period. This solution, though effective, increases the power consumption and the cost of the solution. In [33], a hybrid synchronization scheme is used in which personal area network (PAN) coordinators are synchronized via a wired connection and the associate nodes to a PAN coordinator are synchronized with broadcast beacons. By this method, the authors in [33] have shown a synchronization accuracy of less than ± 10 microseconds.

In [46][47] TS techniques developed specifically for WSNs are used for SHM. In [46], FTSP is used to synchronize a 64-node network deployed at the Golden Gate Bridge in San Francisco (United States). In [47], TPSN is used to synchronize a WSN deployed on medieval tower in Trento (Italy). The reported synchronization error in [47] is 732 μs at the twelfth hop. In these deployments, the collected vibration data lacks the extensive modal analysis and therefore the effect of TS errors on the modal analysis is not evident.

3.5 Time Synchronization Challenges in SHM

In WSNs, the synchronized execution of sampling interval and synchronized sampling at frequencies up to 1 kHz for SHM is hampered by spatial and temporal time uncertainty in the node and across the network

respectively. The spatial time uncertainty occurs among the spatially distributed nodes because of clock skew and drift originated from the variations in the crystal oscillator of the nodes and the imperfect clocks offset adjustments. On the other hand, the temporal time uncertainty takes place inside a node because the sampling application task cannot keep up with aggressive sampling and the logging of the data.

Since the sampling at such a frequency is resource-demanding, the nodes have to suspend other tasks in order to reduce the temporal time uncertainty. Therefore, a time synchronization protocol for re-synchronizing the clocks cannot be functional during the sampling phase. Instead the clocks have to be kept synchronized based on the clock skew estimation from earlier TS points [Publication I]. In addition, the communication overhead inevitably introduced by a TS protocol must be limited, in order to avoid shortening the lifetime of the system.

3.6 μ-Sync Framework for SHM

The μ-Sync scheme presented in Section 2.2.1 is developed further for synchronized sampling in an SHM application in Publication III. Our analysis showed that μ-Sync keeps the one-hop average timer error below 1.74 μs. Also, the relative temporal uncertainty among the collected samples always remains lower than 10 μs at sampling frequencies as high as 1 kHz. The clock skew estimation in the nodes ensures the sampling task synchronization during the extended sampling period when the synchronization may not be feasible.

3.6.1 Time Synchronization Evaluation

Originally, μ-Sync is implemented on Nano.2430 platform. However, μ-Sync is ported to Micro.2420 platform because of its hardware flexibility. The description of these two platforms can be found in Appendix A.

In Micro.2420, the TS clock is based on `Timer-A` configured with a tick resolution of 1 μs. A compare register, `TACCR1`, associated with `Time-A` is utilized to adapt the sampling rate of an accelerometer. At each sampling interval, `TACCR1` generates an interrupt which in turn invokes the sampling task at the application layer. Appendix A.1.1 explains the available timers in Micro.2420.

Among others advantages, Micro.2420 platform has a more stable

crystal oscillator than the Micro.2430. This can be observed by comparing clock skew in Fig. 3.1 and Fig. 2.3. These figures depict the clock skew in the undisciplined clocks with respect to a reference node. In general, the clock skew is linear and varies among nodes. However, the fluctuations in a Micro.2420 clock are much smaller than the ones observed in a Nano.2430, which reached to ± 40 μs.

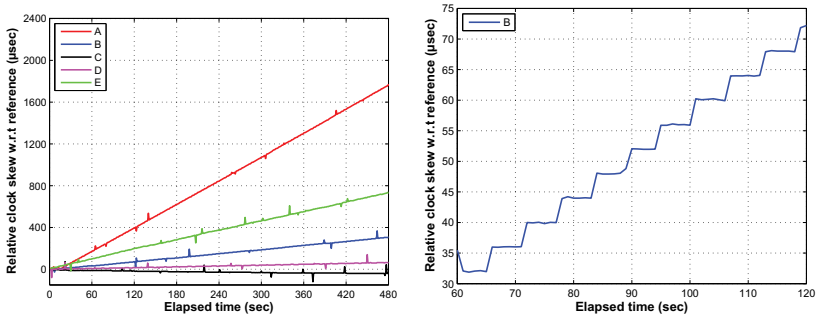

(a) Clock skew in Micro.2420 nodes (b) Magnified view of clock B

Figure 3.1. Clock skew in Sensinode Nano.2420 nodes with respect to a reference node

In the tests for measuring the synchronization accuracy, a reference node transmitted a TS beacon every 1 second. The network nodes adjusted their clock with respect to this reference time. The synchronization error was measured by toggling an I/O pin every 65.535 ms. The absolute average synchronization error was measured to be 1.74 μs and the error remained below 5 μs by 98.6% of the time.

3.6.2 Sampling Task Synchronization

The synchronized execution of the sampling task and maintaining that synchronicity within the collected samples across the network, defined as sampling task synchronization here, is based on the TS service. From this perspective, the TS service adjusts or translates the local time of a node to a global reference, whereas, the task synchronization achieves periodic execution of a task at different nodes in synchrony.

It is implicit that the user task at the application layer demands services from a TS protocol transparently and without the disruption of the user task. Since the clock skew makes the clocks diverge from the reference time at a high rate, the frequent transmission of synchronization beacons is mandatory. This requirement seems to cause an adverse effect on periodic execution of the user task. Therefore, in Publication III the inter-

action of the two tasks, i.e., accelerometer sampling and synchronization are tailored in such a fashion that they run independently from each other while the synchronization is performed even while sampling is in progress. In the proposed solution, the accelerometer sampling and TS tasks run at the application and the MAC layer, respectively.

The user task handles the activation of the synchronization task for a desired synchronization beacon rate and synchronization duration. The synchronization task runs transparently at the MAC layer and the synchronization beacons are characterized by a unique frame-type subfield in the IEEE 802.15.4 frame control field. Before the execution of the sampling task, synchronization beacons are transmitted for removing the clock offset and for clock skew estimation. The clock adjustment and skew estimation procedure is the same as described in Publication I. During the sampling phase, the clock adjustment is based on a node's estimated clock skew with respect to the reference node.

The synchronization phase is followed by a sampling command to the network by the reference node. The command includes the sampling parameters such as sampling rate, measurement period, monitored axes, and accelerometer scale and bandwidth. At the reception of the sampling command, a network node suspends all other tasks, except for `Timer-A` interrupts and the sampling task. This ensures that the application layer sampling task will completely get the microcontroller's processing time, thus reducing the jitter in the acquisition of the samples potentially introduced by other tasks or interrupts. The sampling task at the application layer monitors the state changes in the microcontroller's I/O port, which is driven by the synchronized `Timer-A`, and collects a sample from the accelerometer at each transition. The port is toggled by exploiting the register `TACCR1` and its hardware interrupt, which is triggered each time `TAR` value equals the value stored in `TACCR1`. The register is updated in an interrupt service routine (ISR) according to the sampling frequency specified by the sampling task. During the sampling phase, `TAR` is periodically readjusted by adding the estimated clock skew value.

The synchronized sampling for two different nodes is shown in Fig. 3.2. We measured the task synchronization error between many nodes and it is found that the tasks are always synchronized to less than 10 μs even at a sampling frequency of 1 kHz. The possible factors contributing to the difference between TS accuracy and task synchronization accuracy

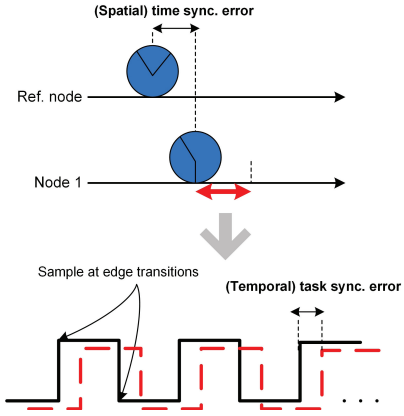

Figure 3.2. Time and task synchronization error

are the jitter in hardware interrupts and the delay in reading the I/O pin transitions by the sampling task. At the end of the accelerometer sampling phase, all the other tasks previously suspended are restored, `Timer-A` interrupts are deactivated and data collection procedure is activated.

A complete flow of the events as being executed by a sink node and the accelerometer nodes is shown in Fig. 3.3.

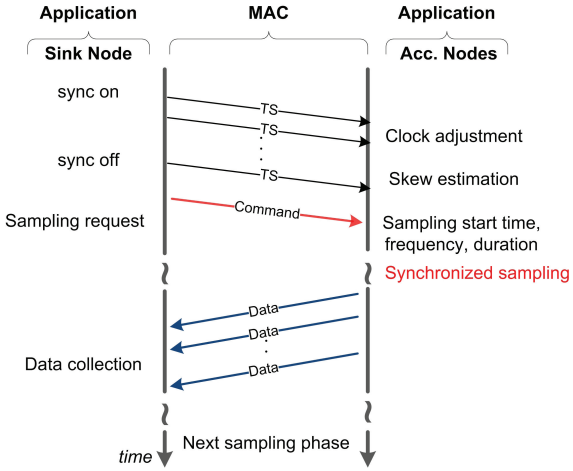

Figure 3.3. The flow of events in SHM application

3.6.3 Results

The proposed time and task synchronization scheme is integrated to a configurable wireless system for SHM. This synchronized wireless system is deployed on a model wooden bridge for experimental modal analysis

in Publication III. A cable-based monitoring system with high-quality accelerometers is installed parallel to the wireless system to provide a baseline for performance comparison. In addition to maintaining the accurate synchronicity in the collected acceleration samples collected by the nodes, the wireless system also takes care of the missing samples in data collection procedure and sampling accuracy.

The structural responses collected by the synchronized wireless system and the wired system are processed by applying the SSI-COV [39][40] method. The analysis identified fourteen modes in the frequency range of 0 to 40 Hz in the model wooden bridge. The absolute average relative difference between the natural frequencies identified with the wireless and wired measurements is 0.422%. The variability of damping ratios is typically very high even between the different wired measurement runs, e.g., 200%. However, the relative difference between the damping ratios estimated with the wireless and wired systems is 42.2%. The modal assurance criterion (ModAC) [48], which measures the consistency of the two mode shapes, has an average value of 0.943.

4. Time-Synchronized Communication

Since their advent, wireless sensor networks (WSNs) have paved their way into home, health and monitoring applications. However, their adoption have thus far been slow in wireless industrial automation owing to the lack of open international standards fulfilling the industrial requirements [49][50].

For industrial applications, the design and operation of WSNs must ensure the the management of energy resources, communication reliability and real-time data delivery. The efficient management of the energy resources hinges on the scheduling of radio up-time and minimizing external interferences. By duty cycling, the radio is turned on only for packet transmission or reception and otherwise, the radio remains in low-power state. By mitigating the effect of external interferences, not only is the the energy spent on packet retransmission minimized, but communication reliability, greatly needed for real-time applications is enhanced.

The radio duty cycling [51] requires a common sense of time in the network so that the node pairs can be scheduled to wake up only at data communication instances. Given that the network communications are appropriately scheduled such that no two pairs of nodes within the interference range of each other communicate at the same time, the intra-network interference can also be removed. Such synchronized radio scheduling enables energy savings by enhancing the packet delivery performance with a minimum number of retransmissions and by keeping the nodes in a low-power state during inactive periods.

A communication channel in low-power WSNs might suffer from fading and interference from the coexisting wireless systems. Communication on such a channel can easily result in packet losses and consequently in packet delays and energy consumption. In order to mitigate the

channel uncertainties, the radio scheduling on all or least interfered channels is the optimal solution [52] [53][Publication VII] as compared to a single-channel communication. Just as with radio scheduling, the ability to schedule channels also demands tight time synchronization in the network.

In summary, a robust synchronization procedure, coupled with a well-designed communication schedule both in time and frequency, can play a significant role in fulfilling the requirements of industrial applications. Working on these lines, several industrial organizations have pushed towards wireless communication standardization in wireless automation. The standards such as WirelessHART [7] and ISA 100.11a [8] are milestones of these efforts.

WirelessHART and ISA 100.11a implement IEEE 802.15.4 direct sequence spread spectrum (DSSS) PHY layer specifications. The medium access and networking schemes, in these standards, are based on time synchronized mesh protocol (TSMP) [54]. TSMP provides time-slotted MAC (i.e., TDMA) with a 10 ms of slot time, channel hopping, channel blacklisting and security. The centralized network manager ensures self-organization and self-healing of the network by maintaining up-to-date routes, routing diversity and communication schedules.

TSMP provides time division multiple access along with a number of enhancements for time synchronization and frequency diversity. TSMP utilizes slot-based synchronization on an agreed upon network communication schedule. The communication schedule is designed by dividing the medium access in time and frequency and each resulting unit is assigned to a pair of nodes for communication. Time is sliced up into *time slots* of equal length and a constant number of slots make up a *slot frame* which repeats itself indefinitely.

In slot-based synchronization, instead of exchanging the explicit timestamps, a node is expected to receive a scheduled packet exactly after *Tx offset* units from the start of a slot. Every packet is thus implicitly timestamped and its comparison with the expected *Tx offset* gives the synchronization error for offsetting the phase of the next slot frame. Figure 4.1 shows the time and frequency schedule highlighting the slot frame adjustments using the *Tx offset*-based synchronization error.

In addition to *Tx offset*-based adjustments, Rx node can also indicate this synchronization error to a transmitter in an ACK packet either explicitly in the packet or implicitly with its reception time. The syn-

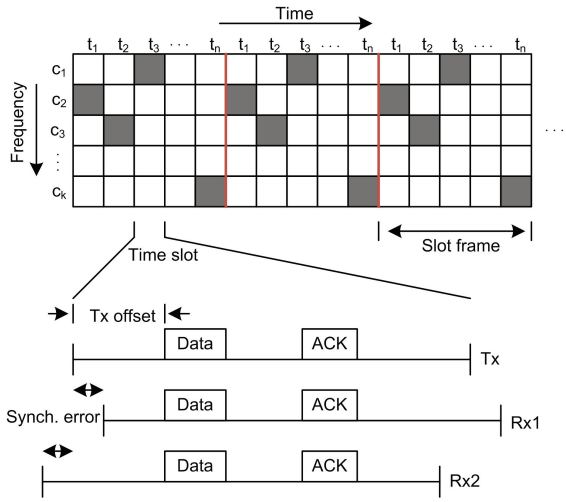

Figure 4.1. Time and frequency scheduling highlighting the slot frame adjustments using the *Tx offset*-based synchronization error

chronization accuracy of slot-based synchronization is less than 1 ms [54].

4.1 A-Stack – A Communication Stack for Industrial Applications

In Publication IV, a TDMA-based communication stack using IEEE 802.15.4 PHY, named A-Stack, is designed. A-Stack provides a flexible development environment for real-time WSN applications such as wireless automation and structural health monitoring. A-Stack includes time-synchronization, multichannel time-slotted communication and network formation schemes. The communication stack is flexible enough to incorporate any packet scheduling algorithm, both in time and frequency, as well as network formation and configuration schemes. A-Stack provides this flexibility with ad-on PC tools that allow network adaptation for given application requirements.

4.1.1 Motivation for A-Stack Development

The diverse nature of WSN applications limits the design of a single generic solution [55]. Therefore, a flexible environment is needed that can ease the development and testing process for application specific protocols and algorithms. A-Stack, in general, aims at providing an open-source prototyping environment capable of ensuring real-time and reliable network operation and, in addition can incorporate any given network management scheme.

Specifically, A-Stack targets the demands of industrial applications such as wireless automation and structural health monitoring. The wireless automation applications demands real-time data collection with high reliability. On the other hand, SHM applications require **a**) collection of the bulk of the acceleration data from the network reliably, **b**) accurate synchronized sampling (in the order of tens of microseconds) of structural responses across the network. In this context, A-Stack provides time and frequency diversity to enhance communication reliability and network bandwidth, and also fulfills the synchronization accuracy demands for synchronized sampling in SHM applications.

4.1.2 A-Stack Design and Tasks

A-Stack is implemented on Micro.2420 platform by extending its preceding communication stack, called NanoStack. A brief overview of the platform and Nanostack is given in Appendix A. A-Stack, runs on FreeRTOS real-time operating system. A-stack design, however, is independent of platform, operating system and communication scheduling scheme. A-stack design includes the following four tasks.

- MAC task: enables time-slotted communication by handling the radio and time-synchronized timer events. Each timer event has an associated event type, event duration, radio channel and communication pair index. Radio channels can be updated from a list of favorable channels.
- Packet manager: handles packets based on their type and destination. It is also responsible for packet routing.
- Service manager: responsible for network configuration and node joining
- Application task: is any application-dependent task, e.g., time-synchronized sampling of structural responses.

These tasks are prioritized within the context of real-time operating system such that time-critical events are executed in deterministic fashion.

4.1.3 Time Synchronization in A-Stack

In order to enable multi-channel time-slotted communication, all the nodes in a network must be synchronized to a common time-reference.

A-stack achieves network-wide synchronization by integrating μ-Sync synchronization service at the MAC layer. The synchronized clock of a node is responsible for generating the desired timer events (i.e., time slots) as well as synchronized sampling in SHM application. The sync-beacons are scaled to a multi-hop network by the addition of synchronization time slots in super-frames.

Timer Events

A-stack uses a set of timer events to define a communication schedule of a node. An event indicates the start of a time-slot within the schedule. The timer events are based on the hardware interrupts of a node's clock which is synchronized to the network's clock.

In A-stack, the synchronization clock is derived from the `Timer-A` of Micro.2420. The basic timer implementation is the same as discussed in Section 3.6.1. The `Timer-A`, in addition to maintaining a synchronized clock, is responsible for initializing the scheduler and to initialize the generation of timer events. The scheduler is activated only after the network-wide time synchronization and the distribution of scheduling information is completed. The timer events are handled in an ISR that is associated to compare register, `TACCR0`, of the `Timer-A`. When a timer interrupt occurs, the event-handling task is invoked and the `TACCR0` is updated with the next timer event duration. Another compare register `TACCR1` of `Time-A` works in parallel to control the execution of a sampling task. The timer event generation and handling interface in A- Stack is shown in Fig. 4.2.

Scheduling Synchronization Beacons

For maintaining a collision-free schedule in the network, the synchronization error among the nodes must be less than the guard time, T_g, in each time-slot. This condition places an upper bound on the synchronization period, T_S

$$T_S = \frac{T_g - \Delta t}{\varepsilon}$$

where ε is the clock accuracy and Δt is the worst time error in μ-Sync. In Micr.2420 platform, ε = $\pm$40 PPM and with T_g = 3 ms and Δt= 5 μs, we have T_S = 37 sec; that is the clocks must be synchronized every 37 sec.

After the network initialization and distribution of the communication schedule as explained in Publication IV, the network is synchronized and time-slotted communication is initiated. During the time-slotted

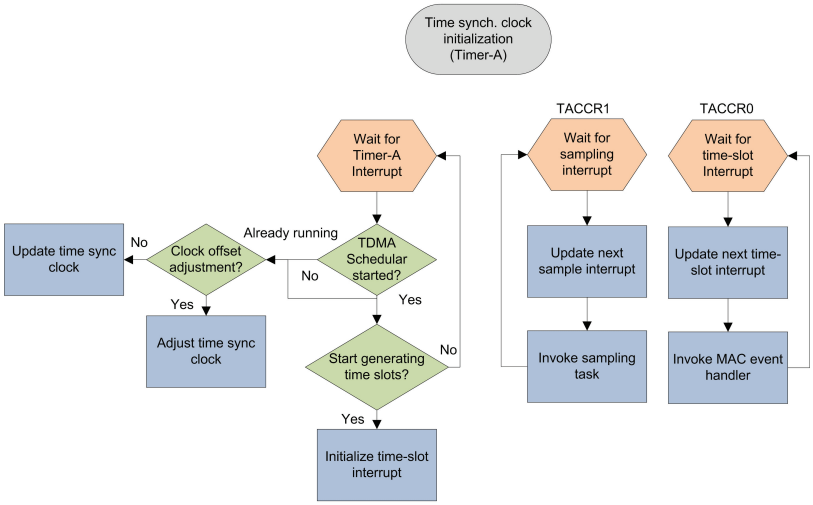

Figure 4.2. Timer event generation and handling interface

communication, periodic synchronization beacons propagate down the network on the dedicated time slots in the transmission schedule.

4.1.4 A-Stack Performance

A-Stack performance is evaluated rigorously in single and multihop network formations deployed in line-of-sight (LOS) and non-line-of-sight (NLOS) environments. The main idea of these tests is to evaluate the nodes' adherence to the schedule. The communication reliability is measured in terms of PDR and latency. In these tests, the time-slot length is 10 ms with 3 ms guard time. The synchronization beacon is sent every 10 super-frames. The multihop test deployment and the used communication schedule are shown in Fig. 4.3(a) and Fig. 4.3(b) respectively.

The PDR results in single-hop LOS tests showed 100 % PDR on all the utilized channels reflecting the success in the generation and handling of the timer events according to the schedule on a node. In multi-hop NLOS tests, the PDR varied among frequency channels from 88-100% which, in addition to propagation losses in an office environment, can be attributed to fading and interference for the co-existing WLANs.

In order to gauge the capability of A-stack to maintain time-slotted communication as well as executing an accelerometer sampling task, we deployed an A-Stack based network for vibration measurements of a pedestrian bridge [56]. Each accelerometer-equipped node collects the

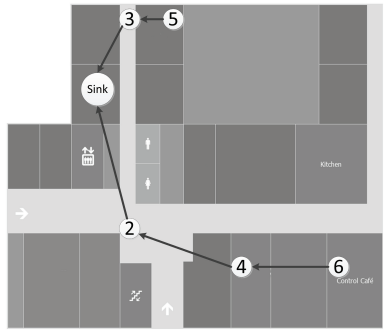

(a) Multihop deployment layout

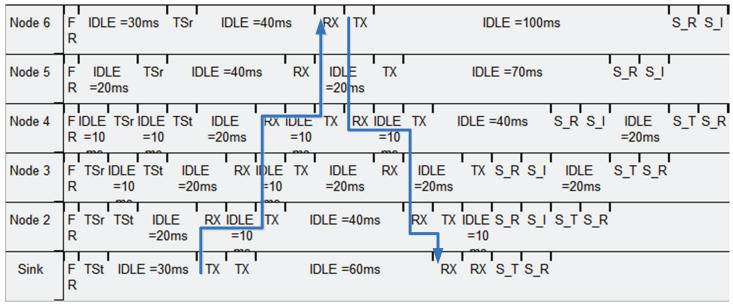

(b) Communication schedule

Figure 4.3. Schedule used in a multi-hop test. Super-frame length is 500 ms. (Last IDLE slots in the schedule are truncated). Transmission pipelining is shown on the schedule with arrows.

vibration measurements of the bridge as explained in Chapter 3. The vibration measurements can amount to as much as 4 MB of data per node with a 30 s measurement time. This SHM application demands high payload throughput requirement in a network of multiple nodes. A-Stack has proven to be a useful framework for SHM applications requiring high data-transfer rates, synchronized sampling and long-term reliable operation.

5. Coexistence Modeling for Link-Quality Analysis

Coexistence and unlicensed spectrum sharing of low-rate wireless personal area networks (LR-WPAN) with WLANs results in their performance degradation as studied extensively in the literature [57, 58, 59, 60]. The performance degradation is caused by higher power WLAN transmissions on the overlapping channels. On the other hand, there is a limited to negligible impact of low power LR-WPAN transmissions on WLAN [61, 62, 63, 58].

In this asymmetric coexistence scenario, the coexistence modeling of LR-WPAN is important for **a)** network performance evaluation **b)** designing the coexistence techniques for mitigating the impact of interference. The coexistence modeling in this chapter is concerned with the design of coexistence models capable of capturing the impact of interference, in terms of its power and traffic characteristics, on the quality of an interfered link. In this context, we proposed packet delivery ratio (PDR) models for link-quality analysis of an interfered LR-WPAN system under WLAN coexistence. A PDR model probabilistically combines the impact of interfering WLAN traffic on LR-WPAN traffic based on the signal-to-noise-ratio (SNR) and signal-to-noise-plus-interference-ratio (SINR) of the link, and the traffic characteristics of the two systems [59].

The contributions in this chapter can be summarized as:

- Coexistence performance modeling of a LR-WPAN link under WLAN interference based on a stochastic packet collision-model
- Spectrum sensing based PDR estimation of an interfered LR-WPAN link with and without packet collision-modeling

5.1 Coexistence Performance Analysis

The coexistence performance analysis of two networks is challenging due to their possible coexistence scenarios and network configurations. For coexistence analysis of WLAN and LR-WPAN, in particular, selection of the following aspects play a critical role for a realistic evaluation study:

- The offset between the operational frequencies and the proximity: these factors can alter the MAC layer operation based on the measured interference energy.
- Typical network traffic characteristics which are variable especially in WLANs, due to adaptive PHY transmission rate and network size.

Some experimental studies investigated the coexistence performance of IEEE 802.15.4 under IEEE 802.11b interference with respect to frequency offset between the two systems [57, 58]. Petrova *et. al.* [58] suggested a minimum frequency offset of 7 MHz for satisfactory IEEE 802.15.4 performance under 3.5 meter's distance separation of IEEE 802.15.4 from the IEEE 802.11b transmitter. However, the IEEE 802.11b traffic characteristics are not given in this study. A probabilistic model is developed in [59], which evaluates the packet error rate (PER) in the IEEE 802.15.4 network based on the frequency offset, duty cycle and distance separation of the IEEE 802.11b interferer. The model assumes that the in-band interference power from IEEE 802.11b to the IEEE 802.15.4 is additive white Gaussian noise (AWGN). The theoretical and simulation analysis, under saturated periodic WLAN traffic, suggest that IEEE 802.15.4 needs 8 meter's distance separation or 7 MHz frequency offset from IEEE 802.11b to maintain the PER below 0.1%.

The received in-band interference power from IEEE 802.11 depends on its distance separation and frequency offset from the IEEE 802.15.4. Therefore, it is more effective to evaluate the PER of a LR-WPAN link with respect to SINR and the activity factor of IEEE 802.11b, as suggested in Publication V. The frequency offset and distance-based performance evaluations are more useful for static network deployment. However, the aforementioned approach can be adopted for frequency-agile communication.

In [64], a coexistence model is proposed to evaluate the throughput performance of IEEE 802.15.4 in different coexistence ranges with IEEE 802.11. The coexistence ranges are defined based on the transmit power

and receiver sensitivity of the two systems. The analysis presented in [59] falls into one of the coexistence ranges, i.e., both the IEEE 802.15.4 and IEEE 802.11 networks do not sense transmissions from each other.

5.1.1 Link-Quality Estimators for Coexisting Networks

The link-quality estimation in wireless sensor networks is a fundamental element of network management for adapting the network parameters and protocols. Various network management mechanisms such as MAC [65], routing [66], topology control [67], clustering [68], channel ranking [PV], and power control [69] rely on link-quality estimation.

The link-quality estimators, in general, can be categorized as hardware-based and software-based estimators [70]. The hardware-based estimators are received signal strength indicator (RSSI), link quality indicator (LQI) and SNR that can be read directly from the radio transceiver. Several studies have investigated the correlation of these estimators with PDR [71, 72, 73, 74, 75]. However, these estimators are ineffective in estimating the link-quality under interference. The software-based estimators are derived from link measurements. The main software-based estimator is packet delivery ratio (PDR) which is computed as a ratio of the successfully received packets to the transmitted packets. A similar metric is the PER, that is PDR $= 1 -$ PER. A comprehensive survey on link-quality estimators in LR-WPAN is presented by Baccour *et. al.* [70].

A PDR estimator can be based on active or passive link monitoring. In active monitoring, PDR is estimated by transmitting training packets and by correlating SINR with PDR [65]. The passive-monitoring-based PDR estimators are more agile to link dynamics, which can be based on either a combination of existing traffic and overhearing [76, 75] or energy detection [77].

In this thesis, energy-detection-based PDR estimation is adopted for further analysis. This technique is already studied by Stabellini *et. al.* [77], however, the underlying coexistence model ignores the traffic characteristics of the interfering network.

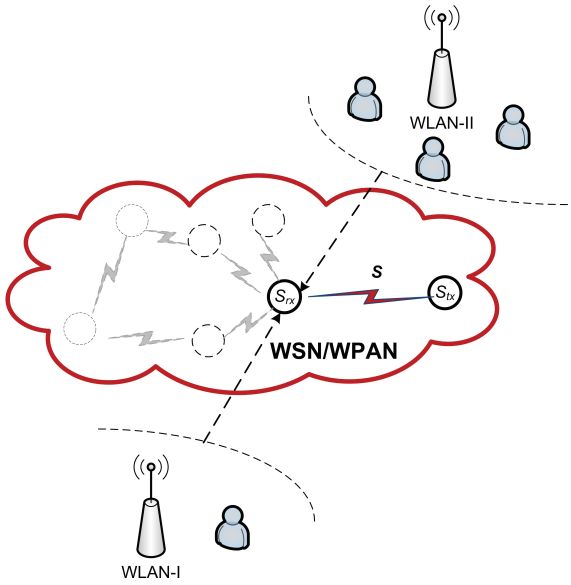

Figure 5.1. Coexistence scenario of a LR-WPAN with WLAN

5.2 Coexistence Model

We consider the coexistence of IEEE 802.15.4-based LR-WPAN and IEEE 802.11g-based WLAN in a 2.4 GHz unlicensed band. Figure 5.1 sketches such a coexistence scenario in which a LR-WPAN link is interfered by WLAN network. The LR-WPAN link, established between a sensor transmitter (S_{tx}) and sensor receiver (S_{rx}), is a part of a large network. The link strength on a candidate channel is S. A geographically co-located WLAN network operates on a channel overlapping with the channel selected for the sensor link.

The sensor link can experience interference from a WLAN network with a single communication flow (WLAN-I) or a composite effect of interfering traffic from a multi-terminal WLAN network (WLAN-II). The objective in either case is to evaluate the link-quality based on the PDR.

5.2.1 PHY Layer Specifications

IEEE 802.15.4

The PHY layer of IEEE 802.15.4 uses offset quadrature phase-shift keying (OQPSK) modulation with half-sine pulse shaping [5]. The PHY layer transmission rate is 250 kbit/s. The bit error rate (BER) of OQPSK

modulation in an AWGN channel is

$$P_e = Q\left(\sqrt{2\zeta E_b/N_o}\right) \tag{5.1}$$

where ζ is the pulse-shaping factor and E_b/N_o is the average energy per bit to the noise spectral density or noise plus interference spectral density at the receiver input.

IEEE 802.11g

The PHY layer transmission rate of the IEEE 802.11g standard, assumed in this thesis, is 12 Mbps. This data rate corresponds to quadrature phase-shift keying - orthogonal frequency division multiplexing (QPSK-OFDM) modulation.

5.2.2 Traffic Models

LR-WPAN

We consider a typical LR-WPAN traffic model for periodically reporting constant size measurement data to a sink node. It is assumed that a sensor transmitter sends a N_b-bit packet at R_b bits/s with packet transmission time, $T_w = N_b/R_b$. The packets are sent at a rate λ. In experimental and numerical evaluations, we use N_b = 480 bits, R_b = 250 kbps and λ = 33 packets/s.

WLAN

We assume a nominal WLAN packet payload size of 500 bytes. Including headers and the PHY layer specifications this corresponds to a packet transmission time of T = 0.374 ms. The considered packet inter-arrival time distributions are stationary periodic, exponential, gamma and hyper-Erlang. The periodic and exponential distributions are used to model the packet arrivals in a single-terminal scenario. The gamma and hyper-Erlnag distributions, as we study later in this chapter, are the potential candidates to model realistic traffic scenarios, for instance, traffic shaped by CSMA/CA mechanisms in a multi-terminal WLAN system.

5.3 Packet Delivery Ratio Model

Consider the transmission of a LR-WPAN packet of length T_w. If there is no interference, the bit error probability is P_{e_0} and E_b/N_o in Eq. (5.1) is a function of $\mathrm{SNR} = S/P_N$. Alternatively, if a bit experiences interference,

the bit error probability is P_{e_1} and E_b/N_o is a function of $\mathrm{SINR} = S/(I + P_N)$. Here, S is the signal power, P_N is the noise power and I is the interference power.

Let us define $q_0 = 1 - P_{e_0}$ and $q_1 = 1 - P_{e_1}$ as the bit success probabilities without and with interference, respectively. Then the success probability of a packet can be determined from Eq. (5.1) as a function of SNR, SINR and the number of interfered bits [59] as

$$\mathrm{PDR} = q_0^{N_b - \ell} q_1^{\ell} \tag{5.2}$$

where ℓ is the number of interfered LR-WPAN bits, i.e., the packet collision-time. The packet collision-time of an interfered link is a function of traffic distributions, packet size and packet inter-arrival time, of the interfering and interfered networks [59][78].

Since the PDR model in Eq. (5.2) requires deterministic knowledge of ℓ, in earlier studies [59, 78], collision-time is analyzed based on deterministic packet collision models. However, these models are limited to periodic inter-arrivals which cannot be generalized to a realistic traffic scenario, for example, a sensor link observing a composite effect of traffic from a multi-terminal WLAN network. Due to this limitation, the collision-time has to be evaluated by simulations [Publication VII].

In Publication VIII, we proposed a PDR model (Eq. (5.3)) based on packet collision-time distribution. In this formulation, $F(T_w, x)$ is the collision-time distribution (CTD) function parametrized by LR-WPAN packet length, T_w, and collision-time, x.

$$\mathrm{PDR} = q_0^{N_b} F(T_w, 0) + \sum_{\ell=1}^{N_b} \left(q_0^{N_b - \ell} q_1^{\ell} \right) \Big(F(T_w, \ell T_b) - F(T_w, (\ell - 1) T_b) \Big) \tag{5.3}$$

Since the interfering traffic is parametrized by packet inter-arrival time and packet-size distributions, the PDR evaluation of LR-WPAN requires derivation of CTD using these parameters.

5.4 Stochastic Packet Collision Model

In Publication VIII, we developed a stochastic packet collision model to capture the temporal effect of WLAN traffic distributions on a LR-WPAN link. The packet collision model is utilized to derive the CTDs of the LR-WPAN link under a realistic interfering traffic distribution such as WLAN traffic originated from multiple terminals and shaped by the CSMA/CA rules of the associated MAC layer.

The proposed collision model is based on the observation that the WLAN traffic can be represented by an alternating renewal process (see Fig. 5.2), where the channel occupancy is one of the states. The statistical properties of alternating renewal processes where the observation starts at the state transition instant are already analyzed by Takács [79]. As the interfered LR-WPAN may access the channel at an arbitrary time, we consider two probable states of residual hold-time before the next state transition occurs, and mix them according to the WLAN activity factor.

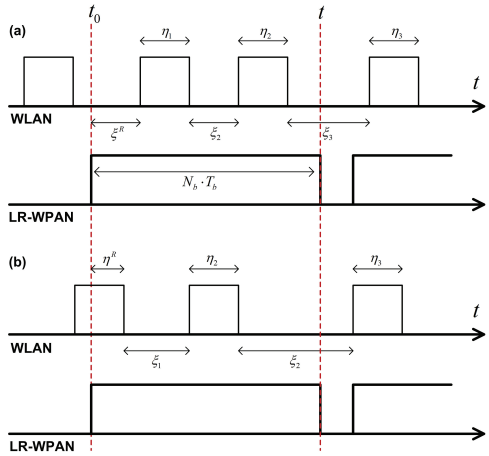

Figure 5.2. The alternating renewal processs representation of WLAN traffic

Consider an alternating renewal process that can be in one of two states: *on* (busy) or *off* (idle). Let ξ denote the length of *off* time and η denote the length of *on* time. The variables $\xi_1, \xi_2, \xi_3, \ldots$ are independent and identically distributed (i.i.d.) random variables (RV) with cumulative distribution function (CDF) $G(x)$ and mean $\bar{\xi}$. Also, $\eta_1, \eta_2, \eta_3, \ldots$ are i.i.d. RV with CDF $H(x)$ and mean $\bar{\eta}$. Let $\chi(t)$ denotes the state of the process at a time instant t. At an arbitrary time instant $t > 0$, we find the system in *on* state with probability ρ and in *off* state with probability $1 - \rho$.

$$\Pr\{\chi(t) = 1\} = \frac{\bar{\eta}}{\bar{\eta} + \bar{\xi}} \triangleq \rho \tag{5.4}$$

Let A denote the set of time instances that the system is in an *off* state and B denote the set of time instances when the system is in an *on* state.

$$\chi(t) = \begin{cases} 0 & \text{if } t \in A \\ 1 & \text{if } t \in B \end{cases}$$

The total time spent in state B in an interval $[t_0, t]$ is given by

$$\beta_o(t) = \int_{t_0}^{t} \chi(\tau)\, \mathrm{d}\tau$$

and the total time spent in state A is given by $\alpha_o(t) = t - \beta_o(t)$. The CDF of the *on* time, $\beta_o(t)$, is obtained by Takács [79] assuming that the system is in *on* state at t_0. At time instant t_0, however, the process $\chi(t)$ can be in an arbitrary state as shown in Fig. 5.2. The first observed state (at t_0) can be either *off* as shown in Fig. 5.2.a or *on* as shown in Fig. 5.2.b. The CDT for each case can be written as

$$\begin{aligned}\omega_0(t,x) &\triangleq \Pr\{\beta_o(t) \le x | \chi(t) = 0\} \\ &= \sum_{n=0}^{\infty} H_n(x) \left[G_n^R(t-x) - G_{n+1}^R(t-x)\right]\end{aligned} \tag{5.5}$$

$$\begin{aligned}\omega_1(t,x) &\triangleq \Pr\{\beta_o(t) \le x | \chi(t) = 1\} \\ &= \sum_{n=0}^{\infty} H_{n+1}^R(x) \left[G_n(t-x) - G_{n+1}(t-x)\right]\end{aligned} \tag{5.6}$$

where

$$\begin{aligned}H_n(x) &= \Pr\left\{\sum_{i=1}^{n} \eta_i \le x\right\}, H_0(x) = 1 \\ G_n(x) &= \Pr\left\{\sum_{i=1}^{n} \xi_i \le x\right\}, G_0(x) = 1 \\ H_n^R(x) &= \Pr\left\{\eta^R + \sum_{i=2}^{n} \eta_i \le x\right\}, H_0(x) = 1 \\ G_n^R(x) &= \Pr\left\{\xi^R + \sum_{i=2}^{n} \xi_i \le x\right\}, G_0(x) = 1\end{aligned} \tag{5.7}$$

$H_n(x)$ and $G_n(x)$ denote the nth iterated convolution of $H(x)$ and $G(x)$ respectively. Also, using ξ^R and η^R as the residual time of ξ and η, $H_n^R(x)$ and $G_n^R(x)$ are the convolutions of $H_{n-1}(x)$ and $G_{n-1}(x)$ with the CDF of ξ^R and η^R, respectively.

Therefore, the joint CDT function from Eqs. (5.4)(5.5)(5.6) is given as

$$F(t,x) \triangleq \rho\omega_1(t,x) + (1-\rho)\,\omega_0(t,x). \tag{5.8}$$

5.4.1 WLAN Traffic Distributions

The packet length and idle-time distributions of WLAN can be used in Eq. (5.8) to determine the distribution of total time overlap of a LR-WPAN

packet in an interval $[t_0, t]$. The CDF function depends on $H_n(x)$, $G_n(x)$, and convolution of these functions with CDF of ξ^R and η^R, respectively.

Busy-time distribution

The packet length of WLAN corresponds to *on* time in renewal process terminology. We assume that WLAN has constant packet length, i.e., $\bar{\eta} = T$, that is equal to the transmission time of a nominal packet size. Thus, the *on* time distribution is given by

$$H_n(x) = \begin{cases} 0 & \text{if } x < nT \\ 1 & \text{if } x \geq nT \end{cases} \tag{5.9}$$

Then, the residual time is uniformly distributed in the interval $[0, T]$

$$H_n^R(x) = \begin{cases} 0 & \text{if } x < (n-1)T \\ \frac{x-(n-1)T}{T} & \text{if } (n-1)T \leq x < nT \\ 1 & \text{if } x \geq nT \end{cases} \tag{5.10}$$

The constant packet length is assumed to simplify the analysis without the loss of generality of the approach. For a given packet length distribution, it is possible to obtain $H_n(x)$ and $H_n^R(x)$.

Idle-time distribution

Similar to busy-time distribution, the idle-time of WLAN traffic corresponds to *off* time in renewal process terminology. In the following we derive $G_n(x)$ and $G_n^R(x)$ for different WLAN inter-arrival distributions.

a) Periodic distribution: For periodic inter-arrival time between packets, the idle-time, $\bar{\xi} = T_{IA} = 1/\lambda$, is deterministic. Therefore, $G_n(x)$ and $G_n^R(x)$ are given by Eq. (5.9) and (5.10) respectively by replacing T with T_{IA}.

b) Exponential distribution: Considering the idle-time between the packets follows exponential distribution with mean $\bar{\xi} = 1/\lambda$, the n-fold convolution is Erlang-n.

$$G_n(x) = 1 - \sum_{j=0}^{n-1} \frac{1}{j!} \left(\frac{x}{\bar{\xi}}\right)^j \exp\left(-\frac{x}{\bar{\xi}}\right) \tag{5.11}$$

Since the residual time is also exponential distributed with the same parameters, $G_n(x) = G_n^R(x)$

c) Gamma and Erlang distributions: For this case, consider a scenario where r independent WLAN nodes are generating traffic each having a common exponential distribution with mean $1/\lambda$. Although the traffic

generated by r independent identical nodes has Erlang-r distribution with mean $\bar{\xi} = r/\lambda$, we consider gamma distribution with shape parameter α and rate parameter β to generalize the analysis. The probability density function (PDF), $g(x)$, and CDF, $G(x)$, of the gamma distribution are given by

$$g(x) = g(x;\alpha,\beta) = \frac{\beta^{\alpha}x^{\alpha-1}\mathbf{exp}(-\beta x)}{\Gamma(\alpha)} \tag{5.12}$$

$$G(x) = G(x;\alpha,\beta) = \frac{\gamma(\alpha,\beta x)}{\Gamma(\alpha)} \tag{5.13}$$

where $\gamma(\cdot)$ is the lower incomplete gamma function and $\Gamma(\cdot)$ is the gamma function. The n-fold convolution of the gamma distribution function (5.13) is also a gamma distribution with shape parameter $n\alpha$

$$G_n(x) = G(x;n\alpha,\beta). \tag{5.14}$$

The PDF of the residual time is defined by CDF of the state [80] as

$$g_1^R(x) = \frac{1-G(x)}{\bar{\xi}} \tag{5.15}$$

Therefore, the CDF of the residual time is given by

$$G_1^R(x) = \frac{\Gamma(\alpha+1)+x\beta\Gamma(\alpha,x\beta)-\Gamma(\alpha+1,x\beta)}{\bar{\xi}\beta\Gamma(\alpha)} \tag{5.16}$$

where $\Gamma(\alpha,x)$ is the upper incomplete gamma function.

The distribution function G_n^R for $n>1$ is

$$\begin{aligned} G_n^R(x) =& \frac{\Gamma((n-1)\alpha+1,x\beta)-x\beta\Gamma((n-1)\alpha,x\beta)}{\bar{\xi}\beta\Gamma((n-1)\alpha)} \\ &+ \frac{\alpha\Gamma(n\alpha)+x\beta\Gamma(n\alpha,x\beta)-\Gamma(n\alpha,x\beta)}{\bar{\xi}\beta\Gamma(n\alpha)} \end{aligned} \tag{5.17}$$

d) Idle-time distribution in a WLAN cell under CSMA/CA medium access: The realistic WLAN traffic properties can be determined only by including the effects of CSMA/CA medium access rules of the associated MAC layer. In this context, we first find the empirical channel idle-time distribution in a multi-terminal WLAN cell and then find an analytical model fitting the empirical distribution. The fitted model is then used in the proposed collision-time model to determine the CDT.

We consider a WLAN cell of three nodes generating packets with exponential inter-arrival times and the same mean packet rate, all destined to a common access point. The nodes are within the carrier sense range of each other. This setup is realized in ns2 to extract the empirical idle-time distribution.

The empirical channel idle-time distribution depicts heavy-tailed behavior and fitting a hyper-Erlang distribution to such distributions is already studied in [81]. The probability density function (PDF) of mixture of M_r mutually independent Erlang distributions is given by

$$g\left(t;\pi,\alpha,\beta\right)=\sum_{j=1}^{M_r}\pi_j\frac{(\beta_j t)^{\alpha_j-1}}{(\alpha_j-1)!}\beta_j\exp(-\beta_j t) \tag{5.18}$$

with mixture probabilities π_j such that $\pi_1+...+\pi_{M_r}=1$, shape parameter α such that the number of phases of the M_rth Erlang distribution are α_{M_r} and scale parameter of the M_rth Erlang distribution is β_{M_r}.

Fitting the hyper-Erlang distribution to the empirical data is a mixture-density parameter estimation problem and the unknown parameters (π,α,β) can be estimated using the algorithm proposed in [81].

The closed-form expressions for n-fold convolution and residual time of the hyper-Erlang distribution are not known and the solution proposed by Ma and King [82] is also computationally extensive. Thus, this distribution cannot be used to find the CDT using Eq. (5.8). As a result, we considered approximating the empirical distribution with gamma distribution by matching the first two moments. The shape (α) and scale (β) parameters of gamma distribution are determined as

$$\alpha=\frac{\mu^2}{\sigma^2},\beta=\frac{\mu}{\sigma^2}$$

where μ is the mean and σ^2 is the variance of the empirical idle-time data set.

In order to test the goodness-of-fit of the fitted gamma and hyper-Erlang distributions, we performed the Kolmogorov-Smirnov (K-S) test [83]. The resulting D and p-values of K-S test showed that hyper-Erlang distribution is a better fit compared to gamma distribution. However, considering the complexity of hyper-Erlang distribution and reasonable K-S test outcome for gamma distribution, the latter is a rational choice. Figure 5.3 shows the CDFs of the empirical data, hyper-Erlang and fitted gamma distributions using the estimated parameters. The gamma distribution parameters can be used in Eq. (5.16) and (5.17) to find $G_n^R\left(x\right)$.

5.4.2 Numerical Evaluation

The proposed CTD model is validated for the inter-arrival time distributions studied in Section 5.4.1 by MATLAB simulations. In simulations, it is assumed that a LR-WPAN packet starts at $t=0$. The initial state of the

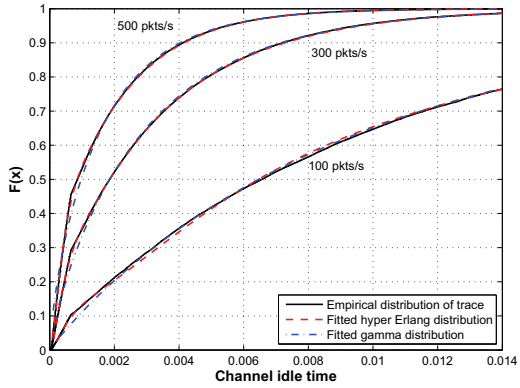

Figure 5.3. Hyper-Erlang and gamma distributions fitting to the empirical idle-time distribution

WLAN traffic distribution process at $t = 0$ is determined by comparing a uniform distributed number against *on* state probability of the process. Considering the WLAN process is in *on* state, the residual on time is uniformly distributed with $\eta^R \sim U(0, T)$. Otherwise, the residual idle-time for each traffic distribution is calculated as

- Periodic: the residual idle-time is uniformly distributed as $\xi^R \sim U(0, T_{IA} - T)$.
- Exponential: the residual idle-time is also exponentially distributed with mean $(T_{IA} - T)$.
- Erlang-r: since Erlang-r is a composite process, the residual idle-time can be calculated by generating a random number from gamma distribution. The shape parameter of gamma distribution is a uniformly distributed integer from the interval $[0, r]$ and its scale parameter is $\left(\frac{T_{IA}-T}{r}\right)$.
- Gamma: the residual idle-time is calculated using Eq. (5.16) and gamma distribution parameters.

We compared the simulated and theoretical CTDs of an interfered LR-WPAN link by K-S test. The K-S test showed a perfect match on the continuous sections of a CDT. As an example, Fig. 5.4(a) shows a comparison for gamma inter-arrivals with packet rate of 400 packets/s. Figure 5.4(b) shows a comparison of the CTDs achieved with the theoretical collision-time model for the studied WLAN inter-arrival distributions.

The impact of WLAN traffic distributions on the PDR of a LR-WPAN link under two different WLAN packet rates is compared in Fig. 5.5.

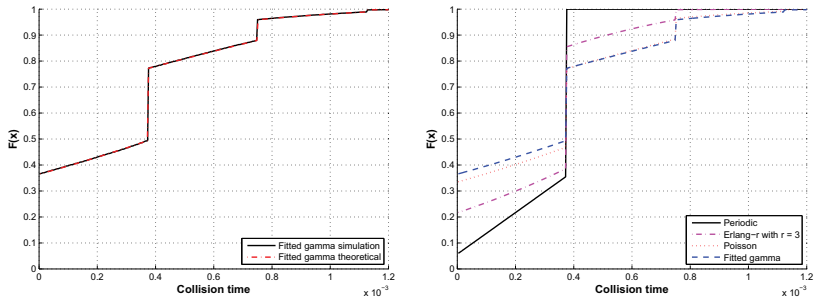

(a) Theoretical and simulated CTD of a LR-WPAN link under gamma inter-arrivals

(b) CTDs for the studied WLAN inter-arrivals with packet rate of 400 packets/s

Figure 5.4. Collision time distributions (CTDs) of a LR-WPAN link

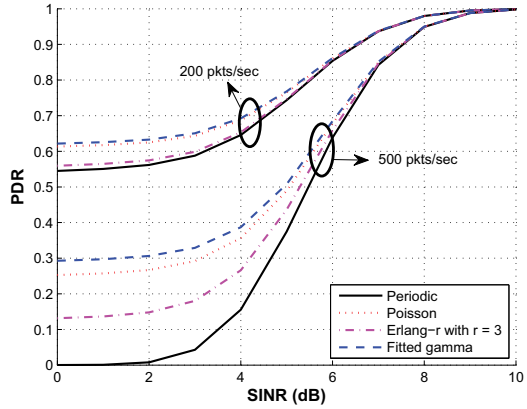

Figure 5.5. Comparison of packet delivery ratio (PDR) under different WLAN traffic distributions (with SNR = 15 dB)

These results are obtained by using the derived collision-time distributions in Section 5.4.1 along with Eq. (5.3). It can be seen that periodic traffic has worse impact on the PDR than any other WLAN traffic distribution.

5.5 PDR Estimation Using Spectrum Sensing

In this section, we present two PDR estimation schemes for LR-WPANs under WLAN interference using energy-detection-based spectrum sensing. The first PDR estimation scheme is based on the PDR models (Eq. (5.2) & (5.3)) which are defined as functions of SNR, SINR, and collision-time. Since the collision-time is defined by the traffic characteristics of the two coexisting systems, the estimation of the interfering traffic characteristics might not be a feasible option with limited

spectrum-sensing time. Therefore, the second PDR scheme concentrates on estimating the link-quality independent of the collision-time.

5.5.1 Spectrum Sensing

Spectrum sensing is one of the most fundamental elements of cognitive radio systems to identify spectrum opportunities or white spaces [84] across frequency, time and space. The spectrum opportunities can be exploited with different spectrum-sharing schemes by secondary users to a licensed spectrum [85, 86], and by coexisting networks in unlicensed bands [87]. The most common spectrum-sensing schemes are matched filtering, energy detection and cyclostationary feature detection which differ from one another based on the principles of detection [88]. Each sensing scheme has an associated complexity versus reliability trade-off [89].

Energy detection is a low-complexity spectrum-sensing technique for the detection of primary signal or interference in noise. An energy detector measures the energy received on a frequency band in a sampling interval. The absence of primary signal or interference is subject to the measured energy less than a threshold. The detection reliability, however, has been the subject of much investigation, since the energy detector is susceptible to uncertainties in background noise power, especially at very low SNR [90].

However, in close-proximity coexistence scenarios, a WLAN's SNR at an LR-WPAN is expected to be substantially larger. Therefore, the concerns of detection reliability are reduced and energy detection can be used effectively. Also, energy detection is the most feasible option for low-complexity sensor devices without any need of extra hardware since the energy detector is an essential part of CSMA/CA based medium access schemes.

A typical energy detector consists of a bandpass filter to reject out of band noise and adjacent signals, an analog-to-digital converter for Nyquest rate sampling, a square-law device and an integrator. In order to measure the energy of the received signal, the output signal of the bandpass filter with width W is squared and integrated over a sampling interval T_s. The number of complex samples collected during the sampling interval are $N = W \cdot T_s$.

The energy detector output in IEEE 802.15.4-compliant radio transceivers is always averaged over 8 symbol periods ($T_s = 128\ \mu$s) [5].

This average channel energy is called as received signal strength indicator (RSSI). With bandpass filter bandwidth $W = 2$ MHz, the number of complex samples in the sampling interval is $N = 256$.

5.5.2 PDR Estimation I – Using Packet Collision Model

The PDR estimation using PDR models in Eq. (5.2) requires the estimation of interfering network parameters such as signal strength, activity factor, packet size and inter-arrival-time distributions. The interference signal strength and activity factor are estimated by spectrum measurements in Publication VII. However, given the interfering traffic parameters are known, the existing deterministic packet collision models [78, 59], apart from simple traffic distributions, cannot be utilized for theoretical PDR evaluation in realistic traffic scenarios. Therefore, the temporal effect of coexisting traffic distributions on the PDR is evaluated by simulations in Publication VII. On the other hand, the stochastic collision-time model proposed in Publication VIII can be utilized for PDR evaluation under an arbitrary interfering packet size and inter-arrival-time distributions.

Concerning the identification of inter-arrival time distributions, the authors in [87, 91, 92] have studied the statistical modeling of channel idle periods in a 2.4 GHz band. By using this approach, in Publication VIII, we showed that packet inter-arrivals in a realistic multi-terminal WLAN scenario can be approximated with gamma distribution, which is mathematically more tractable without compromising its goodness-of-fit as compared to other distributions in terms of Kolmogorov-Smirnov (K-S) tests. As in [92], the channel energy measurement can be used for the estimation of the distribution parameters.

Interference Estimators

A sensor receiver estimates the interference strength and activity factor from energy measurements. A spectrum energy sample is realization of one of the following hypotheses

$$X[n] = \begin{cases} W[n] & H_0 \\ Y[n] + W[n] & H_1 \end{cases} \tag{5.19}$$

where H_0 is the hypothesis corresponding to no signal transmitted and H_1 to signal transmitted, $W[n]$ is a noise sample and $Y[n]$ is the WLAN signal sample.

At a certain time instant a channel can be in either an idle or a busy state. The distribution of the two states depends on the WLAN traffic distribution. In idle state each energy sample contains pure noise and can be modeled by a zero mean Gaussian random variable with variance P_N, where P_N stands for the noise power. In a busy state each sample contains WLAN signal embedded into noise. Since the time domain distribution of an OFDM signal can be approximated to be Gaussian [93], these samples can also be modeled by a zero mean Gaussian random variable with variance $(P_N + I)$, where I is the WLAN signal power.

The decision statistic, L, for an energy detector is

$$L = \sum_{n=1}^{N} |X[n]|^2 \tag{5.20}$$

The L is compared with a threshold, γ, to decide whether a WLAN signal is present or not. The L is known to follow Chi-square distribution [94]. When N is large, Chi-square distribution can be well approximated with Gaussian distribution [94]. Under this assumption the distributions of L under two hypotheses are

$$\begin{aligned} p(L|H_0) &\sim \mathcal{CN}\left(NP_N, NP_N^2\right) \\ p(L|H_1) &\sim \mathcal{CN}\left(N(P_N + I), N(P_N + I)^2\right) \end{aligned} \tag{5.21}$$

where $\mathcal{CN}$ stands for the complex Gaussian distribution.

Assuming that the interference level is higher compared to the noise level and thus, the miss-detection probability is practically zero. Therefore, we set the threshold γ based on the probability of false alarm, Pr_{fa},

$$\mathrm{Pr}_{fa} = \int_{\gamma}^{\infty} p(L|H_0)\, dL \approx \frac{1}{2}\mathrm{erf}\left(\frac{\gamma - NP_N}{\sqrt{2NP_N^2}}\right) \tag{5.22}$$

The interference level, $\hat{I}$, is estimated by calculating the sample mean

$$\hat{I} = \frac{1}{\hat{N}}\sum_{j=1}^{\hat{N}} L_j - P_N \tag{5.23}$$

where $\hat{N}$ is the number of times the calculated decision statistic exceeds the decision threshold, $L > \gamma$.

Similarly the activity factor sample mean estimate, $\hat{\rho}$, is

$$\hat{\rho} = \frac{\hat{N}}{N_{T_s}} \tag{5.24}$$

where N_{T_s} is the total number of times the decision statistic is evaluated.

5.5.3 PDR Estimation II – Independent of the Packet Collision Model

The complexity associated with link-quality evaluation of an interfered network based on the PDR models, given in Eq. (5.2) & (5.3), is their dependence on collision-time. As discussed in Section 5.3, the collision-time depends on the activity factor and, packet size and packet inter-arrival time distributions of the two coexisting systems. With known parameters, the PDR can be estimated based on the packet collision model proposed in Section 5.4. However, in reality, these parameters cannot be determined satisfactorily with limited channel energy measurements.

In Publication IX, a PDR estimation scheme independent of collision-time estimation is developed using limited spectrum measurements. In this scheme, the spectrum measurements are adjusted with respect to the traffic characteristics of the sensor link such that the interference and noise characteristics can be identified accordingly. The PDR is estimated based on these measurements in association with the link strength and the BER specifications of the interfered system. The effectiveness of the proposed estimation scheme is verified using a Micro.2420 sensor platform against the empirical PDR in emulated multipath fading channels.

Spectrum Measurement Model

The spectrum measurement scheme schedules the energy measurements instances according to the traffic model of the LR-WPAN link. The motivation for this scheme is to identify the noise and interference characteristics that a sensor receiver might experience on the scheduled link traffic.

A set of successive energy samples completely covering a single packet duration is collected. A single energy sample is named as a micro-sample and the set of micro-samples belonging to a single packet as a macro-sample. Each micro-sample contains average channel energy over a certain number of packet bits. In total, M macro-samples $X^1, X^2, ..., X^M$ are collected with a time interval of $T_I = 1/\lambda$. Figure 5.6 shows this measurement scheme where $x^{i,j}$ indicates the jth collected micro-samples belonging to ith macro-samples.

PDR Estimation Model

By using the proposed measurement scheme, PDR is estimated by averaging the successful packet reception corresponding to a macro-sample over

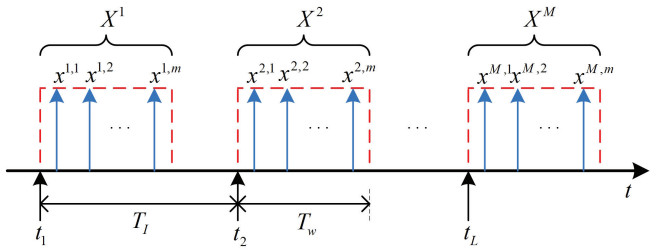

Figure 5.6. Channel energy measurement scheme

M macro-samples. Here, the packet success is achieved as the product of success probability of bits in all micro- samples belonging to a macro-sample. The success probability of bits is obtained by translating SINR, which is obtained from the signal level of the sensor link and the micro-sample energy, into a given BER. The signal level of the link is obtained by transmitting probe packets.

Given that the bit errors occur independently of each other, the packet success probability for N_b-bit packet can be calculated from Eq. (5.1)

$$\Pr\{\text{packet success}\} = \prod_{i=1}^{N_b} \left(1 - Q\left(\sqrt{2\zeta \text{SINR}^i}\right)\right) \tag{5.25}$$

where SINR^i is the SINR corresponding to the ith bit of the packet.

With known link strength (S), we can define $\text{SINR}^{i,j}$ as [Publication V]

$$\text{SINR}^{i,j} = S - x^{i,j} \tag{5.26}$$

where $\text{SINR}^{i,j}$ represents the SINR at the receiver corresponding to ith bit of the jth packet. Assuming the interference is changing slowly within the two consecutive micro-samples, the SINR for N_b/ℓ consecutive bits can be assumed to be the same. In this case, the packet success probability considering only the ith macro-sample can be expressed as

$$\Pr\{\text{packet success}\} = \prod_{j=1}^{\ell} \left(1 - Q\left(\sqrt{2\zeta \text{SINR}^{i,j}}\right)\right)^{\left(\frac{N_b}{\ell}\right)} \tag{5.27}$$

The PDR estimate can be obtained by averaging Eq.(5.27) over M collected macro-samples.

$$\text{PDR} = \frac{1}{M} \sum_{i=1}^{M} \prod_{j=1}^{\ell} \left(1 - Q\left(\sqrt{2\zeta \text{SINR}^{i,j}}\right)\right)^{\left(\frac{N_b}{\ell}\right)}. \tag{5.28}$$

Experimental Evaluation

An experimental setup is designed to evaluate the accuracy of the PDR estimation model given in Eq.(5.28) under WLAN interference. The

experimental setup measures the empirical PDR of a LR-WPAN link under the emulated LOS/NLOS indoor multi-path propagation conditions of the interfering signal. In the same environment, the receiver node collects channel energy samples to estimate the PDR.

A wired link is established between two Micro.2420 sensor nodes. A PC equipped with IEEE 802.11(b/g) PCI wireless adapter is used as WLAN interfering node. The WLAN signal first undergoes fading in a channel emulator [95] and then it is combined with an LR-WPAN link before its reception at the receiver node.

The WLAN generates multicast packets using MGEN v.5.02 [96] at a fixed packet rate with periodic inter-arrival times. The other traffic characteristics of LR-WPAN and WLAN are the same as given in Section 5.2.2.

Empirical PDR: The empirical PDR is calculated as a ratio of successfully received packets to the total transmitted packets and it is correlated with SINR. The signal energy from the transmitter node is changed with an attenuator to obtain PDR ranging from the minimum possible value to 100%. The average SINR is calculated by taking the difference between the average packet RSSI and the average of channel RSSI samples exceeding the decision threshold (γ). The γ differentiates between noise samples and interference-plus-noise samples. For a given probability of misinterpreting noise from an interfering signal, that is the probability of false alarm, the γ can be calculated from Eq.(5.22).

Estimated PDR: In the same channel and interference conditions, the receiver node collects RSSI samples while the transmitter node remains silent. These RSSI samples are collected according to the LR-WPAN traffic model such that the time spacing among macro-samples is $T_I = 30$ ms and each macro-sample has a sampling interval equal to the LR-WPAN packet duration of 1.984 ms. Since $T_s = 128$ μs, a macro-sample contains 16 non-overlapping micro-samples. These energy samples are used for PDR estimation using Eq. (5.28).

Results

The empirical and estimated PDRs are compared under different WLAN packet rates and wireless channel models. Two single-input single-output (SISO) WLAN channel models A and D [97, 98] are defined separately in the channel emulator. The channel models A and D introduce fading in an interfering WLAN signal corresponding to NLOS and LOS channel

conditions respectively.

The receiver node performs the channel measurements according to the intended traffic pattern from the transmitter node under different interference conditions. The first ten macro-samples collected from each interferer condition are shown in Figure 5.7.

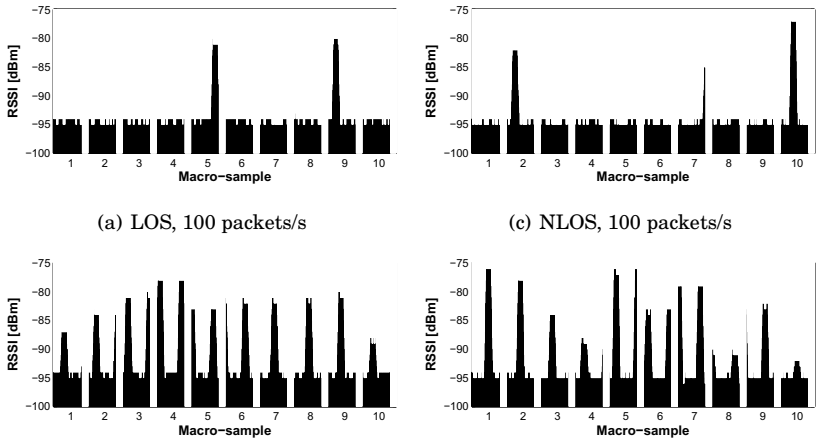

(a) LOS, 100 packets/s

(c) NLOS, 100 packets/s

(b) LOS, 700 packets/s

(d) NLOS, 700 packets/s

Figure 5.7. Captured macro-samples under WLAN interference

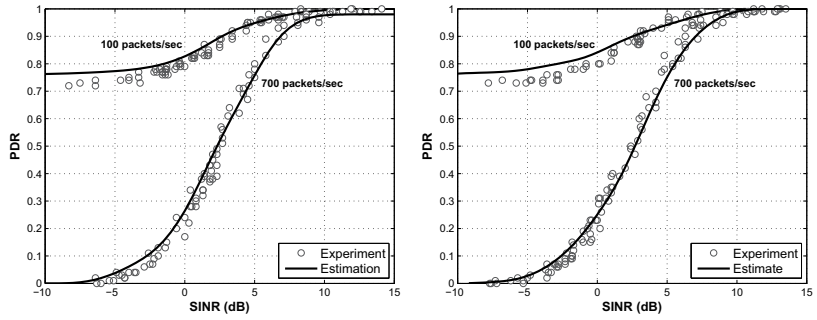

(a) LOS, 100 / 700 packets/s

(b) NLOS, 100 / 700 packets/s

Figure 5.8. Empirical and estimated PDR under WLAN interference

The estimated and empirical PDRs are compared in Figure 5.8. The estimated PDR closely follows the empirical PDR and the error is less than 5% in most cases. The transmitter node signal strength in these experiments is kept such that the SNR at the receiver is greater than 10 dB. Consequently, the receiver node can receive the interference-free packets correctly. This condition clarifies the relationship between the lowest PDR and the interference-free macro-samples for any WLAN packet rate. The PDR under interference with 100 packets/s starts at

around 80% (Fig. 5.8) which corresponds to 8 out of 10 interference-free macro-samples (Fig. 5.7.a & c). For a packet rate of 700 packets/s, PDR starts from 0% (Fig. 5.8) since all the macro-samples are collided with WLAN packet transmissions (Fig. 5.7.b & d).

The accuracy of the proposed PDR estimation depends mainly on the number of channel samples. A sufficient number of channel samples will ensure that the interference traffic and fading conditions are taken into account properly. However, there is an energy cost associated with the spectrum sensing. In order to determine the minimum required number of channel samples, we estimated PDR using a different number of macro-samples. It is observed that the PDR estimation accuracy is low with 20 macro-samples, whereas, PDR follows the experimental results closely with 40 macro-samples and insignificant improvement is observed with 60 macro-samples.

5.6 Summary

From network organization to communication protocols, link-quality estimation is crucial for network management. If incorporated appropriately, it can enhance communication reliability; consequently it can also reduce communication delays and energy consumption. The link-quality estimation, however, in interfered LR-WPANs is challenging due to the lack of coexistence models which can reflect the impact of interference power and realistic traffic characteristics on the link-quality.

In this chapter, we proposed a PDR-based coexistence performance model. It can evaluate the link-quality of an interfered link under realistic interfering traffic distributions by using a stochastic packet collision model. The existing models, whereas, are either limited to simple traffic distributions [59] or ignore the impact of traffic distributions [77].

We also studied this model for PDR estimation using channel energy measurements. The PDR estimation requires the estimation of interference signal strength, activity factor and traffic distribution. In Publication VII, we studied the estimation of strength and activity factor. A simple model to approximate the traffic distribution proposed in Publication VIII together with a channel energy measurement based traffic distribution estimation scheme [92] can also effectively contribute to the PDR estimation. On the other hand, for PDR estimation with limited channel energy measurements, we proposed a PDR model independent

of traffic estimation. In this model, the spectrum measurements are adjusted to identify the interference characteristics on the intended traffic of a sensor link. These measurements together with link strength and BER specifications are used for accurate PDR estimation.

In the next chapter, we exploit the link-quality analysis presented here to enhance the coexistence performance in LR-WPANs by identifying the suitable communication channels.

6. Coexistence Enhancement by Channel Ranking

As the spectral congestion mounts with the proliferation of heterogeneous wireless technologies and the associated applications, the reliable operation of a host system in unlicensed bands requires interference management techniques. Without interference management, the lack of interference mitigation capability at the physical layer and medium access coordination may lead to disruptive mutual interference in close proximity coexistence scenarios. The issue of coexistence and interference management becomes more critical for WSNs consisting of low-power embedded nodes when competing for medium access along with high-power and less resource-constrained nodes. Therefore, low-complexity coexistence enhancement solutions, enabling sensing and adaptation of the link layer procedures, must be integrated into such networks to provide communication reliability. The coexistence enhancement capability can be achieved by exploiting the spectrum opportunities, i.e., spectrum holes [99, 84] in frequency and/or time. By learning these spectrum access opportunities and adapting the behavior of the interfered system accordingly such that the interference can be avoided can be seen as implicit medium-access coordination in unlicensed bands [100].

With the overlapping channel allocations in LR-WPAN and WLAN, if not coordinated properly, even a single interference-free channel may not be guaranteed for LR-WPAN. The severity of the interference from WLANs is also verified in a measurement campaign conducted at an industrial assembly hall (see Fig. 6.1), an environment where WSNs find applications for industrial monitoring and control. The performance analysis of LR-WPAN under WLAN interference in Chapter 5 already gave an understanding of the coexistence concerns in WSNs. In this context, providing some intelligence to WSN nodes to analyze the environment and find the channel facing least interference is necessary to guarantee

a reliable operation under interference. This chapter proposes low-complexity coexistence enhancement solutions which can take advantage of a wider channel set, namely, *channel ranking*.

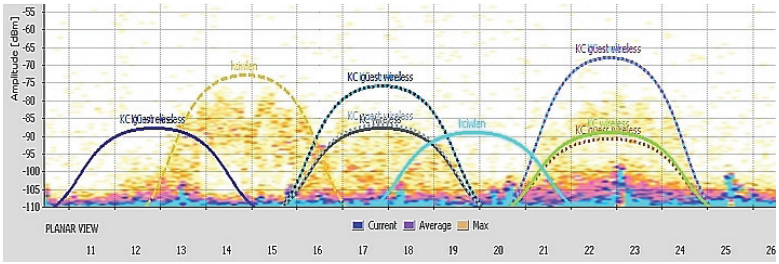

Figure 6.1. WLAN activity on IEEE 802.15.4 channels in an industrial assembly hall surrounded by offices with many operational WLANs

Channel ranking here is concerned with the ordering of the available channels by the sensor nodes with respect to a channel quality metric (CQM) that reflects the interference severity on the WSN. To this end, the nodes exploit the scanning capability of the embedded radios to quantify the perceived interference parameters on the candidate channels. These interference parameters are incorporated into CQM such that an individual node can interpret the interference disruption on its link-quality when acting as a receiver with neighboring nodes on each channel. Such a receiver-centric channel ranking approach can easily be integrated into a distributed multichannel MAC protocol [101].

Our contributions on channel ranking, depending on the design of CQM, can be summarized as:

- We propose channel ranking schemes using a CQM designed only from the interference characteristics, signal strength and activity factor. Since the link-connectivity information (i.e., link strengths with adjacent neighbors) is unavailable at network initialization, the problem we address is how to consider the individual effect of interference parameters in the CQM.

- Given the link-connectivity information available, we propose channel ranking schemes by using PDR as a CQM. Based on our coexistence analysis in the previous chapter, we address the challenges (such as estimating the interfering traffic distributions) and analyze the performance of PDR-estimation-based channel ranking schemes.

6.1 Coexistence Enhancement Solutions

In general, the link-layer solutions enhancing heterogeneous internetwork coexistence in unlicensed bands, excluding inherent CSMA/CA - listen before talk, can be based on the following two approaches:

- The *Reactive approach* orthogonalizes the medium access of a system by identifying the spectrum access opportunities in frequency and/or time domain, also known as dynamic spectrum access (DSA) [99].
- The *Passive approach* adapts the medium-access, usually in frequency domain, based on the communication performance under learning based methods (see, e.g., references [102, 103]).

DSA techniques can alleviate the problems of low spectrum utilization in licensed bands as well as the spectral congestion in unlicensed bands. In either role, the unused spectrum is identified by spectrum sensing, a spectrum decision on the most suitable resource is made and the resource is updated if the lately selected renders unsuitable for communication. Although, with equal medium-access rights, the notion of primary and secondary users is irrelevant in unlicensed bands, however, the DSA techniques utilized in licensed bands can also be utilized in unlicensed bands to orthogonalize a system under study against interference.

In DSA, a system can separate the transmissions in time or frequency domain. In the time domain, a frequency channel is accessed opportunistically by moving in time to avoid transmissions from the interfering system. The frequency domain finds the interference-free or least interfered channels among the candidate channels. A combination of the two schemes, for example opportunistic medium access on a least interfered channel, is also possible. Since each approach identifies the spectrum opportunities through spectrum sensing, the associated energy overhead and complexity in quantifying and modeling the time domain channel availability is unsuitable for resource-constrained LR-WPANs. Therefore, we restrict our discussion here on frequency-domain-based coexistence enhancement solutions. The time domain exploitation of spectrum opportunities is addressed in [92, 104, 105, 106]. In the following discussion, channel-management-based coexistence enhancement solutions for multichannel systems/standards are presented.

The IEEE 802.15.4e-2012 [107] has proposed two methods for MAC layer enhancement called *channel adaptation* and *channel hopping*. Channel adaptation is an on-demand method in which a channel is not changed until the operational channel quality drops lower than a threshold value. Whereas, in channel hopping the channel is switched periodically according to a channel-hopping sequence.

In literature, a varity of channel adaptation schemes have been proposed such as channel surfing [108, 109], channel adaptation [110] and channel switching [111]. In channel surfing [108, 109], the idea is to switch to a new channel once the interference is detected by a jamming/interference detection module [112] on the current channel. Two different approaches for channel surfing are introduced in [108, 109] namely *coordinated channel switching*, and *spectral multiplexing*. The latter approach is similar to the adaptive radio channel allocation scheme proposed earlier by Won Xu *et. al.* [110]. In coordinated channel switching, the entire network adjusts it channel. However, in spectral multiplexing, the nodes located in an interfered region switch their channel while the nodes on the boundary of the region act as radio relays between two spectral zones. The channel-switching proposal by Min *et. al.* [111] selects candidate channels based on their estimated utilization and proactively switches to a throughput-maximizing candidate channel.

The standard specifications offering networking solutions based on IEEE 802.15.4 MAC/PHY such as Zigbee [6], WirelessHART [7] and ISA 100.11a [8] have also introduced channel management schemes. Zigbee uses a method called frequency agility similar to the channel adaptation. WirelessHART and ISA100.11a implement channel hopping along with TDMA. Channel blacklisting, a feature which allows avoiding the unreliable channels, is an optional feature in WirelessHART whereas ISA100.11a employs adaptive blacklisting [49]. The general MAC layer protocol proposals exploiting the multichannel diversity in wireless sensor networks can be found in [53, 113, 114].

A concept similar to adaptive blacklisting is adaptive channel hopping (ACH): hopping sequence is adapted to avoid congested channels [115, 116, 117]. The ACH algorithm proposed by Yoon *et. al.* [115], implements channel hopping within a cluster. The cluster-head periodically generates the hopping pattern based on ordering of the candidate channels using link-quality information of each child node on each channel. Han *et. al.* [116, 117] developed a demand-based frequency-hopping in which

the network coordinator switches from normal single-channel to multi-channel transmission mode upon interference detection. The multi-channel mode is used only to identify the best channel and the network network resumes single-channel operation on a newly selected channel.

Dynamic channel selection is another reactive channel management scheme whereby a channel with least interference or primary activity is searched. The objective here is to maximize the communication reliability under interference in unlicensed bands [60, 118, 119, 120] or spectrum access probability in licensed bands [121, 122, 123, 124, 125]. There are two different approaches to channel selection: the first approach, utilizes a channel quality metric to establish an order of the candidate channels, which is further studied in this chapter, and selects the best channel whereas the second approach stops the channel search as soon as a channel satisfying a criteria is found. The channel selection is followed by a coordination procedure which is studied in the context of multichannel MAC protocols. The MAC layer protocols making use of dynamic channel selection can be found in [126, 127].

6.2 Channel Quality Metrics for Channel Ranking

The design factors of a meaningful CQM can be identified by studying the wireless interference in packet-based coexisting networks. The interference is caused by the simultaneous packet transmissions on an overlapping frequency channel. However, the amount of damage that one packet causes to another is partially determined by the SINR at the respective receiver, which is the ratio of the received signal strength to that of the interference and noise. Besides signal strength, the activity factor of the interference defines the degree of interference [128]. In this perspective, the relevance of the interference characteristics, signal strength and activity factor, in the CQM to a sensor node is with respect to its link strength with its adjacent neighbors. This relationship have already been modeled by PDR in Chapter 6 which can also be used as CQM. However, the identification of an interference traffic pattern is beyond the scope of resource-constrained WSNs. In addition, the connectivity information at network initialization is unknown and the channel ranks have to be inferred only using the interference characteristics. In this case, the intuitive question is which channel to be preferred more, the one with lower signal strength or the one with lower activity factor.

A group of existing channel management schemes exploit the various characteristics of interference such as average interference strength, activity factor, and traffic burstiness, based on channel energy measurements. These techniques, however, usually consider only one aspect of interference characteristics for channel quality evaluation. For example, authors in [60, 120] utilized interference activity factor to determine the channel quality. Similarly, Noda *et. al.* [118] determines the channel ordering based on the burstiness of interfering traffic. The average interference energy exceeding a certain threshold is utilized to trigger the channel adaptation in a number of proposals [108, 6, 116]. Since the preference of one channel over the other depends on the relative influence of interference strength and activity factor on a sensor link, in this thesis we consider estimating and combining these two parameters for channel quality evaluation at network initialization.

Packet delivery ratio (PDR), which is accurate in capturing the link dynamics under interference, is also used for channel adaptations in different manners. For example, PDR as a performance metric is used for channel blacklisting in channel-hopping algorithms [8]. On the other hand, PDR is used as a CQM for channel selection where PDR is determined by active approach (using probe packets) [65] or passive approach (by energy measurements) [77]. The passive approach is further studied in Publication V and Publication IX. Also, in [102], based on the rewards assigned to packet transmission outcomes on each channel, a control strategy is developed for tracking an optimal channel. In this chapter, based on the coexistence analysis in Chapter 5, we developed channel ranking schemes using sensing-based PDR estimation such that the effect of interference traffic distribution is considered appropriately. The earlier closely related work, [77], neglects the effect of traffic distribution and also instead of channel ranking the first channel satisfying a certain packet error rate target is selected.

The other channel ranking schemes, given the network connectivity information is available, use channel capacity [119] and spectrum access probability [129, 130] as CQM. However, in [119] the interfering traffic distribution is ignored. In [129, 130], the optimal channel sensing order is proposed such that in each time-slot the spectrum access probability is maximized. However, in [129], the mean SINR is assumed to be a priori known whereas in [130] channel activity factor is assumed to be a *priori* known.

6.3 System Model

Consider a wireless sensor network with sensor nodes employing low-power IEEE 802.15.4 compliant radios. The WSN is deployed in a place where it has to share the radio spectrum with IEEE 802.11 b/g-based WLAN(s). The WSN performance, depending on its channel selection, can be harmfully influenced by the WLAN(s) interference (see Fig. 6.2). In order to enhance WSN performance, we design channel ranking strategies enabling WSN to react autonomously to interference by selecting the optimum communication channel(s). In this scenario, each sensor node estimates the local interference characteristics, interference strength ($\hat{I}_k$) and activity factor ($\hat{\rho}_k$) where $k = 1, \ldots, C$ on the candidate channels by spectrum sensing. The link strength of a sensor node on a channel k with a neighboring node is denoted by S_k, which is unknown at network initialization. The physical layer and traffic models for the two systems are the same as given in Section 5.2.1 and Section 5.2.2. In addition, we make the following assumptions for channel ranking:

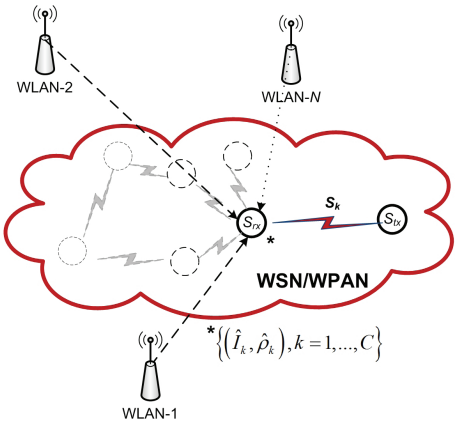

Figure 6.2. Channel ranking in WSN under WLAN coexistence

- WSN is loosely synchronized during the spectrum measurement phase during which sensors do not communicate.
- Each node ranks the channel using a receiver-centric approach
- The nodes exchange their estimated ranks through a beacon period [53] or dedicated control channel [131] in multichannel protocols to agree on the preferred channels or utilize each node's individual preference in a distributed way through a decentralized channel-selection algorithm [101]

In the following sections, the channel quality metrics used for channel ranking are described.

6.3.1 Interference Estimators

In the absence of link-connectivity information in the WSN, the channel quality metric for channel ranking has to be designed exclusively from the interference characteristics. The perceived interference on a sensor location is mainly characterized by its signal strength and activity factor. Therefore, a sensor node must estimate these interference characteristics on a channel and use them together for defining the interference severity for a sensor node.

6.3.2 Packet Delivery Ratio

In Chapter 5, we discussed PDR as a link-quality metric in LR-WPANs under coexisting WLANs and proposed PDR modeling and estimation schemes. We briefly summarize these schemes here to know their associated complexity and challenges before applying these models to channel ranking.

The PDR models given in Section 5.3 are built on the BER evaluation of a link with and without interference in association with the packet-collision time. Depending on the deterministic knowledge on packet collision-time or its distribution, two PDR models are given in Eq. 6.1 and Eq. 6.2 respectively.

$$\text{PDR} = q_0^{N_b-\ell} q_1^{\ell} \tag{6.1}$$

$$\text{PDR} = q_0^{N_b} F\left(T_w, 0\right) + \sum_{\ell=1}^{N_b} \left(q_0^{N_b-\ell} q_1^{\ell}\right) \Big(F\left(T_w, \ell T_b\right) - F\left(T_w, (\ell-1) T_b\right) \Big) \tag{6.2}$$

where $q_0 = 1 - Q\left(\sqrt{2\zeta \text{SNR}}\right)$ and $q_1 = 1 - Q\left(\sqrt{2\zeta \text{SINR}}\right)$. Also, T_w is the packet transmission time of an N_b-bit LR-WPAN packet with bit duration T_b, ℓ is the number of interfered bits in a LR-WPAN packet, i.e., the packet collision time and $F\left(\cdot\right)$ is its distribution. Figure 6.3 shows the PDR of a link with respect to SINR under periodic and Poisson interfering traffic distributions.

The PDR estimation using these models requires the estimation of link strength S, interference strength I and packet collision-time. The collision-time of an interfered link is a function of activity factor ρ and traffic distributions, packet size and inter-arrival time, of the interfering

and interfered network. In Section 5.5.2, the estimation of $\hat{I}$ and $\hat{\rho}$ based on energy measurements is given. However, the estimation of realistic traffic distributions with limited energy measurements is not feasible. We will discuss later how we can develop a channel ranking scheme using PDR as a performance metric without estimating the traffic distributions.

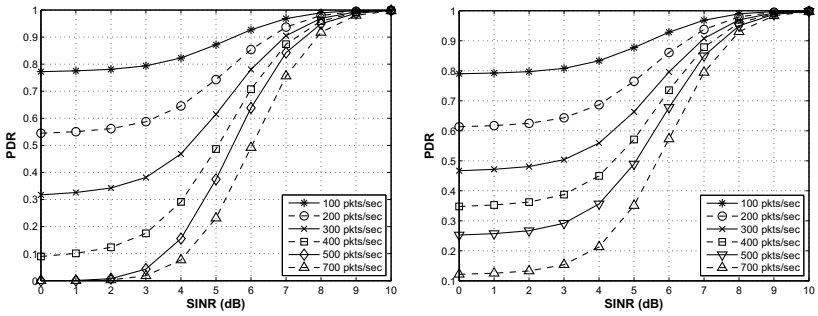

(a) Periodic traffic (b) Poisson traffic

Figure 6.3. PDR-SINR curves of an interfered sensor link under periodic and Poisson traffic distributions of WLAN

The PDR model presented in Section 5.5.3 is independent of the packet collision-time. This model measures the interference characteristics during the scheduled LR-WPAN traffic using spectrum sensing. These measurements are used for PDR estimation in association with the link strength and BER of the LR-WPAN system as

$$\text{PDR} = \frac{1}{M}\sum_{i=1}^{M}\prod_{j=1}^{\ell}\left(q^{i,j}\right)^{\left(\frac{N_b}{\ell}\right)} \tag{6.3}$$

where

$$q^{i,j} = 1 - Q\left(\sqrt{2\zeta \text{SINR}^{i,j}}\right)$$

and PDR is estimated using M macro-samples.

6.4 Interference-Characteristics-Based Channel Ranking

In this section, we present two channel ranking schemes based on the interference estimators. These ranking schemes are named as *heuristic* and *decision theoretic* channel ranking. In each scheme, the estimators are derived from the spectrum measurements at a sensor node. In heuristic ranking, the candidate channels are ranked based on interference strength and activity estimates independently and a combination of the

respective rank gives the final ranks of the channels. On the other hand, in decision theoretic ranking, at first each estimator is weighted according to its impact on a sensor location and then combined together to establish ranking.

6.4.1 Interference Estimators

In Publication V and Publication VI, we proposed different estimators for estimating the interference strength and activity factor using energy samples. The properties of an energy detector in an IEEE 802.15.4-compliant radio has already been discussed in Section 5.5.1. In this section, we present these estimators and evaluate their performance in a scenario with known interfering WLAN traffic.

Let L_i be the ith decision statistic or RSSI sample. Also, N_{T_s} is the total energy samples collected during a sampling time T_s. Using these samples, we identify these statistics: minimum channel energy (noise level), $I_{\min} = \min_i (L_i)$, maximum channel energy, $I_{\max} = \max_i (L_i)$, mean channel energy, $\bar{I} = \frac{1}{N_{T_s}} \sum_{i=1}^{N_{T_s}} L_i$, mean interference energy, $\hat{I} = \frac{1}{\hat{N}} \sum_{i=1}^{\hat{N}} [L_i > \gamma]$ where $\hat{N}$ is the number of times L_i is greater than the threshold γ. Threshold γ, together with acceptable probability of false alarm, is used to decide the presence or absence of a WLAN signal. Based on these statistics Type-I and Type-II interference estimators are proposed in Publication V and Type-III in Publication VI. Table 6.1 gives a summary of these estimators.

Table 6.1. Interference strength and activity factor estimators

Type	Strength	Activity	Remarks
Type-I	$I_{\max}$	$\frac{\bar{I}-I_{\min}}{I_{\max}-I_{\min}}$	Closer the $\bar{I}$ to $I_{\max}$, higher the activity
Type-II	$\hat{I}$	$\frac{\bar{I}-I_{\min}}{\hat{I}-I_{\min}}$	Closer the $\bar{I}$ to $\hat{I}$, higher the activity
Type-III	$\hat{I}$	$\frac{\hat{N}}{N_{T_s}}$	

We verified these estimators under the interference from a coexisting WLAN in an indoor office environment. We realized 15 interfered channels for a sensor node by varying the packet rate and signal strength of a WLAN interferer as shown in Fig. 6.4. This arrangement can be viewed as: a sensor node observes fifteen different channels where the five different activity factors are observed from an interferer with the same interference level and there are three such interference levels in total. In this setup, the WLAN interferer generates broadcast packets periodically

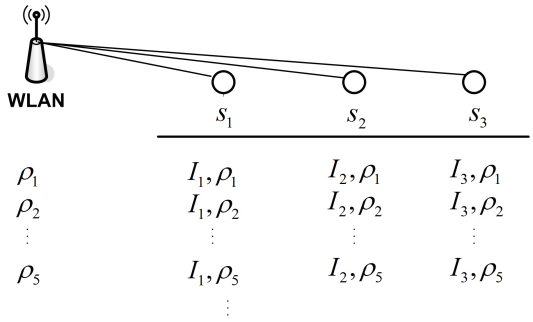

Figure 6.4. Measurement setup

with constant payload using a traffic generator [96]. The sensor node collects N_{T_s} samples in each channel at a sampling interval T_I = 5 ms. The consecutive sampling time instants are observed at $t_{i+1} \geq t_i + T_I$ where the inequality is owing to the hardware-induced delays.

6.4.2 Heuristic Ranking

In Publication V, two channel ranking schemes are proposed based on Type-I & II estimators. Each estimator type is evaluated using the energy measurements in the preceding scenario and channels are ranked with respect to strength and activity independently. Intuitively, the strength rank (R_I) of a channel at location s_1 should be lower than the strength ranks at s_2 and s_3. Similarly, the activity rank (R_ρ) of the channels at ρ_1 should be higher than the activity ranks at any other ρ. We observed that the Type-I estimator makes errors both in activity and strength ranks whereas Type-II and Type-III estimators are accurate in both. The ranks R_I and R_ρ based on the Type-II estimator are given in Table 6.2.

Table 6.2. Channel ranks

Activity (ρ)	s_1			s_2			s_3		
	R_I	R_ρ	R	R_I	R_ρ	R	R_I	R_ρ	R
100	12	2	14	6	1	7	3	3	6
200	11	6	17	8	5	13	1	4	5
300	14	9	23	10	8	18	4	7	11
500	13	12	25	7	11	18	2	10	12
700	15	15	30	9	14	23	5	13	18

In order to infer the channel ranking, the following two channel groups are formed:

Group 1: This group maintains the R_I ranks.

Group 2: This group maintains the R_I and R_ρ ranks. In addition, a final ranking (R) is developed which is the one-to-one addition of R_I and R_ρ ranks.

In Publication V, based on the coexistence performance of IEEE 802.15.4 under WLAN interference, it is recommended to select the channels from first group given that the SINR on those channels is more than 15 dB. If no such channel is available either due to low SINR or if sensor link strength is unknown, the channel has to be picked from the second group.

The final rankings in Table 6.2, which heuristically combines strength and activity ranks, has certain discrepancies. First, often the final ranks are the same and it is not apparent to give preference to a channel with better strength rank or better activity factor rank. Therefore, a node cannot decide on such channels without knowing the effect the two estimators have on channel quality. Second, when the strength and activity values are ranked beforehand then the magnitude or cardinal utility of the estimators is lost and we encounter a voting paradox for preferring one channel over another. Therefore, in the next section, we propose to utilize actual channel occupancy and strength estimates and scale/weight each estimator as per their impact on channel quality.

6.4.3 Decision Theoretic Ranking

The performance degradation in an interfered sensor link can best be understood from PDR curves which are drawn as a function of SINR and interference activity factor. Figure 6.3 shows that the PDR decreases with the increase in interference packet rate for a given SINR. Also, the PDR increases with the increase in SINR. In short, the effect of interferer strength and activity factor on the PDR is relative to the signal strength of the sensor link. However, given that the sensor link strength is unknown, first it is difficult to establish a performance metric based on the interference estimates and secondly the degree to which each interference parameter will degrade the channel quality is not obvious for a sensor node.

In Publication VI, channel ranking is based on a fitness function of weighted interference parameters which is synthesized using the decision theoretic framework of the Analytic Hierarchy Process (AHP) [132]. The fitness function assigns the weights based on the influence of each interference parameter on the channel quality from an interfered receiver perspective. To this end, the fitness function provides a mapping of

interference parameters to the PDR without knowing the sensor link strength. We show that weighting the interference parameters according to their individual influence on the channel quality, as compared to the heuristic approach adopted in Publication V, achieves significant improvement in channel ranking performance.

In Publication VI, the interference parameters are estimated for each channel realization in Fig. 6.4 using Type-III estimators given in Table 6.2. These low-complexity estimators achieved the same rankings as given in Table 6.2, however the problems associated with a heuristic combination of interference estimates remains the same.

The channel fitness function (F_k) from the interference estimators $(\hat{I}_k)$ and $(\hat{\rho}_k)$ at a channel k must be defined using an interference function $f(\cdot)$ such that it gives a point mapping on the PDR curves for the given link strength and interference parameters.

$$F_k = f\left(\hat{\rho}_k, \hat{I}_k\right) \tag{6.4}$$

Therefore, the interference function with respect to PDR curves must observe the following properties

$$\begin{cases} 0 \leq f(\rho, I) \leq 1 & \forall\, [\rho, I] \\ f(\rho_1, I_1) \geq f(\rho_2, I_2) & \rho_1 < \rho_2, I_1 < I_2 \\ f(\rho, I) \geq f(\alpha\rho, I) & \alpha > 1 \end{cases}$$

Using these properties, we come to the following definition for relative channel ranking.

Definition 1: A function $f(\rho, I)$ is a mapping function such that for a given ρ_1, I_1 and ρ_2, I_2 if $\text{PDR}(\rho_1, I_1) > \text{PDR}(\rho_2, I_2)$ then the order $f(\rho_1, I_1) > f(\rho_2, I_2)$ is also preserved.

Considering the degree of influence of each interference parameter in PDR curves, the interference parameters in Eq. (6.4) must be scaled appropriately. For this purpose, we structure this problem using the AHP decision theoretic approach. AHP is a multiple criteria decision-making technique which have been applied to design a routing protocol [133], cluster-head selection [134] and modeling the application requirements [135].

AHP has three phases namely decomposition, comparative judgment and synthesis [132]. The *decomposition* phase for channel ranking problem is shown in Fig.6.5. This top-down structure builds a relationship among goal (fitness of channels), criteria (interference parameters)

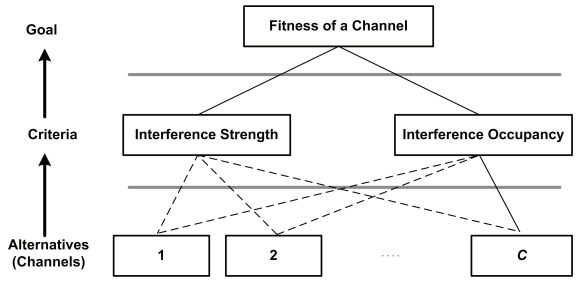

Figure 6.5. AHP structuring of the channel ranking problem under the interference estimates

and alternatives (channels). In *comparative* judgment, the interference parameters are compared pairwise as to the strength of their individual influence on the fitness of the channels. These comparisons may be taken from actual measurements or from a fundamental scale. Saaty [132] suggested a nine-point scale from z_1 to z_9 to quantify the pairwise preferences where z_1 represents indifference of the elements and z_9 the extreme dominance of one element to the other. The pairwise comparison matrix $\mathbf{A}$ for I and ρ is

$$\mathbf{A} = \begin{array}{c} \\ I \\ \rho \end{array} \begin{array}{c} \begin{array}{cc} I & \rho \end{array} \\ \begin{bmatrix} \frac{z_I}{z_I} & \frac{z_I}{z_\rho} \\ \frac{z_\rho}{z_I} & \frac{z_\rho}{z_\rho} \end{bmatrix} \end{array} \tag{6.5}$$

where a_{ij} is the ratio of the scale of the ith element to the scale of the jth element. The $\mathbf{A}$ is a consistent matrix and the normalized principle eigenvector from $\mathbf{A}\mathbf{w} = \lambda^{'}\mathbf{w}$ gives the desired weight vector $\mathbf{w} = (w_I, w_\rho)$.

In the final *synthesis phase*, the rankings are established by assigning the weights to each of the criteria. The resulting fitness (F_k) function is

$$\begin{bmatrix} F_1 & F_2 & \dots & F_C \end{bmatrix} = \begin{bmatrix} w_I \\ w_\rho \end{bmatrix}^T \begin{bmatrix} I_1^{'} & I_2^{'} & \dots & I_C^{'} \\ \rho_1^{'} & \rho_2^{'} & \dots & \rho_C^{'} \end{bmatrix} \tag{6.6}$$

where $I_k^{'} = \frac{\hat{I}_k}{I_{\min}}$ normalizes the interference strength estimate of a channel k with the minimum interference strength estimate of a channel in the channels set such that $I_k^{'} \in [0, 1]$. Similarly $\rho_k^{'} = \frac{\hat{\rho}_k}{\rho_{\max}}$, where the temporal occupancy estimate of a channel is normalized with the maximum occupancy estimate. Equation (6.7) computes the fitness of a channel by summing the contributions as

$$F_k = w_\rho \rho_k^{'} + w_I I_k^{'} \tag{6.7}$$

which evaluates the fitness of a channel by assigning the weights to the normalized values of two interference estimators with $F_k \in [0, 1]$.

Scaling Interference Estimators for Channel Ranking

The PDR curves (Fig. 6.3), do not clearly describe the degree to which the interference estimators will degrade the channel quality when the desired link strength is unknown. In order to determine the weights for interference estimators and find channel ranking, we followed a four-step procedure:

- *True* channel ranking is obtained from the PDR curves (Fig. 6.3.a). Assuming a sensor s_1 (Fig. 6.4) has a certain SINR with sensor s_2, the PDR is observed at that SINR for all activity factors. Another SINR point is selected for location s_2 and s_3 and the procedure is repeated. We get PDR for fifteen channels and determine the true ranking.
- Assuming that the interference strength perceived on a channel affects z times more than the activity factor on the same channel where $z \in \left[\frac{1}{9}, 9\right]$ and $z \neq 0$. Then the weight of each estimator is determined from the eigenvector of Eq. (6.5) and the normalized values of the interference estimates are weighted to establish *estimated* ranking from Eq.(6.7).
- The true and estimated channel rankings are compared element by element and channel ranking error is computed by the Euclidean norm of the difference between the two rankings.
- The above steps are repeated for all z.

This procedure is iterated for extensive SINR selections. At first, the SINR difference between s_1–s_2 and s_2–s_3 is kept small to replicate the scenario in which the interference strength varies slightly among the channels. We called these channels as *Type-I channels*. For such channels, the ranking error is lower if the two interference estimators are scaled equally. Later, the SINR difference is increased significantly. Here, the minimum ranking error occurs when the strength estimate is scaled 7-8 times more than the activity factor. We called these channels *Type-II channels*. The transition from Type-I to Type-II channels occurs if the SINR difference between any two locations is greater than 1.4 dB. The ranking error for these channel types is shown in Fig. 6.6.a. The vertical bars along each trend line indicates the confidence interval of ranking error. The possibility of finding a single best channel under these scales is shown in Fig. 6.6.b where check mark ($\surd$) indicates that the best channel is always found otherwise it is crossed (X).

From definition 1, the uniqueness of a channel rank is true given that for any two channels i and j if $\text{PDR}(\rho_i, I_i) > \text{PDR}(\rho_j, I_j)$ then with the appropriate selection of weights w_ρ and w_I our estimated channel ranks also follow $f(\rho_i, I_i) > f(\rho_j, I_j)$. In our channel ranking, this condition is closely satisfied for all the channels while it is strictly satisfied for the unique least interfered channel. This behavior leads to the definition of two distinct decision rules for assigning weights to the interference estimators; especially when a node cannot estimate SINR and only interference estimators are available. The rules are independent from the PDR-SINR model and a transitional boundary governs the transition between the rules depending on the spread of the energy level estimator of interfered channels. The rules are applicable without loss of generality to any modulation type employed by the sensors for channel ranking. This distinction makes our proposal for finding the least interfered channels for network initialization unique.

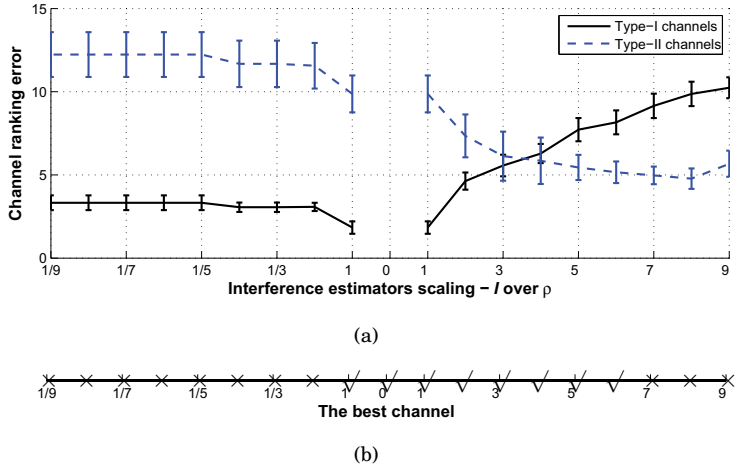

Figure 6.6. Channel ranking error in two channel types with respect to the preference scale of interference estimators

6.4.4 Comparison of Heuristic and Decision Theoretic Ranking

We compared the ranking error in heuristic and decision theoretic approaches with respect to true channel ranks. The ranking error is given in Table 6.3 for different SINR separations. Channel ranking under decision theoretic approach is shown to have better performance than heuristic ranking. For any selection of SINR separations, decision theoretic channel ranking outperforms the HCR.

We also observed the impact of channel ranking error on packet loss for

Table 6.3. Ranking error performance of heuristic and decision theoretic channel ranking

Channel type	SINR (dB)			Ranking approach	
	s_1	s_2	s_3	Heuristic	Decision theoretic
Type-I	2.0	2.4	2.6	8.7	2.4 (z = 1)
	2.0	2.7	3.4	8.1	1.6 (z = 1)
	2.0	3.4	4.8	6.7	2.2 (z = 1)
Type-II	2.0	4.4	6.8	6.3	4.9 (z = 8)
	2.0	4.0	9.0	6.8	5.7 (z = 8)
	2.0	7.0	9.0	6.4	3.9 (z = 8)

two approaches. Assuming only the five best-ranked channels are used by a node, we calculated the additional packet loss because of choosing the wrong channels in the channel set. It is observed that the decision theoretic approach can mostly identify the ranks accurately and the additional packet loss is less than 16% as an estimated channel rank, although misplaced, is ordered quite close to true channel rank. Whereas, the HCR approach can lead to a packet loss of up to 48%.

6.5 PDR-Estimation-Based Channel Ranking

In this section, we present two PDR-estimation-based channel ranking schemes. The first scheme determines the relative ranks of the channels such that the effect of interfering traffic distribution is incorporated although cannot be estimated by low-power sensors. The second scheme develops channel ranks based on the accurate PDR estimation.

6.5.1 Scheme I

If the PDR of an interfered link is estimated accurately, it can be directly used as a channel quality metric for channel ranking. The PDR estimation using Eq. (6.1) or Eq. (6.2) requires the estimation of interferer characteristics. The signal strength level and activity factor can be estimated easily, however, it is difficult to estimate the realistic WLAN traffic distributions accurately for each measured channel. The realistic WLAN traffic can be modeled by phase-type distributions [91] that is also verified in Publication VIII. However, the parameter estimation of such distributions is difficult with limited energy measurements.

Owing to the constraint on traffic distribution estimation, the exact PDR cannot be estimated. However, the objective is not to estimate

the exact PDR but to determine the relative ranks of the channels, that is, find the channels which can yield the highest PDR. Therefore, a relative channel ranking scheme is formulated in Publication VII by studying the effect of different traffic distributions on channel ranking performance by extensive simulations. The ranking performance under a traffic distribution is measured in two-steps as: **(a)** PDR is estimated for each measured channels based on their SINR and activity factor estimates, and by assuming a traffic distribution, **(b)** channels are ranked with respect to estimated PDRs and the ranking error probability (REP) is measured. A channel ranking algorithm is proposed based on the traffic distribution giving the upper bound on REP for PH traffic. In addition, a numerical approximation to calculate the lower and upper bound on REP is presented such that for a given REP target the appropriate channel measurement time can be set.

Ranking Error Probability

A channel ranking algorithm is reliable if the ranks of the channels are mostly determined correctly. A channel ranking error occurs when a channel with the higher PDR is ranked lower than the channel with the lower PDR channel. The channel ranking performance can be described in terms of REP. We studied the effect of traffic distributions on the REP by simulations.

The simulations are carried out for two channels such that the PDR in channel 1 is always higher than that of channel 2. In each simulation run we first compute the interference and activity estimates for both channels. Then, we calculate their PDR for periodic, Poisson and PH traffic distributions. If the PDR for channel 1 is estimated to be lower than that of channel 2, a ranking error occurs. The REP is computed as an average of such ranking errors. The REP for these traffic distributions is shown in Fig. 6.7. The notable observations from Fig. 6.7 are:

- The REP decreases with the increase in measurement time, since the errors in interference and activity estimates decrease.
- The REP decreases with the decrease in SINR. A rational justification for this observation is the slope of the PDR curves with respect to SINR (see Fig. 5.5).
- The REP for PH traffic always falls within that of periodic and Poisson distributions. This behavior suggests that a single periodic

and Poisson flow can be used as the lower and upper bounds on REP for any interfering traffic distribution.

Channel Ranking Algorithm

As observed in Fig. 6.7, the periodic and Poisson traffic distributions give the lower and upper bound respectively on REP for PH traffic, a channel ranking algorithm can be designed such that a sensor node estimates the interference level and the activity factor for all the channels and subsequently their PDR by using Poisson traffic. The channel with the highest PDR estimate is ranked higher and it is favored for communication.

The channel ranking must be established based on the upper bound on ranking error in case the sensor must guarantee a certain REP. In addition, a lower bound on the REP can be obtained by estimating the PDRs by using periodic traffic distribution. Hence, even though the WLAN interfering traffic is usually modeled with phase-type (PH) distributions, the periodic and the Poisson traffic distributions allow us to bypass the traffic estimation process and relatively rank the channels based on their SINR and activity factor estimates. In the next section, a numerical approximation to calculate these bounds quickly is presented.

Channel Ranking Error Approximation

A low complexity and fast method for evaluating REP is desirable such that a sensor can determine the measurement time quickly for a target REP. In this section one such method to estimate the REP for Poisson and periodic traffic is proposed.

Assuming the interference level is well above the noise level, the miss-detection probability is practically zero. Also, by maintaining the false alarm rate under 10^{-3} we can make the following approximation: in the N_{T_S} times the decision statistic is evaluated at most one false alarm event may occur. Therefore, one may assume there are only four possible outcomes (or cases) when the activity is estimated. The Case 1 corresponds to the situation where a false alarm does not occur for any channel. The Cases 2 and 3 correspond to the situation where one false alarm occurs for the second and first channel, respectively. Finally, the Case 4 describes the situation where both channels suffer from a false alarm. Therefore, the REP can be approximated as a sum of only four terms.

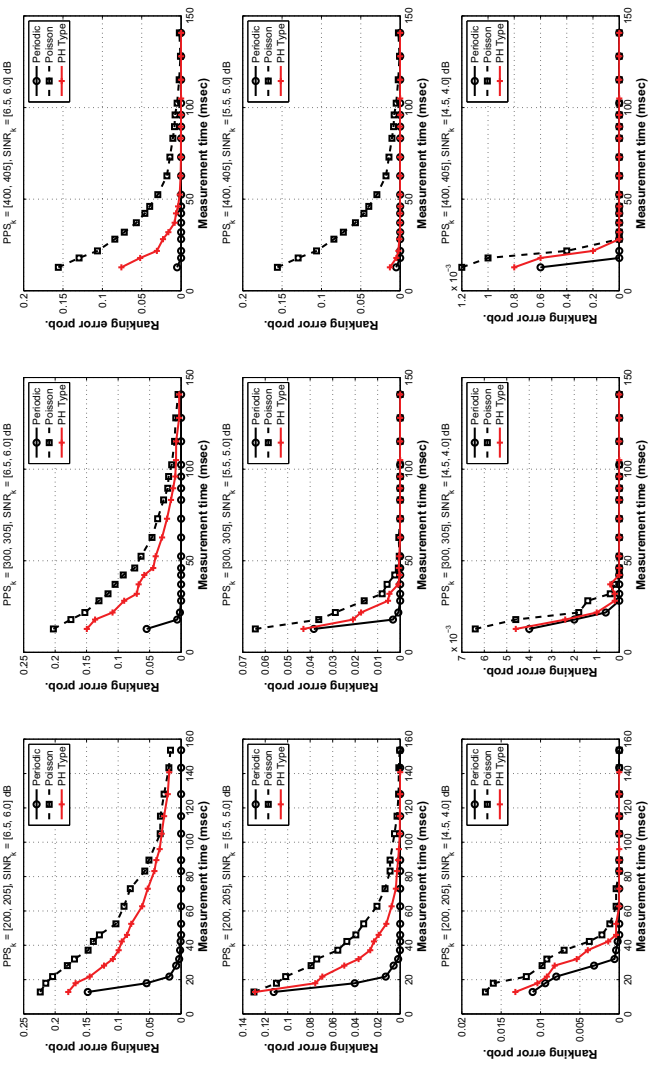

Figure 6.7. Ranking error probability under different interfering traffic patterns

$$\mathrm{Pr}_{\varepsilon} \approx \sum_{j=1}^{4} \mathrm{Pr}_{cj} \cdot \mathrm{Pr}_{\varepsilon j} \tag{6.8}$$

where the Pr_{ϵ} stands for the REP, $\mathrm{Pr}_{cj}, j = 1, \ldots, 4$ stands for the probability that the jth case occurs and $\mathrm{Pr}_{\epsilon j}$ denotes the REP in the jth case.

In order to calculate $\mathrm{Pr}_{\epsilon j}, j = 1, \ldots, 4$, it is assumed, without any loss of generality, that the channel 1 is characterized by the lower PDR. While calculating the PDR curves in Fig. 6.3, the interference level is discretized. Let us assume that N_I interference levels are utilized, $I_i^{(j)}, j = 1, \ldots N_I$, and the discretization step is denoted by dI. Given the actual interference level, I_i, the probability the interference level is estimated to be $I_i^{(j)}$ is obtained by integrating the PDF of $1/N_i \sum_{j=1}^{N_i} L_i^{(j)}$ in the interval $I_i^{(j)} \pm dI/2$. Since the sum of normal random variables follows the normal distribution, one can calculate the parameters of the distribution $1/N_i \sum_{j=1}^{N_i} L_i^{(j)}$. For instance, for case 1 the mean value of $1/N_i \sum_{j=1}^{N_i} L_i^{(j)}$ is $\mu_i = I_i + P_N$ because no false alarm is assumed to occur.

Assume $\mathrm{PDR}_{1,j}$ is the PDR in channel 1 when the interference level takes the jth out of the N_I total possible values. Then, the interference level of channel 2, I_2', resulting in a PDR equal to $\mathrm{PDR}_{1,j}$ can be obtained by moving horizontally until the PDR curve of channel 2 is met. The REP $\mathrm{Pr}_{\epsilon i}$ is computed by integrating over the set of interference levels making the PDR of channel 2 lower than $\mathrm{PDR}_{1,j}$. This is equal to the CDF value of a normal distribution with parameters μ_2, σ_2 evaluated at I_2'. Mathematically, the REP $\mathrm{Pr}_{\epsilon i}$ can be expressed as:

$$\mathrm{Pr}_{\varepsilon i} = \sum_{j=1}^{N_I} \left(\int_{I_1^{(j)} - dI/2}^{I_1^{(j)} + dI/2} \frac{1}{\sqrt{2\pi\sigma_1^2}} e^{-\frac{(x + P_N - \mu_1)^2}{2\sigma_1^2}} dx \right) \times \frac{1}{2} \left(1 + \mathrm{erf}\left(\frac{I_2' + P_N - \mu_2}{\sqrt{2\sigma_2^2}} \right) \right) \tag{6.9}$$

In Table 6.4, the proposed method to evaluate the REP is validated against simulation results for periodic and Poisson traffic using exemplary values. The results illustrate that the four terms are enough to obtain a sufficient approximation for the REP.

6.5.2 Scheme II

The PDR formulation in Eq. (5.2) requires the estimation of interfering traffic distribution which is not feasible for power-limited WSNs. Owing to this constraint, the channel ranking scheme presented in the previous

Table 6.4. REP results for periodic and Poisson traffic by simulations and numerical approximation. In each row the top value refers to the simulation result and the bottom value to the numerical approximation

Traffic type	Activity (PPS)	SINR (dB)	
		6.5/6.0	5.5/5.0
Periodic	200/205	0.1482	0.1124
		0.1436	0.1095
	300/305	0.0602	0.0384
		0.0588	0.0381
Poisson	200/205	0.2236	0.1300
		0.2196	0.1278
	300/305	0.2028	0.0644
		0.2013	0.0632

section resorts to relative channel ranking based on PDR estimation, from SINR and activity factor estimates, assuming the traffic distribution giving upper bound on ranking error.

However, the PDR model presented in Publication IX and discussed in Section 5.5.3 allows accurate PDR estimation and therefore can directly be used for channel ranking. This model estimates PDR of an interfered link with a spectrum measurement scheme which incorporates the interfering traffic characteristics the link will experience on its scheduled traffic. In Publication IX, the channel ranking performance of this model is verified by ranking the channels in a IEEE 802.15.4-based sensor network in the presence of WLAN interference.

The considered environment is an indoor office space. In this environment, the spectral activity from co-located WLANs on the candidate channels to the sensor network is such that a sensor node can sense WLAN activity on any channel other than channels 25 and 26. A snapshot of perceived interference at a sensor location is shown in Fig. 6.8. This sensor acts as a receiver and establishes a LOS communication link with another sensor. The sensor estimates PDR on each channel and then ranks all 16 available channels based on the estimated PDRs.

The PDR estimation on a channel depends on the the link strength and interference characteristics. We measured the average link strength over a channel with probe packets. It was observed that the link strength did not vary much on a given channel however it varied significantly across channels due to frequency-selective fading [52]. On the other hand, the interference characteristics were taken into account by collecting 40 macro-samples. After estimating PDR on a channel, empirical PDR is

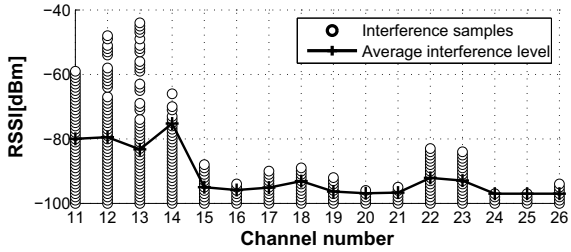

Figure 6.8. Perceived interference strength on IEEE 802.15.4 channels

calculated over 1000 packets. These steps are repeated for all 16 channels and the channels are sorted according to PDRs. Table 6.5 shows the estimated and actual ranks.

Table 6.5. Channel ranking based on PDR estimation and empirical PDR

	PDR		Channel Rank	
Channel #	Experiment	Estimate	Experiment	Estimate
11	70	78	16	15
12	71	76	15	16
13	76	79	14	14
14	78	80	13	13
15	99	99	6	6
16	97	96	8	8
17	97	95	9	9
18	86	82	12	12
19	99	99	7	7
20	100	100	1	1
21	100	100	2	2
22	90	95	10	10
23	90	90	11	11
24	100	100	3	3
25	100	100	4	4
26	100	100	5	5

Table 6.5 shows that the estimated ranks based on PDR estimation are as accurate as the ranks based on the empirical PDR. There is one ranking mistake in which channels 11 and 12 are misplaced due to the fact that these channels had very close PDRs.

These results highlight the effectiveness of the proposed PDR estimation scheme for channel ranking in WSN. Under this scheme, the PDR can be estimated without prior knowledge or estimation of the interfering traffic patterns. Also, in a large sensor network given that all the sensors have with the same traffic model, a receiver node can determine the PDR estimates of the associated links with a single set of channel measurements.

6.6 Summary

In this chapter, low-complexity channel ranking schemes are proposed for coexistence enhancement in WSNs in the presence of WLAN interference. The channel ranking schemes are receiver-centric; that is, a receiver estimates the link-quality to an adjacent node on the candidate channels and determines the channel ranks accordingly. The link-quality is estimated using a channel quality metric (CQM) that is designed with respect to the availability of connectivity information in a sensor network; for instance at network initialization the link strengths to the adjacent nodes are not known whereas it is known at network operation phase.

For channel ranking at network initialization, interference parameters, signal strength and activity factor are used in Publication V and Publication VI. How these parameters individually effect a sensor link with unknown link strengths is also considered.

We further studied packet delivery ratio based channel ranking schemes in Publication VII and Publication IX. Since PDR estimation requires interfering traffic distribution, our first scheme establishes a relative channel ranking with respect to a traffic distribution giving a bound on the ranking error. In the second scheme, channel ranking is based on the exact PDR estimation scheme.

7. Conclusions and Future Work

7.1 Conclusions

By enabling to instrument and gather information through untethered sensors, WSNs provide an efficient infrastructure to interact with the physical world. WSNs are a low-cost and easy-to-deploy alternative to wired remote sensing networks with higher monitoring fidelity and fault-tolerance. In the past decade, these attributes encouraged numerous WSN-based sensing and actuation applications. Realizing an application, however, greatly depends on the network management protocols and algorithms that can guarantee coordination and connectivity among sensors over low-power wireless links.

In this thesis, the author studied network management functions that enable the usage of WSNs for time- and reliability-sensitive applications. These applications require an accurate timing service for coordinated task execution and energy-efficient medium-access scheduling. The medium access, whereas, must be scheduled on the portions of the allocated spectrum that guarantee communication reliability. In this respect, the studied management functions are time synchronization, and interference awareness under spectral coexistence.

Time synchronization is provided by a combination of a messaging protocol and clock synchronization algorithm.

The messaging protocol diffuses the reference time in the network using either handshake or broadcast schemes. Broadcast schemes are appreciated for their low energy demands. In this thesis, a broadcast-based scheme is studied with a focus on the elaboration of associated synchronization aspects.

The clock synchronization algorithms are responsible for time correction

in the nodes based on the received reference time reports. The time correction is achieved by offset adjustment in a local clock with respect to the reference clock. The author analyzed the factors contributing to the clock offset budget in the sender-receiver path of the reference broadcasts. Together with MAC layer timestamping, this analysis provided accurate synchronization as validated using a sensor platform. In addition, a method for scalable diffusion of reference time reports is hypothesized.

The offset adjustment provides instantaneous synchronization only because the clocks deviate with time. The deviations originate from the inaccuracy and instability of the oscillator driving a clock. As a result, the nodes rely on periodic reference time reports, which causes drainage of resources. However, the identification of clock skew (change in phase difference with time) can provide time correction frequently with less frequent reference time reports. In this thesis, the author investigated a LS linear-regression-based clock skew estimator. It is shown how the non-linearity in the clock skew affects the synchronization accuracy unless the regression size is adapted according to the synchronization period. The author also provided the clock skew data of sensors to validate a recursive ML clock skew estimator. The ML estimator achieves smallest estimation error variance by utilizing a time relation model that reflects correlation in the clock offset measurements.

The question of how well the synchronization service translates into the application requirements asks for the design of interfaces using synchronized clocks. In this thesis, the author extending the synchronization service to task synchronization in an SHM application and time-slotted communication. The task synchronization was aimed at maintaining tight synchronicity among acceleration samples collected by distributed sensors. By enabling such synchronicity among the sensors, WSN provided accurate extraction of modal analysis parameters. The author also developed a synchronization interface for communication scheduling in a protocol stack. This interface allowed reliable execution of a schedule which exploits time and channel diversity.

In the past decade, IEEE 802.15.4 has emerged as a *de facto* PHY layer standard for low-power WSNs. It operates universally on a 2.4 GHz unlicensed band. The 2.4 GHz band, however, is crowded by standards with heterogeneous medium access rules. The spectrum sharing under geographical coexistence had been a reliability concern for IEEE 802.15.4, specifically from WLAN systems. In this thesis, the author addressed this

concern by modeling the coexistence performance of WSNs and extended it to formulate interference-aware coexistence enhancement schemes.

Under spectral coexistence, the link-quality in an interfered network is a function of SNR, SINR and packet collision-time. The collision-time itself depends on the activity factor, packet size and packet inter-arrival time distributions of the two coexisting networks. By combining all these factors, the link-quality can be effectively modeled in terms of PDR. However, modeling collision-time is a complex process and there exist deterministic models only in the literature. In this thesis, the author proposed a stochastic packet collision model which provided theoretical evaluation of collision-time distribution for a given traffic scenario. The model is demonstrated to be effective for link-quality analysis in the presence of simple to realistic interfering traffic distributions.

Given the PDR is estimated quickly and efficiently, it can play a vital role in network management. The author studied two energy-detection-based PDR estimation models. The first PDR model requires the estimation of interference parameters. The estimation of these parameters is discussed with respect to their complexity for sensors. In reality, these parameters cannot be determined satisfactorily with limited energy measurements. The second PDR model is independent of estimating the parameters separately. Instead, in this scheme, the energy measurements are collected considering the traffic on the sensor link. The PDR is then estimated using these measurements in association with the link strength and the BER specifications of the interfered system.

The coexistence analysis reveals the severity of WLAN interference. Unless, an interference-aware operation on favorable channels is enforced, a WSN cannot ensure reliability to the application. In this respect, the author developed low-complexity channel ranking schemes for coexistence enhancement. The channel ranking is based on a channel quality metric (CQM). In general, the CQM design is such that a node, acting as a receiver, can interpret the quality of an interfered link on a channel. The CQM design, in particular, depends on the availability of network connectivity information. If available, PDR can also serve as CQM otherwise the CQM has to be designed using interference parameters only.

At network initialization, the signal strengths of the links to the neighbors are unknown. The question then arises: which channel should be preferred more, the one with lower signal strength or the one with lower activity factor?. This thesis studied two solutions to the problem:

heuristic combination of interference parameters and a decision-theoretic weighted combination of each parameter. The ranking under decision theoretic approach resulted in fewer ranking errors. The challenges in using PDR as CQM for channel ranking are also explored in this thesis. The author studied the impact of interfering traffic distributions on channel ranking error for a given measurement time. In order to bypass the traffic estimation process, an algorithm to establish relative channel ranking is proposed. For this purpose, traffic distribution setting upper bound on ranking error is utilized for ranking and a numerical method to calculate the ranking error probability is developed. In addition, the ranking performance of the PDR estimation scheme, which does not rely on separate estimation of interference parameters, is also validated.

7.2 Future Work

We briefly discuss here the directions for future work that are closely related to the motivation of this thesis.

The time synchronization error grows with the number of hops from the reference clock. A possible future direction is to model the behavior of networked clocks to keep the synchronization error bounded. In addition, we noticed that the clock mismatch observed in the distributed collection of acceleration samples is higher than the original clock mismatch. A study is required to analyze and compensate for the factors contributing to the time errors in distributed task execution.

We analyzed the effect of interfering packet distributions on the packet delivery ratio of an interfered link. In this analysis, mean SINR is assumed for multi-terminal scenarios. Modeling SINR distribution under realistic node locations and channel fading, and formulating the PDR model accordingly is an interesting research problem. For channel ranking, the possible future topic of research is collaborative ranking. The motivation for this study is to minimize the sensing overhead by scanning fewer channels at a node and using neighbors' recommendations to find the ranks of the remaining channels.

A. Sensinode WSN Platforms

In this appendix we briefly describe the hardware and software components of WSN platforms developed by Sensinode [136]. These platforms, in this thesis, are referred to as Micro.CC2420 and Nano.CC2430 based on the utilized radio transceivers. The software, operating system and communication stack, are common in both platforms. Although, Sensinode has discontinued these platforms, the main components on which these platforms are built on are widely accepted by the WSN community.

A.1 Hardware Components

The hardware description mainly covers the microcontroller unit (MCU) and radio chip of a platform.

A.1.1 Micro.CC2420

Micro.2420 platform integrates Texas Instruments' MSP430 MCU and CC2420 radio. The MCU has an 8 MHz clock source, 10 KB RAM and 256 KB flash memory. CC2420 is a low-power IEEE 802.15.4-compliant radio transceiver with an effective data rate of 250 Kbps. Micro.2420 platform is powered by a battery voltage of 1.5 V to 2.6 V. The platform supports additional sensors through two external connectors.

Hardware Timers
The MCU of Micro.2420 provides two 16-bit timers, `Timer-A` and `Timer-B`. `Timer-B` runs as local clock of the node for task scheduling and other MAC layer operations, for example random back-off, acknowledgments expiry time, etc. `Timer-A` is free and it is used for time synchronization in Publication III and Publication IV. `Timer-A` has one 16-bit counter (`TAR`) and three 16-bit configurable compare/control registers (`TACCRx`). The

source of Timer-A is 8 MHz clock derived from an external 16 MHz crystal oscillator which can be further divided to take on the user's desired tick resolution.

A.1.2 Nano.CC2430

Nano.CC2430 platform is based on Texas Instruments' CC2430 System-on-Chip (SoC) solution. The SoC is designed specifically for IEEE 802.15.4 and Zigbee applications. CC2430 combines the performance of CC2420 radio with 8051 MCU. The CC2430 clock source is a 32 MHz crystal oscillator with 8 KB RAM and 128 KB flash memory. Nano.CC2430 supply voltage range is 2.0 V to 3.6 V.

Hardware Timers
Nano.CC2430 has one 16-bit timer (`Timer1`), one 24-bit Sleep Timer, one MAC timer (`Timer2`) and two 8-bit timers (`Timer3`, `Timer4`). Sleep Timer is used to maintain the local clock and task scheduling. `Timer2` and `Timer3` are used to implement backoff and ACK expiry time. We used `Timer1` to realize a time synchronization clock in Publication I. `Timer1` has one 16-bit counter (`T1CCTx`) and three independent compare/capture channels. The clock source of the timer is 32 MHz crystal oscillator. The counter increments at each active clock edge while the clock edge frequency can be varied from 0.25 MHz to 32 MHz.

A.2 Software Components

The integral software components of the platforms are explained in the following sections.

A.3 Protocol Stack – NanoStack

NanoStack is a protocol stack which implements IEEE 802.15.4 MAC and also provides drivers for CC2420 and CC2430 radios. The stack includes 6LoWPAN, User Datagram Protocol (UDP), Internet Control Message Protocol (ICMP) and Simple Sensor Interface (SSI). A custom protocol can be defined for NanoStack as a protocol element.

NanoStack v1.x provides a socket interface to the application layer for data communication. It also provides memory management features for

flexible buffer operation. For further details on NanoStack architecture and buffer management, one can refer to the work by Sergio *et al.* [137]. NanoStack was initially distributed under GPL license but as of January 2009 the stack is closed.

A.4 Operating System – FreeRTOS

FreeRTOS is an open-source real-time operating system for small embedded systems [138]. It supports large variety of processor architectures and compilers. FreeRTOS provides a micro-kernel with a scheduler, MCU-specific code, memory allocation, queues, and semaphores along with system-timer functionality. The scheduler is capable of running tasks in preemptive, cooperative and hybrid modes. By using scheduler and inter-task communication, FreeRTOS can switch between different tasks and run them apparently concurrently.

NanoStack v1.x is executed as a single task in the FreeRTOS environment. It uses FreeRTOS timing facilities and implements some extensions, such as an asynchronous timer service. The FreeRTOS source tree used by NanoStack is not modified, which gives NanoStack the flexibility to upgrade the FreeRTOS version without update patches.

Bibliography

[1] I. F. Akyildiz, W. Su, Y. Sankarasubramaniam, and E. Cayirci, "A survey on sensor networks," *IEEE Communications Magazine*, vol. 40, no. 8, pp. 102–114, 2002. *Cited on page(s): 1*

[2] J. Yick, B. Mukherjee, and D. Ghosal, "Wireless sensor network survey," *Computer Networks*, vol. 52, no. 12, pp. 2292–2330, Aug. 2008. *Cited on page(s): 1*

[3] IBM: A Smarter Planet, http://www.ibm.com/smarterplanet/, accessed: 07/07/2013. *Cited on page(s): 1*

[4] Z. Shelby and C. Bormann, *6LoWPAN: The Wireless Embedded Internet*. Wiley Publishing, 2010. *Cited on page(s): 2*

[5] IEEE Std.802.15.4, "IEEE standard for wireless medium access control (MAC) and physical layer (PHY) specifications for low-rate wireless personal area networks (LR-WPANs)," pp. 1–320, 2006. *Cited on page(s): 2, 44, 54*

[6] ZigBee Alliance, "Zigbee specification 053474r17," 2007. *Cited on page(s): 2, 66, 68*

[7] WirelessHART, "Hart field communication protocol specification, revision 7.0," *HART Communication Foundation*, Sept. 2007. *Cited on page(s): 2, 34, 66*

[8] ISA-100.11a-2009 Standard, "Wireless systems for industrial automation: Process control and related applications," *Intl. Society of Automation (ISA)*, 2009. *Cited on page(s): 2, 34, 66, 68*

[9] L. Stabellini, "Toward reliable wireless sensor networks: Energy-aware distributed interference management for unlicensed bands," Ph.D. dissertation, KTH, 2010. *Cited on page(s): 2*

[10] D. Mills, "Internet time synchronization: the network time protocol," *IEEE Transactions on Communications*, vol. 39, no. 10, pp. 1482–1493, 1991. *Cited on page(s): 9, 26*

[11] E. Serpedin and Q. M. Chaudhari, *Synchronization in Wireless Sensor Networks: Parameter Estimation, Peformance Benchmarks, and Protocols*. Cambridge University Press, 2009. *Cited on page(s): 9, 11*

[12] S. Ganeriwal, R. Kumar, and M. Srivastava, "Timing-sync protocol for sensor networks," in *Proceedings of the 1st ACM Intl. Conference on Embedded Networked Sensor Systems*, 2003, pp. 138–149. *Cited on page(s): 9, 12*

[13] J. Elson, L. Girod, and D. Estrin, "Fine-grained network time synchronization using reference broadcasts," *ACM SIGOPS Operating Systems Review*, vol. 36, no. SI, pp. 147–163, 2002. *Cited on page(s): 9, 10, 11, 17*

[14] M. Maróti, B. Kusy, G. Simon, and Á. Lédeczi, "The flooding time synchronization protocol," in *Proceedings of the 2nd ACM Intl. Conference on Embedded Networked Sensor Systems*, 2004, pp. 39–49. *Cited on page(s): 9, 11, 14, 17*

[15] Y.-C. Wu, Q. Chaudhari, and E. Serpedin, "Clock synchronization of wireless sensor networks," *IEEE Signal Processing Magazine*, vol. 28, no. 1, pp. 124–138, 2011. *Cited on page(s): 10, 11*

[16] J. Elson and K. Römer, "Wireless sensor networks: A new regime for time synchronization," *ACM SIGCOMM Computer Communication Review*, vol. 33, no. 1, pp. 149–154, 2003. *Cited on page(s): 11, 12*

[17] E. Kaplan and C. Hegarty, *Understanding GPS: principles and applications*. Artech House Publishers, 2006. *Cited on page(s): 11*

[18] IEEE Std 1588-2008 (Revision of IEEE Std 1588-2002), "IEEE standard for a precision clock synchronization protocol for networked measurement and control systems," pp. c1 –269, 24 2008. *Cited on page(s): 11, 26*

[19] B. Sundararaman, U. Buy, and A. D. Kshemkalyani, "Clock synchronization for wireless sensor networks: a survey," *Ad Hoc Networks*, vol. 3, no. 3, pp. 281–323, 2005. *Cited on page(s): 11*

[20] W. Su and I. F. Akyildiz, "Time-diffusion synchronization protocol for wireless sensor networks," *IEEE/ACM Transactions on Networking*, vol. 13, no. 2, pp. 384–397, 2005. *Cited on page(s): 12*

[21] S. Yoon, C. Veerarittiphan, and M. L. Sichitiu, "Tiny-sync: Tight time synchronization for wireless sensor networks," *ACM Transactions on Sensor Networks (TOSN)*, vol. 3, no. 2, p. 8, 2007. *Cited on page(s): 12*

[22] J. Van Greunen and J. Rabaey, "Lightweight time synchronization for sensor networks," in *Proceedings of the 2nd ACM Intl. conference on Wireless sensor networks and applications*, 2003, pp. 11–19. *Cited on page(s): 12*

[23] IEEE Std 802.11s-2011, "IEEE standard for information technology–telecommunications and information exchange between systems–local and metropolitan area networks–specific requirements part 11: Wireless lan medium access control (MAC) and physical layer (PHY) specifications amendment 10: Mesh networking," pp. 1–372, 2011. *Cited on page(s): 16*

[24] G. J. Pottie and W. J. Kaiser, "Wireless integrated network sensors," *Communications of the ACM*, vol. 43, no. 5, pp. 51–58, 2000. *Cited on page(s): 16*

[25] K.-L. Noh, E. Serpedin, and K. Qaraqe, "A new approach for time synchronization in wireless sensor networks: Pairwise broadcast synchronization," *IEEE Transactions on Wireless Communications*, vol. 7, no. 9, pp. 3318–3322, 2008. *Cited on page(s): 17*

[26] G. Strang, "Linear algebra and its applications. thomson–brooks," *Cole, Belmont, CA, USA*, 2005. *Cited on page(s): 18*

[27] H. W. Sorenson, *Parameter estimation: principles and problems*. Marcel Dekker New York, 1980. *Cited on page(s): 19*

[28] C. Farrar and K. Worden, "An introduction to structural health monitoring," *Philosophical Transactions of the Royal Society A: Mathematical, Physical and Engineering Sciences*, vol. 365, no. 1851, pp. 303–315, 2007. *Cited on page(s): 23*

[29] A. Rytter, "Vibrational based inspection of civil engineering structures," Ph.D. dissertation, Dept. of Building Technology and Structural Engineering, Aalborg University, 1993. *Cited on page(s): 23*

[30] S. W. Doebling, C. R. Farrar, M. B. Prime, and D. W. Shevitz, "Damage identification and health monitoring of structural and mechanical systems from changes in their vibration characteristics: a literature review," Los Alamos National Lab., NM (United States), Tech. Rep., 1996. *Cited on page(s): 23*

[31] M. Celebi, "Seismic instrumentation of buildings (with emphasis on federal buildings)," *Special GSA/USGS Project, an administrative report*, 2002. *Cited on page(s): 24*

[32] C. R. Farrar, "Damage prognosis: current status and future needs," *Technical Report: LA-14051-MS, Los Alamos National Laboratory, Los Alamos*, 2003. *Cited on page(s): 24*

[33] V. Krishnamurthy, K. Fowler, and E. Sazonov, "The effect of time synchronization of wireless sensors on the modal analysis of structures," *Smart Materials and Structures*, vol. 17, no. 5, p. 055018, 2008. *Cited on page(s): 24, 25, 26*

[34] G. Yan and S. Dyke, "Structural damage detection robust against time synchronization errors," *Smart Materials and Structures*, vol. 19, no. 6, p. 065001, 2010. *Cited on page(s): 24, 25*

[35] T. Nagayama, S. Sim, Y. Miyamori, and B. Spencer Jr, "Issues in structural health monitoring employing smart sensors," *Smart Structures and Systems*, vol. 3, no. 3, pp. 299–320, 2007. *Cited on page(s): 24, 25*

[36] Y. Lei, A. Kiremidjian, K. Nair, J. Lynch, and K. Law, "Algorithms for time synchronization of wireless structural monitoring sensors," *Earthquake Engineering & Structural Dynamics*, vol. 34, no. 6, pp. 555–573, 2005. *Cited on page(s): 25*

[37] T. Nagayama, B. Spencer, G. Agha, and K. Mechitov, "Model-based data aggregation for structural monitoring employing smart sensors," in *Proceedings of the 3rd Intl. Conference on Networked Sensing Systems*, 2006, pp. 203–210. *Cited on page(s): 25*

[38] J. Juang and R. Pappa, "An eigensystem realization algorithm for modal parameter identification and model reduction," *Journal of Guidance, Control, and Dynamics*, vol. 8, no. 5, 2012. *Cited on page(s): 25*

[39] P. Overschee, B. Moor, D. Hensher, J. Rose, W. Greene, K. Train, W. Greene, E. Krause, J. Gere, and R. Hibbeler, *Subspace Identification for the Linear Systems: Theory–Implementation*. Boston: Kluwer AcademicPublishers, 1996. *Cited on page(s): 25, 31*

[40] A. Guyader and L. Mevel, "Covariance-driven subspace methods: input/output vs. output-only," in *Proceedings of the 21st Intl. Modal Analysis Conference*, 2003. *Cited on page(s): 25, 31*

[41] T. Nagayama, M. Abe, Y. Fujino, and K. Ikeda, "Structural identification of a nonproportionally damped system and its application to a full-scale suspension bridge," *Journal of Structural Engineering*, vol. 131, no. 10, pp. 1536–1545, 2005. *Cited on page(s): 25*

[42] M. Fraser, A. Elgamal, and J. P. Conte, "UCSD powell laboratory smart bridge testbed," *SSRP 06/06, Department of Structural Engineering, University of California, San Diego, La Jolla, CA, USA*, 2006. *Cited on page(s): 25*

[43] K. Behrendt, K. Fodero *et al.*, "The perfect time: An examination of time-synchronization techniques," in *Proceedings of the 60th Annual Georgia Tech Protective Relaying Conference*, 2006. *Cited on page(s): 26*

[44] H. Li, J. Ou, X. Zhao, W. Zhou, H. Li, Z. Zhou, and Y. Yang, "Structural health monitoring system for the shandong binzhou yellow river highway bridge," *Computer-Aided Civil and Infrastructure Engineering*, vol. 21, no. 4, pp. 306–317, 2006. *Cited on page(s): 26*

[45] M. Whelan, M. Gangone, K. Janoyan, and R. Jha, "Real-time wireless vibration monitoring for operational modal analysis of an integral abutment highway bridge," *Engineering Structures*, vol. 31, no. 10, pp. 2224–2235, 2009. *Cited on page(s): 26*

[46] S. Kim, S. Pakzad, D. Culler, J. Demmel, G. Fenves, S. Glaser, and M. Turon, "Health monitoring of civil infrastructures using wireless sensor networks," in *Proceedings of the 6th IEEE Intl. Symposium on Information Processing in Sensor Networks (IPSN)*, 2007, pp. 254–263. *Cited on page(s): 26*

[47] M. Ceriotti, L. Mottola, G. Picco, A. Murphy, S. Guna, M. Corra, M. Pozzi, D. Zonta, and P. Zanon, "Monitoring heritage buildings with wireless sensor networks: The torre aquila deployment," in *Proceedings of the IEEE Intl. Conference on Information Processing in Sensor Networks*, 2009, pp. 277–288. *Cited on page(s): 26*

[48] R. Allemang, "The modal assurance criterion–twenty years of use and abuse," *Sound and Vibration*, vol. 37, no. 8, pp. 14–23, 2003. *Cited on page(s): 31*

[49] S. Petersen and S. Carlsen, "WirelessHART Versus ISA100.11a: The format war hits the factory floor," *IEEE Industrial Electronics Magazine*, vol. 5, no. 4, pp. 23 –34, Dec. 2011. *Cited on page(s): 33, 66*

[50] T. Lennvall, S. Svensson, and F. Hekland, "A comparison of WirelessHART and Zigbee for industrial applications," in *IEEE Intl. Workshop on Factory Communication Systems (WFCS)*, may 2008, pp. 85–88. *Cited on page(s): 33*

[51] K. Chintalapudi and L. Venkatraman, "On the design of mac protocols for low-latency hard real-time discrete control applications over 802.15. 4 hardware," in *Proceedings of IEEE Intl. Conference on Information Processing in Sensor Networks (IPSN)*, 2008, pp. 356–367. *Cited on page(s): 33*

[52] D. Sexton, M. Mahony, M. Lapinski, and J. Werb, "Radio channel quality in industrial wireless sensor networks," in *Proceedings of IEEE Sensors for Industry Conference*, 2005, pp. 88–94. *Cited on page(s): 34, 84*

[53] S. Nethi, J. Nieminen, and R. Jantti, "Exploitation of multi-channel communications in industrial wireless sensor applications: Avoiding interference and enabling coexistence," in *Proceedings of IEEE Wireless Communications and Networking Conference (WCNC)*, 2011, pp. 345–350. *Cited on page(s): 34, 66, 69*

[54] K. Pister and L. Doherty, "Tsmp: Time synchronized mesh protocol," *IASTED Distributed Sensor Networks*, pp. 391–398, 2008. *Cited on page(s): 34, 35*

[55] J. Yick, B. Mukherjee, and D. Ghosal, "Wireless sensor network survey," *Computer networks*, vol. 52, no. 12, pp. 2292–2330, 2008. *Cited on page(s): 35*

[56] E. Cosar, A. Mahmood, and M. Björkbom, "A-stack: a tdma framework for reliable, real-time and high data-rate wireless sensor networks," *Technical Report, Aalto University*, 2012. *Cited on page(s): 38*

[57] A. Sikora and V. F. Groza, "Coexistence of ieee802. 15.4 with other systems in the 2.4 ghz-ism-band," in *Proceedings of IEEE Instrumentation and Measurement Technology Conference (IMTC)*, vol. 3, 2005, pp. 1786–1791. *Cited on page(s): 41, 42*

[58] M. Petrova, J. Riihijarvi, P. Mahonen, and S. Labella, "Performance study of ieee 802.15. 4 using measurements and simulations," in *Proceedings of IEEE Wireless Communications and Networking Conference (WCNC)*, vol. 1, 2006, pp. 487–492. *Cited on page(s): 41, 42*

[59] S. Y. Shin, H. S. Park, and W. H. Kwon, "Mutual interference analysis of ieee 802.15.4 and ieee 802.11b," *Computer Networks*, vol. 51, no. 12, pp. 3338 – 3353, 2007. *Cited on page(s): 41, 42, 43, 46, 55, 61*

[60] R. Musaloiu-E. and A. Terzis, "Minimising the effect of wifi interference in 802.15.4 wireless sensor networks," *Intl. Journal of Sensor Networks*, vol. 3, no. 1, pp. 43–54, Dec. 2008. *Cited on page(s): 41, 67, 68*

[61] S. Pollin, I. Tan, B. Hodge, C. Chun, and A. Bahai, "Harmful coexistence between 802.15.4 and 802.11: A measurement-based study," in *Proceedings of 3rd IEEE Intl. Conference on Cognitive Radio Oriented Wireless Networks and Communications (CrownCom)*, 2008, pp. 1–6. *Cited on page(s): 41*

[62] K.-J. Myoung, S. Soo-Young, and K. Wook-Hyun, "Ieee 802.11 b performance analysis in the presence of ieee 802.15. 4 interference," *IEICE transactions on communications*, vol. 90, no. 1, pp. 176–179, 2007. *Cited on page(s): 41*

[63] I. Howitt and J. A. Gutierrez, "Ieee 802.15.4 low rate-wireless personal area network coexistence issues," in *Proceedings of IEEE Wireless Communications and Networking Conference (WCNC)*, vol. 3, 2003, pp. 1481–1486. *Cited on page(s): 41*

[64] W. Yuan, X. Wang, and J. P. M. G. Linnartz, "A coexistence model of ieee 802.15.4 and ieee 802.11b/g," in *Proceedings of the 14th IEEE Symposium on Communications and Vehicular Technology in the Benelux*, Nov., pp. 1–5. *Cited on page(s): 42*

[65] M. Sha, G. Xing, G. Zhou, S. Liu, and X. Wang, "C-mac: Model-driven concurrent medium access control for wireless sensor networks," in *Proceedings of IEEE Intl. Conference on Computer Communications (INFOCOM)*, 2009, pp. 1845–1853. *Cited on page(s): 43, 68*

[66] P. Jiang, Q. Huang, J. Wang, X. Dai, and R. Lin, "Research on wireless sensor networks routing protocol for wetland water environment monitoring," in *Proceedings of 1st IEEE Intl. Conference on Innovative Computing, Information, and Control (ICICIC)*, vol. 3, 2006, pp. 251–254. *Cited on page(s): 43*

[67] J. Zhao and R. Govindan, "Understanding packet delivery performance in dense wireless sensor networks," in *Proceedings of the 1st Intl. Conference on Embedded Networked Sensor Systems*. ACM, 2003, pp. 1–13. *Cited on page(s): 43*

[68] C. Gao and R. Jäntti, "Link-state clustering based on ieee 802.15.4 MAC for wireless ad-hoc/sensor networks," in *Proceedings of IEEE Wireless Communications and Networking Conference (WCNC)*, vol. 1, 2006, pp. 499–504. *Cited on page(s): 43*

[69] S. Lin, J. Zhang, G. Zhou, L. Gu, J. A. Stankovic, and T. He, "Atpc: adaptive transmission power control for wireless sensor networks," in *Proceedings of the 4th ACM Intl. Conference on Embedded Networked Sensor Systems*, 2006, pp. 223–236. *Cited on page(s): 43*

[70] N. Baccour, A. Koubâa, L. Mottola, M. A. Zúñiga, H. Youssef, C. A. Boano, and M. Alves, "Radio link quality estimation in wireless sensor networks: a survey," *ACM Transactions on Sensor Networks (TOSN)*, vol. 8, no. 4, p. 34, 2012. *Cited on page(s): 43*

[71] K. Srinivasan and P. Levis, "RSSI is under appreciated," in *Proceedings of the 3rd Workshop on Embedded Networked Sensors (EmNets*, 2006. *Cited on page(s): 43*

[72] K. Srinivasan, P. Dutta, A. Tavakoli, and P. Levis, "Understanding the causes of packet delivery success and failure in dense wireless sensor networks," in *Proceedings of the 4th ACM Intl. Conference on Embedded Networked Sensor Systems*, vol. 31, 2006, pp. 419–420. *Cited on page(s): 43*

[73] ——, "An empirical study of low-power wireless," *ACM Transactions on Sensor Networks (TOSN)*, vol. 6, no. 2, p. 16, 2010. *Cited on page(s): 43*

[74] Y. Ma, "Improving wireless link delivery ratio classification with packet SNR," in *Proceedings of IEEE Intl. Conference on Electro Information Technology*, 2005, pp. 6–pp. *Cited on page(s): 43*

[75] M. Senel, K. Chintalapudi, D. Lal, A. Keshavarzian, and E. J. Coyle, "A kalman filter based link quality estimation scheme for wireless sensor networks," in *Proceedings of IEEE Global Telecommunications Conference (GLOBECOM)*, 2007, pp. 875–880. *Cited on page(s): 43*

[76] A. Woo and D. Culler, "Evaluation of efficient link reliability estimators for low-power wireless networks," EECS Department, University of California, Berkeley, Tech. Rep. UCB/CSD-03-1270, 2003. [Online]. Available: http://www.eecs.berkeley.edu/Pubs/TechRpts/2003/6239.html *Cited on page(s): 43*

[77] L. Stabellini and J. Zander, "Energy-efficient detection of intermittent interference in wireless sensor networks," *Intl. Journal of Sensor Networks*, vol. 8, no. 1, pp. 27–40, 2010. *Cited on page(s): 43, 61, 68*

[78] N. Golmie, *Coexistence in Wireless Networks: Challenges and System-Level Solutions in the Unlicensed Bands*. Cambridge University Press, 2006. *Cited on page(s): 46, 55*

[79] L. Takács, "On certain sojourn time problems in the theory of stochastic processes," *Acta Mathematica Hungarica*, vol. 8, pp. 169–191, 1957. *Cited on page(s): 47, 48*

[80] L. Kleinrock, *Queueing Systems, Theory, Volume 1*. Wiley-Interscience, 1975. *Cited on page(s): 50*

[81] A. Thummler, "A novel approach for fitting probability distributions to real trace data with the em algorithm," in *Proceedings of the Intl. Conference on Dependable Systems and Networks*, Washington, DC, USA, 2005, pp. 712–721. *Cited on page(s): 51*

[82] N.-Y. Ma and R. P. King, "The n-fold convolution of generalized exponential-sum distribution functions," *Appl. Math. Comput.*, vol. 142, no. 1, pp. 23–33, Sep. 2003. *Cited on page(s): 51*

[83] S. Ross, *Simulation-Statistical Modeling and Decision Science*. Academic Press, 1997. *Cited on page(s): 51*

[84] S. Haykin, "Cognitive radio: brain-empowered wireless communications," *IEEE Journal on Selected Areas in Communications*, vol. 23, no. 2, pp. 201–220, 2005. *Cited on page(s): 54, 63*

[85] I. F. Akyildiz, W.-Y. Lee, M. C. Vuran, and S. Mohanty, "Next generation/dynamic spectrum access/cognitive radio wireless networks: a survey," *Computer Networks*, vol. 50, no. 13, pp. 2127–2159, 2006. *Cited on page(s): 54*

[86] S. Huang, X. Liu, and Z. Ding, "Opportunistic spectrum access in cognitive radio networks," in *Proceedings of IEEE Intl. Conference on Computer Communications (INFOCOM)*, 2008, pp. 1427–1435. *Cited on page(s): 54*

[87] S. Geirhofer, L. Tong, and B. M. Sadler, "Cognitive radios for dynamic spectrum access-dynamic spectrum access in the time domain: Modeling and exploiting white space," *IEEE Communications Magazine*, vol. 45, no. 5, pp. 66–72, 2007. *Cited on page(s): 54, 55*

[88] A. Ghasemi and E. S. Sousa, "Spectrum sensing in cognitive radio networks: requirements, challenges and design trade-offs," *IEEE Communications Magazine*, vol. 46, no. 4, pp. 32–39, 2008. *Cited on page(s): 54*

[89] T. Yucek and H. Arslan, "A survey of spectrum sensing algorithms for cognitive radio applications," *IEEE Communications Surveys & Tutorials*, vol. 11, no. 1, pp. 116–130, 2009. *Cited on page(s): 54*

[90] A. Sonnenschein and P. M. Fishman, "Radiometric detection of spread-spectrum signals in noise of uncertain power," *IEEE Transactions on Aerospace and Electronic Systems*, vol. 28, no. 3, pp. 654–660, 1992. *Cited on page(s): 54*

[91] S. Geirhofer, L. Tong, and B. M. Sadler, "Dynamic spectrum access in wlan channels: empirical model and its stochastic analysis," in *Proceedings of the 1st ACM Intl. Workshop on Technology and Policy for Accessing Spectrum*, New York, NY, USA, 2006. *Cited on page(s): 55, 79*

[92] L. Stabellini, "Quantifying and modeling spectrum opportunities in a real wireless environment," in *Proceedings of IEEE Wireless Communications and Networking Conference (WCNC)*, 2010, pp. 1–6. *Cited on page(s): 55, 61, 65*

[93] C. Snow, L. Lampe, and R. Schober, "Analysis of the impact of WiMAX-OFDM interference on multiband ofdm," in *Proceedings of IEEE Intl. Conference on Ultra-Wideband (ICUWB)*, 2007, pp. 761–766. *Cited on page(s): 56*

[94] D. Cabric, A. Tkachenko, and R. Brodersen, "Experimental study of spectrum sensing based on energy detection and network cooperation," in *Proceedings of the first ACM Intl. Workshop on Technology and Policy for Accessing Spectrum*, 2006. *Cited on page(s): 56*

[95] Elektrobit Propsim C8. Visited on 13.03.2013. [Online]. Available: http://www.elektrobit.com/ *Cited on page(s): 59*

[96] Multi-Generator (MGEN), http://cs.itd.nrl.navy.mil/work/mgen/index.php, accessed: 20/02/2013. *Cited on page(s): 59, 73*

[97] J. Medbo and P. Schramm, "Channel models for hiperlan/2 in different indoor scenarios," *ETSI BRAN doc. 3ERI085b*, 1998. *Cited on page(s): 59*

[98] V. Erceg, "Tgn channel models," *IEEE 802.11 document 03/940r4*, 2004. *Cited on page(s): 59*

[99] Q. Zhao and B. Sadler, "A survey of dynamic spectrum access," *IEEE Signal Processing Magazine*, vol. 24, no. 3, pp. 79–89, 2007. *Cited on page(s): 63, 65*

[100] S. Geirhofer, J. Z. Sun, L. Tong, and B. M. Sadler, "Cognitive frequency hopping based on interference prediction: Theory and experimental results," *ACM SIGMOBILE Mobile Computing and Communications Review*, vol. 13, no. 2, pp. 49–61, 2009. *Cited on page(s): 63*

[101] C. Cormio and K. R. Chowdhury, "A survey on MAC protocols for cognitive radio networks," *Ad Hoc Networks*, vol. 7, no. 7, pp. 1315 – 1329, 2009. *Cited on page(s): 64, 69*

[102] A. Motamedi and A. Bahai, "Optimal channel selection for spectrum-agile low-power wireless packet switched networks in unlicensed band," *EURASIP Journal on Wireless Communications and Networking*, vol. 2008, p. 9, 2008. *Cited on page(s): 65, 68*

[103] S. Pollin, M. Ergen, M. Timmers, A. Dejonghe, L. Van der Perre, F. Catthoor, I. Moerman, and A. Bahai, "Distributed cognitive coexistence of 802.15. 4 with 802.11," in *Proceedings of 1st IEEE Intl. Conference on Cognitive Radio Oriented Wireless Networks and Communications*, 2006, pp. 1–5. *Cited on page(s): 65*

[104] L. Stabellini and J. Zander, "Energy-aware spectrum sensing in cognitive wireless sensor networks: A cross layer approach," in *Proceedings of IEEE Wireless Communications and Networking Conference (WCNC)*, 2010, pp. 1–6. *Cited on page(s): 65*

[105] S. Geirhofer, L. Tong, and B. M. Sadler, "Cognitive radios for dynamic spectrum access-dynamic spectrum access in the time domain: Modeling and exploiting white space," *IEEE Communications Magazine*, vol. 45, no. 5, pp. 66–72, 2007. *Cited on page(s): 65*

[106] J. Huang, G. Xing, G. Zhou, and R. Zhou, "Beyond co-existence: Exploiting wifi white space for zigbee performance assurance," in *Proceedings of the 18th IEEE Intl. Conference on Network Protocols (ICNP)*, 2010, pp. 305–314. *Cited on page(s): 65*

[107] IEEE Std 802.15.4e-2012 (Amendment to IEEE Std 802.15.4-2011), "IEEE standard for local and metropolitan area networks–part 15.4: Low-rate wireless personal area networks (LR-WPANs) amendment 1: MAC sub-layer," pp. 1–225, 2012. *Cited on page(s): 66*

[108] W. Xu, W. Trappe, and Y. Zhang, "Channel surfing: defending wireless sensor networks from interference," in *Proceedings of the 6th ACM Intl. Conference on Information Processing in Sensor Networks (IPSN)*, 2007, pp. 499–508. *Cited on page(s): 66, 68*

[109] ——, "Defending wireless sensor networks from radio interference through channel adaptation," *ACM Transactions on Sensor Networks (TOSN)*, vol. 4, no. 4, p. 18, 2008. *Cited on page(s): 66*

[110] C. Won, J.-H. Youn, H. Ali, H. Sharif, and J. Deogun, "Adaptive radio channel allocation for supporting coexistence of 802.15.4 and 802.11b," in *Proceedings of 62nd IEEE Vehicular Technology Conference (VTC)*, vol. 4, 2005, pp. 2522–2526. *Cited on page(s): 66*

[111] A. W. Min and K. G. Shin, "Exploiting multi-channel diversity in spectrum-agile networks," in *Proceedings of IEEE Intl. Conference on Computer Communications (ICC)*, 2008, pp. 1921–1929. *Cited on page(s): 66*

[112] W. Xu, W. Trappe, Y. Zhang, and T. Wood, "The feasibility of launching and detecting jamming attacks in wireless networks," in *Proceedings of the 6th ACM intl. symposium on Mobile ad hoc networking and computing*, 2005, pp. 46–57. *Cited on page(s): 66*

[113] J. Borms, K. Steenhaut, and B. Lemmens, "Low-overhead dynamic multi-channel mac for wireless sensor networks," in *Wireless Sensor Networks*. Springer, 2010, pp. 81–96. *Cited on page(s): 66*

[114] Y. Kim, H. Shin, and H. Cha, "Y-mac: An energy-efficient multi-channel mac protocol for dense wireless sensor networks," in *Proceedings of the 7th IEEE Intl. Conference on Information Processing in Sensor Networks (IPSN)*, 2008, pp. 53–63. *Cited on page(s): 66*

[115] S.-U. Yoon, R. Murawski, E. Ekici, S. Park, and Z. H. Mir, "Adaptive channel hopping for interference robust wireless sensor networks," in *Proceedings of IEEE Intl. Conference on Communications (ICC)*, 2010, pp. 1–5. *Cited on page(s): 66*

[116] J.-S. Han, H.-S. Kim, J.-S. Bang, and Y.-H. Lee, "Interference mitigation in ieee 802.15.4 networks," in *Proceedings of IEEE Global Telecommunications Conference (GLOBECOM)*, 2011, pp. 1–5. *Cited on page(s): 66, 68*

[117] J.-S. Han, S.-H. Lee, H.-S. Kim, and Y.-H. Lee, "Performance improvement of ieee 802.15.4 in the presence of co-channel interference," in *Proceedings of Wireless Communications and Networking Conference (WCNC)*, 2011, pp. 49–54. *Cited on page(s): 66*

[118] C. Noda, S. Prabh, M. Alves, C. A. Boano, and T. Voigt, "Quantifying the channel quality for interference-aware wireless sensor networks," *SIGBED Rev.*, vol. 8, no. 4, pp. 43–48, Dec. 2011. *Cited on page(s): 67, 68*

[119] F. Penna, C. Pastrone, M. A. Spirito, and R. Garello, "Measurement-based analysis of spectrum sensing in adaptive WSNs under Wi-Fi and Bluetooth interference," in *Proceedings of the 69th IEEE Vehicular Technology Conference (VTC)*, 2009, pp. 1–5. *Cited on page(s): 67, 68*

[120] L. Stabellini, "Energy-aware channel selection for cognitive wireless sensor networks," in *Proceedings of the 7th Intl. Symposium on Wireless Communication Systems (ISWCS)*, 2010, pp. 892–896. *Cited on page(s): 67, 68*

[121] A. Azarfar, J.-F. Frigon, and B. Sanso, "History-aware channel search schemes in cognitive radio networks," in *Proceedings of the 22nd IEEE Intl. Symposium on Personal Indoor and Mobile Radio Communications (PIMRC)*, 2011, pp. 379–383. *Cited on page(s): 67*

[122] X. Wang, A. Wong, and P.-H. Ho, "Stochastic channel prioritization for spectrum sensing in cooperative cognitive radio," in *Proceedings of the 6th IEEE Consumer Communications and Networking Conference (CCNC)*, 2009, pp. 1–6. *Cited on page(s): 67*

[123] Y. Song, Y. Fang, and Y. Zhang, "Stochastic channel selection in cognitive radio networks," in *Proceedings of IEEE Global Telecommunications Conference (GLOBECOM)*, 2007, pp. 4878–4882. *Cited on page(s): 67*

[124] H. Kim and K. G. Shin, "Efficient discovery of spectrum opportunities with mac-layer sensing in cognitive radio networks," *IEEE Transactions on Mobile Computing*, vol. 7, no. 5, pp. 533–545, May 2008. *Cited on page(s): 67*

[125] J. Cai and A. S. Alfa, "Optimal channel sensing in wireless communication networks with cognitive radio," in *Proceedings of IEEE Intl. Conference on Communications (ICC)*, 2009, pp. 1–5. *Cited on page(s): 67*

[126] J. Ansari, T. Ang, and P. Mahonen, "Spectrum agile medium access control protocol for wireless sensor networks," in *Proceedings of the 7th Annual IEEE Communications Society Conference on Sensor Mesh and Ad Hoc Communications and Networks (SECON)*, 2010, pp. 1–9. *Cited on page(s): 67*

[127] J. Jia, Q. Zhang, and X. Shen, "Hc-mac: A hardware-constrained cognitive mac for efficient spectrum management," *IEEE Journal on Selected Areas in Communications*, vol. 26, no. 1, pp. 106–117, 2008. *Cited on page(s): 67*

[128] Y. Liu, W. Wu, B. Wang, T. He, S. Yi, and Y. Xia, "Measurement-based channel management in wlans," in *Proceedings of IEEE Wireless Communications and Networking Conference (WCNC)*. IEEE, 2010, pp. 1–6. *Cited on page(s): 67*

[129] H. Jiang, L. Lai, R. Fan, and H. V. Poor, "Cognitive radio: How to maximally utilize spectrum opportunities in sequential sensing," in *Proceedings of IEEE Global Telecommunications Conference (GLOBECOM)*, 2008, pp. 1–5. *Cited on page(s): 68*

[130] Q. Zhao and B. Krishnamachari, "Structure and optimality of myopic sensing for opportunistic spectrum access," in *Proceedings of IEEE Intl. Conference on Communications (ICC)*, 2007, pp. 6476–6481. *Cited on page(s): 68*

[131] S.-L. Wu, C.-Y. Lin, Y.-C. Tseng, and J.-L. Sheu, "A new multi-channel mac protocol with on-demand channel assignment for multi-hop mobile ad hoc networks," in *Proceedings of IEEE Intl. Symposium on Parallel Architectures, Algorithms and Networks (I-SPAN)*, 2000, pp. 232–237. *Cited on page(s): 69*

[132] T. L. Saaty, *The Analytic Hierarchy Process*. McGraw-Hill, New York, 1980. *Cited on page(s): 74, 75, 76*

[133] A. M. Alkahtani, M. Woodward, and K. Al-Begain, "The analytic hierarchy process applied to best effort qos routing with multiple metrics: A comparative evaluation," *IET*, 2003. *Cited on page(s): 75*

[134] Y. Yin, J. Shi, Y. Li, and P. Zhang, "Cluster head selection using analytical hierarchy process for wireless sensor networks," in *Proceedings of the 17th IEEE Intl. Symposium on Personal, Indoor and Mobile Radio Communications*, 2006, pp. 1–5. *Cited on page(s): 75*

[135] J. Haapola, F. Martelli, and C. Pomalaza-Ráez, "Application-driven analytic toolbox for wsns," in *Ad-Hoc, Mobile and Wireless Networks*. Springer, 2009, pp. 112–125. *Cited on page(s): 75*

[136] Sensinode Ltd., http://www.sensinode.com, accessed: 07/07/2013. *Cited on page(s): 91*

[137] S. Lembo, J. Kuusisto, and J. Manner, "Internal map of the nanostack 6LoWPAN stack," in *Recent Trends in Networks and Communications*.

Springer Berlin Heidelberg, 2010, vol. 90, pp. 619–633. *Cited on page(s): 93*

[138] FreeRTOS, http://www.freertos.org, accessed: 07/07/2013. *Cited on page(s): 93*

Aalto-DD 8/2014

ISBN 978-952-60-5536-7
ISBN 978-952-60-5537-4 (pdf)
ISSN-L 1799-4934
ISSN 1799-4934
ISSN 1799-4942 (pdf)

Aalto University
School of Electrical Engineering
Department of Communications and Networking
www.aalto.fi

BUSINESS + ECONOMY

ART + DESIGN + ARCHITECTURE

SCIENCE + TECHNOLOGY

CROSSOVER

DOCTORAL DISSERTATIONS